

OHIO SEMITRONICS INC.

1205 CHESAPEAKE AVENUE • COLUMBUS, OHIO 43212
AREA CODE 614
TELEPHONE 486-9561

April 15, 1973

National Aeronautics and Space Administration
George C. Marshall Space Flight Center
Marshall Space Flight Center, Alabama 35812

Attention: William J. McKinney, A and TS-PR-M

Gentlemen:

Attached you will find the Third Quarterly Report on our Systems Analysis effort relative to "Thermoelectric Thin Film Thermal Coating Systems, "Contract No. NAS8-28519, which covers the period January 1 to March 31, 1973.

During this period the Intermediate TED analysis phase was completed. Characterization is given over a range of sink temperatures from 270°K to 330°K and optimization of change in heat flow and in total heat flow was found based on the Geometric Factor (λ/a)A and the input electrical power.

The concept study was completed resulting in defining six possible applications of TED's. Two unique areas were analyzed on a preliminary basis to demonstrate feasibility. One of these was a practical utilization of thin films for spacecraft thermal control. It is anticipated that the other, utilization of heat pipes, will be further analyzed as a specific TED application during the final quarter period of this contract.

Additional data was generated for the Phase B comparison study. It was shown that heat rejection requirements of the Phase B Space Station can be met for worst and average orbit positions and the degree of control determined

Our March costs were \$4,990.00 and the applicable fee was \$349.37. Total contract costs through March 31, 1973, excluding fee, were \$38,461.97. The applicable fee was \$2692.33. Total man-hours to date were 3405.5.

(NASA-CR-124256) THERMOELECTRIC THIN FILM
THERMAL COATING SYSTEMS Quarterly
Progress Report, 1 Jan. - 31 Mar. 1973
(Ohio Semitronics, Inc.) 85 p HC \$6.25

N73-24935

CSSL 20M G3/33

Unclas
17699

Our analysis of the program tasks and effort involved indicates that the allocated funds should be sufficient to meet the contract objectives as shown in the attached program chart.

Very truly yours,

OHIO SEMITRONICS INC.

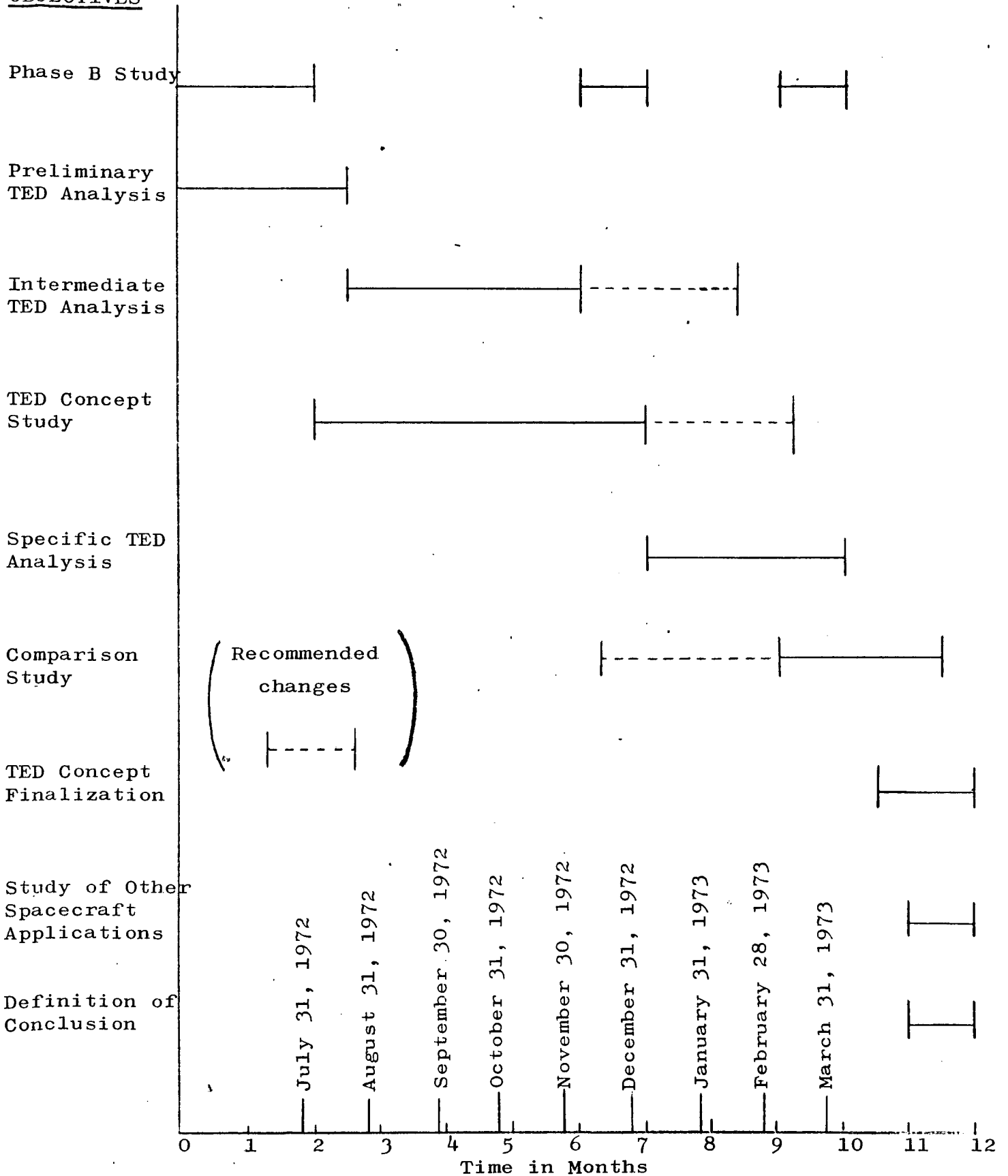
W. E. Bulman

W.E. Bulman, President

J.W.C. Harpster

J.W.C. Harpster, Manager
Materials and Devices R and D

OBJECTIVES



Program Objectives Chart

THIRD QUARTERLY PROGRESS REPORT

on

THERMOELECTRIC THIN FILM THERMAL
COATING SYSTEMS

CONTRACT NO. NAS8-28519

1-2-50-23676(1F)

for the period

January 1, 1973 to March 31, 1973

to

GEORGE C. MARSHALL SPACE FLIGHT CENTER
NATIONAL AERONAUTICS AND SPACE ADMINISTRATION
GEORGE C. MARSHALL SPACE FLIGHT CENTER, ALABAMA

REPORT PREPARED BY

J.W.C. Harpster, W.E. Bulman, A.E. Middleton
P.R. Swinehart and F.D. Braun

April 15, 1973

TABLE OF CONTENTS

	Page
<u>LIST OF FIGURES</u>	i
<u>LIST OF TABLES</u>	ii
<u>ABSTRACT</u>	iii
<u>PURPOSE</u>	v
<u>DERIVATION OF THE PHASE B FLUID LOOP TEMPERATURE PROFILE EXPRESSION WITH TED'S ATTACHED</u>	1
<u>INTERMEDIATE COMPARISON OF PHASE B MODEL</u>	6
<u>INTERMEDIATE TED ANALYSIS</u>	10
<u>Introduction</u>	10
<u>Basic Analysis</u>	10
<u>TED Operation In General</u>	19
<u>Optimization With Respect To ΔQ</u>	39
<u>Optimization With Respect To Q</u>	51
<u>Correlation With Phase B Results</u>	65
<u>Summary</u>	65
<u>CONCEPTS STUDY</u>	68
<u>Introduction</u>	68
<u>TED's With Heat Pipe Radiator</u>	69
<u>Thin Film TED Radiators</u>	71
<u>PLANS FOR FUTURE WORK</u>	74
<u>REFERENCES</u>	75

LIST OF FIGURES

<u>Figure</u>		<u>Page</u>
1	Physical Basis of Four Starting Equations.	2
2	Three Positions Analyzed in Set IV Orbit.	7
3	Heat Sink Model With TED.	11
4	Analog Circuit For Heat Sink Model.	14
5	Magnitude of the Thompson Effect.	16
6	Effects of Incident Flux Intensity on TED Operation.	20
7	Effects of Heat Sink Temperature on TED Operation.	21
8	Three-Dimensional Views of ΔQ on Sun Side.	24-25
9	Variation of Optimum $(\ell/a)A$ With Input Power, VI.	26
10	Three-Dimensional Views of ΔQ on Dark Side.	27-28
11	Three-Dimensional Views of COP.	30-31
12	Three-Dimensional Views of COP x ΔQ .	32-34
13	Three-Dimensional Views of Fin Temperature.	35-38
14	Parametric Dependence of ΔQ Optimum On Input Flux.	40-41
15	Parametric Dependence of Radiator Temperature on Input Flux.	42-43
16	Parametric Dependence of VI on Input Flux.	44-45
17	Parametric Dependence of $(\ell/a)A$ on Input Flux.	46-47
18	Parametric Dependence of COP on Input Flux.	48-49
19	Sun Side Three-Dimensional Views of Total Net Heat Flow, Q.	52-54
20	Dark Side Three-Dimensional Views of Total Net Heat Flow, Q.	55-56
21	Three-Dimensional View of COP x Q_{\max} .	58-60
22	Temperature Dependence of $(\ell/a)A$ Optimum for Q_{\max} on Input Flux.	61
23	Temperature Dependence of Q_{\max} On Input Flux.	62
24	Optimum Input Power for Q_{\max} on Input Flux.	63
25	Correlation With Phase B Results.	66
26	TED's With Heat Pipe Radiator.	70
27	Schematic of a Thin Film Radiator.	72

LIST OF TABLES

<u>Table</u>		Page
I	Quantitative Comparison of Phase B Model	8
II	Definitions of Parameters	12
III	Working Equations	17
IV	Partial Derivatives of ΔQ	18
V	Control Capability of a TED-Heat Pipe Radiator	71

ABSTRACT

Derivation of the fluid loop temperature profile for the Phase B model with TED's attached is developed as a function of position, incident radiation intensity, input fluid loop temperature and TED current. The associated temperature of the radiator is also developed so that the temperature difference across the TED can be determined for each position. The temperature difference is used in determining optimum operating conditions and available generated electrical power.

Additional comparison data is presented for the Phase B model. It is shown for a degraded surface that the TED system has more or less heat rejection capability depending on the orbit position used in the comparison. The TED system is favored in high incident radiation flux positions and the Phase B radiator is favored in low incident radiation flux positions. It is shown for all positions considered that the required heat rejection capacity of the Phase B model is either met under powered conditions with the TED system or exceeded under zero input electrical power conditions.

The Intermediate TED Analysis is given in completed form. Heat sinked TED's are considered over a range in temperature from 270°K to 330°K under various radiation environments and α/ϵ from .1 to 1.0. Data is given which permits determination of optimum $(l/a)A$ and input electrical power for maximum heat transferred and dynamic range of control. The COP is given for maximum heat transferred as well as showing dramatic improvements in COP at somewhat reduced heat rejection capability. Good correlation has been established between the model used in this study and closed form expressions used in the Phase B study.

Two different concepts were analyzed in a preliminary manner to show feasibility. These were a TED-heat pipe configuration and a thin film TED-radiator arrangement. Both systems have merit and should be further studied. The thin film radiator has a feature which permits better zero current heat rejection capability than the bulk approach taken in our present study.

PURPOSE

The purpose of this investigation is to perform a systems analysis of active thermal control using thermoelectric devices and compare the results with performance data and requirements of the McDonnell Douglas Astronautics Company, Phase B Space Station.

DERIVATION OF THE PHASE B FLUID LOOP TEMPERATURE PROFILE
EXPRESSION WITH TED'S ATTACHED

A differential equation has been found which when solved for a given set of conditions gives the temperature of the freon in a given fluid loop of a Phase B radiator with TED's attached as a function of current and position along the loop. Conditions such as incident radiation flux and inlet temperature may be varied. The differential equation can be derived from four basic equations. The first two equations are for the heat flowing into the spacecraft per couple. See Fig. 1(a).

$$Q/\text{couple} = 2SI T_1 + I^2 \rho \ell / a - 2k(a/\ell)(T_1 - T_S) \quad (1)$$

$$Q/\text{couple} = \bar{\Phi}_0 - KA(T_S - T_0) + 2SI(T_1 - T_S) + 2I^2 \rho \ell / a \quad (2)$$

where S=Seebeck coefficient, I=current, ρ =resistivity, ℓ/a =ratio of leg length to leg cross-sectional area, k =thermal conductivity, $\bar{\Phi}_0$ =absorbed radiation flux, and $KA(T_S - T_0)$ is the linearized T^4 radiation law.

The second two equations are for an increment of heat, dQ , entering the fluid loop along a length of tubing $d\ell'$ in which the fluid temperature changes by an amount dT_F . See Fig. 1(b).

$$dQ = C(T_1 - T_F)d\ell' \quad (3)$$

$$dQ = \dot{m} C_p dT_F, \quad (4)$$

where C is the thermal conductance of material between T_1 and T_F for 1 cm of tubing length, \dot{m} is the fluid mass flow rate, and C_p is the specific heat of the fluid.

Equation (1) is solved for T_S , and T_S is substituted into equation (2) giving,

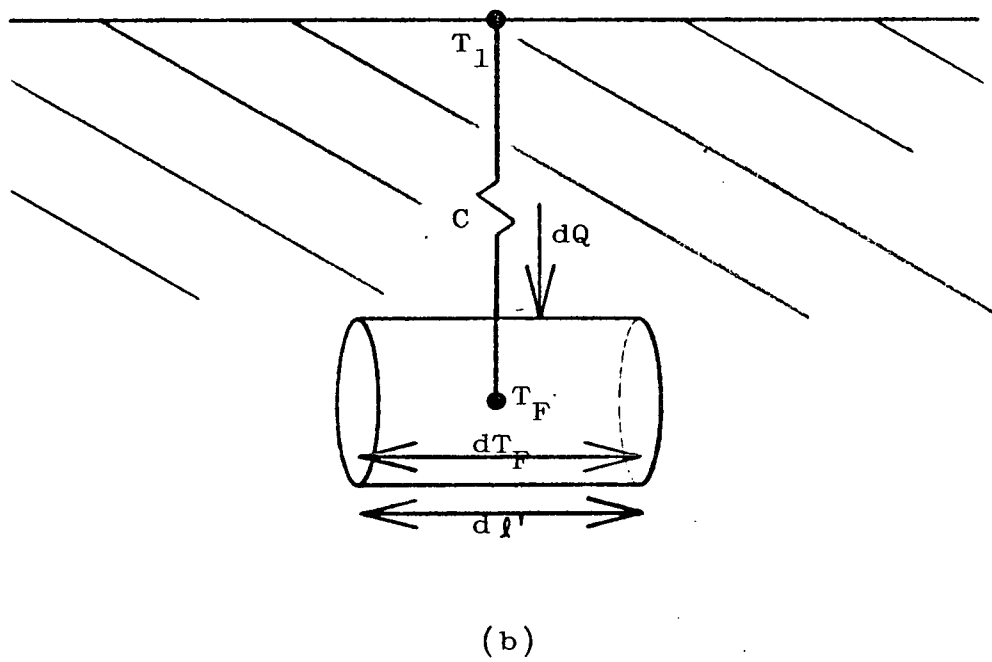
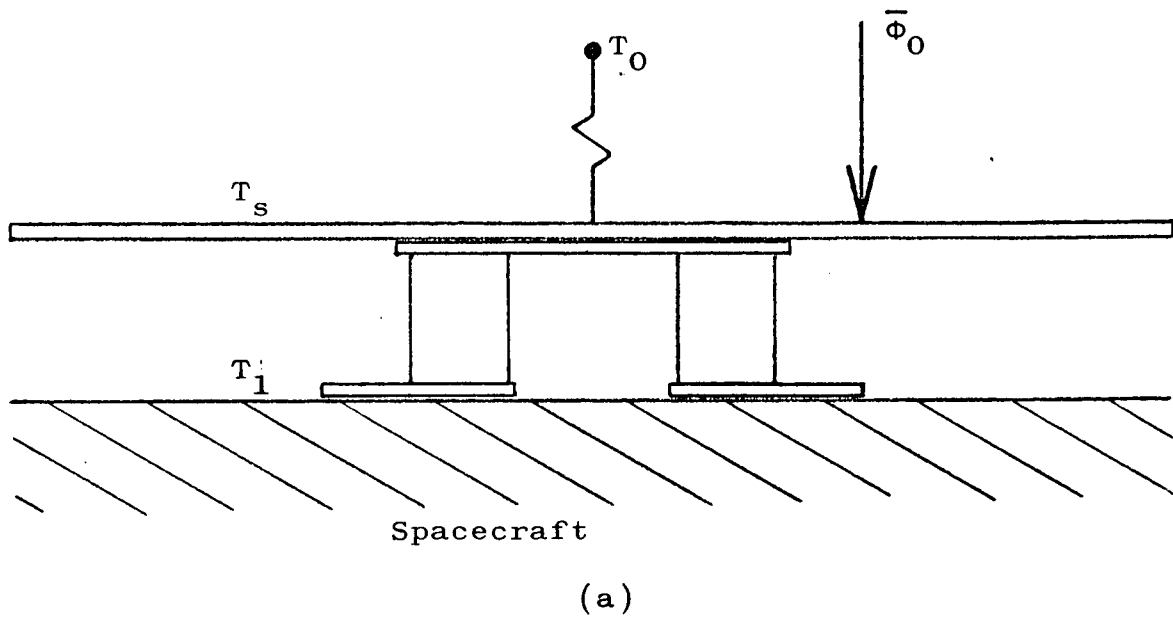


Figure 1. Physical Basis of Four Starting Equations.
 (a) TED and radiator fin arrangement. See Fig. 3 for more detail. (b) Fluid loop segment.

$$Q/\text{couple} = 2k/(2+(\ell/a)(KA+2SI)) \left[\bar{\phi}_0 + KAT_0 - (\ell/a)(KA+2SI) \right. \\ \left. \times (-2SIT_1 - I^2 \rho \ell/a + 2k(a/\ell)T_1) / 2k + 2SIT_1 + 2I^2 \rho \ell/a \right] \quad (5)$$

Equations (3) and (4) are set equal and solved for T_1 giving,

$$T_1 = (\dot{m}C_p/C)dT_F/d\ell' + T_F \quad (6)$$

which is substituted for T_1 in equation (5). Hence,

$$Q/\text{couple} = 2k/(2k+(\ell/a)(KA+2SI)) \left[\bar{\phi}_0 + KAT_0 - (\ell/a)(KA+2SI) \right. \\ \left. \times ((2k a/\ell - 2SI)((\dot{m}C_p/C)dT_F/d\ell' + T_F) - I^2 \rho \ell/a) / 2k \right. \\ \left. + 2SI((\dot{m}C_p/C)dT_F/d\ell' + T_F) + 2I^2 \rho \ell/a \right] \quad (7)$$

It is necessary to eliminate Q/couple from this expression in order to get an equation in which T_F is the only unknown variable. We assume there is one thermoelectric couple per cm of tubing length. Hence, there is $(d\ell'/1 \text{ cm})$ number of couples per length $d\ell'$. Multiplying Q/couple by $(d\ell'/\text{cm})$ gives us dQ . Therefore, we can multiply equation (7) by $(d\ell'/\text{cm})$ and set it equal to equation (4). Rearranging terms and setting $\bar{\phi}_0 = \alpha \phi A \sin(\pi \ell'/L)$ we get a differential equation of the form:

$$dT_F/d\ell' + A'T_F = G \sin(\pi \ell'/L) + E \quad (8)$$

The solution to this equation is,

$$T_F(\ell', I) = Y e^{-A'\ell'} + \left[A'G \sin(\pi \ell'/L) - (\pi/L)G \cos(\pi \ell'/L) \right] \\ \div \left[(\pi/L)^2 + A'^2 \right] + E/A' , \quad (9)$$

where

$$Y = T_{\text{inlet}} + (\pi/L)G / \left[A'^2 + (\pi/L)^2 \right] - E/A'$$

T_{inlet} = fluid temperature at $\ell' = 0$

L = total length of one fluid loop

$$A' = \left\{ \dot{m}C_p/C - \left[\dot{m}C_p (2k + (KA + 2SI)\ell/a) \right] + \left[-2kKA + 2SI(KA + 2SI)\ell/a \right] \right\}^{-1}$$

ℓ' = length of tubing between a given point on a fluid loop and the inlet manifold.

$$G = -2Ck\alpha\phi A / \left\{ \dot{m}C_p \left[(KA + 2SI)(2SI - C)\ell/a - 2k(KA + C) \right] \right\}$$

$$E = -2Ck \left\{ KAT_0 + \left[(\ell/a)(KA + 2SI)/2k + 2 \right] I^2 \rho \ell/a \right\} \\ + \dot{m}C_p \left[(KA + 2SI)(2SI - C)\ell/a - 2k(KA + C) \right]$$

Equation (9) is the desired expression which characterizes the performance of TED's as applied to the phase B space station model. It is useful in obtaining the fluid temperature over the full loop or any portion thereof.

An expression for T_1 as a function of position and current is found by solving equation (8) for $dT_F/d\ell'$ and substituting for $dT_F/d\ell'$ in equation (6). Then once T_F from equation (9) has been found, T_1 may be calculated for identical position and current from,

$$T_1(\ell', I) = T_F(\ell', I) \left[1 - \dot{m}C_p A'/C \right] + \dot{m}C_p/C \left[G \sin(\pi \ell'/L) + E \right].$$

An expression for T_S is found by setting equations (1) and (2) equal and solving for T_S ,

$$T_S(\ell', I) = T_1(\ell', I) \left[2k(a/\ell) / (2k(a/\ell) + KA + 2SI) \right] \\ + (\bar{\theta}_0 + KAT_0 + I^2 \rho \ell/a) + (2k(a/\ell) + KA + 2SI)$$

These expressions for T_F , T_1 , and T_S are used in finding the heats rejected and electrical input powers as presented in the section comparing the Phase B Model with and without TED's.

INTERMEDIATE COMPARISON OF PHASE B MODEL

The average heat rejection capability of the Phase B Space Station without TED's attached and with a surface absorptivity, α , of .4 was found by averaging the heat rejection capability in Set I, IV, V, VI, and VII conditions. The number thus obtained is approximately 19,420 watts. A certain position under Set IV orbit conditions has been found for which the heat rejection capability of the Phase B Model without TED's (19,450 watts), is close to this average. This position is taken as an average orbit position and is labeled as position no. 2 in Figure 2. One side of the Space Station is in full sun light while the other side is in complete darkness. The simplifying assumption is made that no Earth radiation is incident on the radiator surfaces of the module. Position no. 1, shown in Figure 2, is the case for worst possible radiation loading, having full Sun flux incident on one side and Earth infrared radiation and albedo on the other side. Position no. 3 is in the Earth's shadow, with Earth infrared radiation incident on one side and darkness on the other.

Through computer evaluation of the expression for the fluid loop temperature as a function of TED current and position along the loop, the outlet fluid temperature was found for both sides of the Space Station for each of the three positions shown in Figure 2. The heat lost from the fluid between the inlet and outlet manifolds was then calculated from the relation:

$$Q_{\text{rejected/loop}} = \dot{m}C_p(T_{F,\text{in}} - T_{F,\text{out}})$$

where $T_{F,\text{in}}$ is the fluid temperature at the inlet manifold, C_p is the specific heat of the fluid, and \dot{m} is the mass flow rate of the fluid through the loop. A summary of the heat rejected for both sides of the spacecraft in the three orbit positions is given in Table 1. Comparison is made between the Phase B Model with TED's attached and powered at optimum current (constant current throughout each fluid loop) and the Phase B

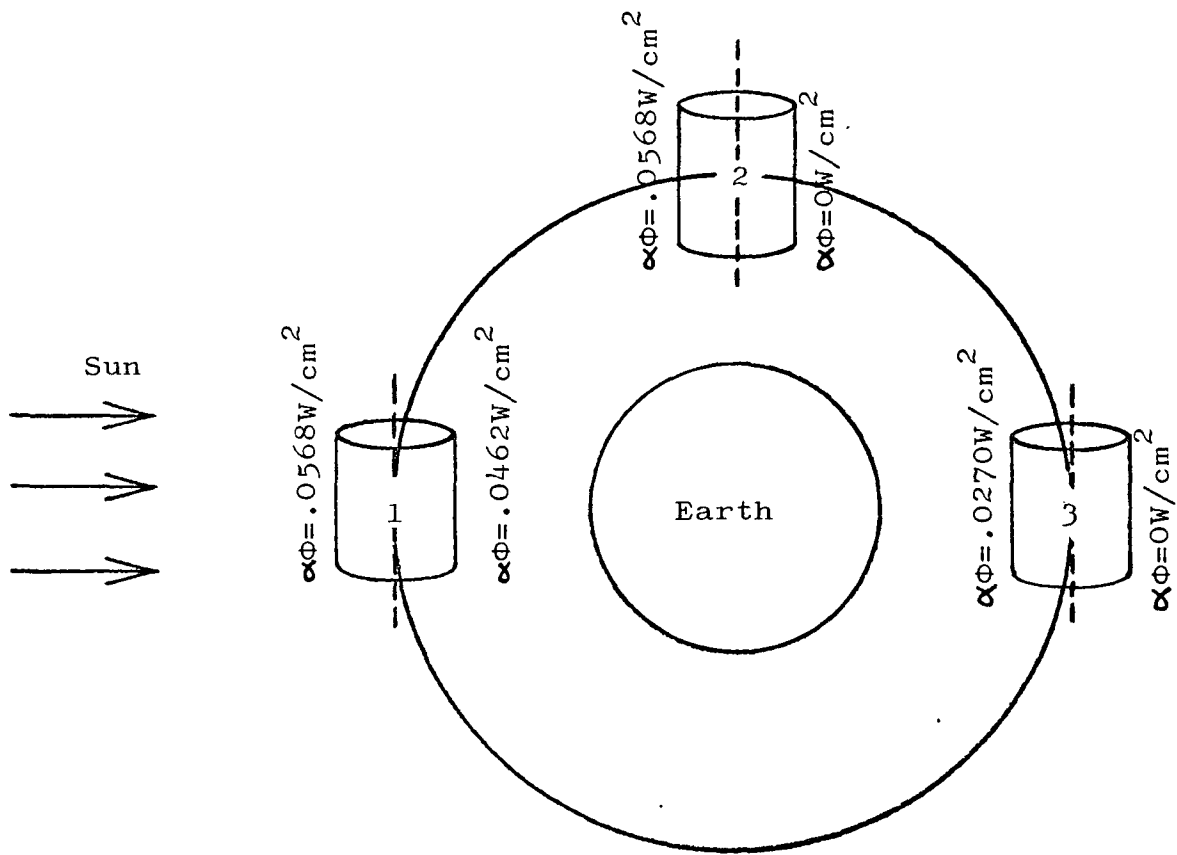


Figure 2. Three Positions Analyzed in Set IV Orbit.

TABLE I
 QUANTITATIVE COMPARISON OF PHASE B MODEL

PHASE B MODEL WITHOUT TED'S
 (Heat Rejected)

Position	Left Side	Right Side	Total
1	2,401	4,910	7,311
2	2,401	17,049	19,450
3	9,738	17,049	26,787

PHASE B MODEL WITH TED'S POWERED
 FOR MAXIMUM HEAT REJECTION
 (Heat Rejected/Electrical Input Power)

Position	Left Side	Right Side	Total
1	4,719/11,920	5,919/11,551	10,638/23,471
2	4,719/11,920	14,512/2,647	19,231/14,567
3	9,438/6,637	14,512/2,647	23,950/9,284

PHASE B MODEL WITH TED'S POWERED TO
 APPROXIMATE HEAT REJECTION OF PHASE B MODEL WITHOUT TED'S
 (Heat Rejected/Input Power)

Position	Left Side	Right Side	Total
1	2,782/1,494	4,937/1,636	7719/3,130
2	2,782/1,494	N.A.	N.A.
3	9,438/6,637	N.A.	N.A.

Heat rejection and input power is given in watts.

Model without TED's attached. Input power for optimum current is given for powered TED's.

Note that on the Sun side in position no. 1, the system with TED's powered at optimum current rejects approximately twice as much heat as the system with no TED's. In position no. 2, the total heat rejected is about the same with and without TED's and is about 4,000 watts above the defined Phase B requirement of 15,350 watts. In position no. 3 the system with TED's powered at optimum current rejects 3,000 watts less than the system with no TED's but still rejects 8,600 watts more than the requirement. It should be emphasized that position no. 2 does not represent an average position for Set IV heat rejection but represents a general average position not associated with any specific Set condition. The average Phase B heat rejection without TED's in Set IV conditions has been given as 15,400 watts, whereas the heat rejection in position no. 2 of Fig. 2 is 19,450 watts, well above the Set IV average. The current needed to meet the required 15,350 watts is -1.3 amps on both sides of the spacecraft in position no. 2. No current is needed to meet the requirement in position no. 3 since 18,100 watts are rejected at zero current. Using the TED's as power generators in position no. 3 would not only produce extra power, but also increase heat rejection capability over the zero current value of 18,100 watts. The output power in position no. 3 with the TED's electrically in series with a load of resistance equal to the sum of the TED resistances would be 213.5 watts. The current flowing through the TED's would be -.6 amps, and the new value of heat rejected would be 19,818 watts. Where possible, in Table I, the electrical input power is given that is needed to match the heat rejection capability of the Phase B Model with no TED's.

INTERMEDIATE TED ANALYSIS

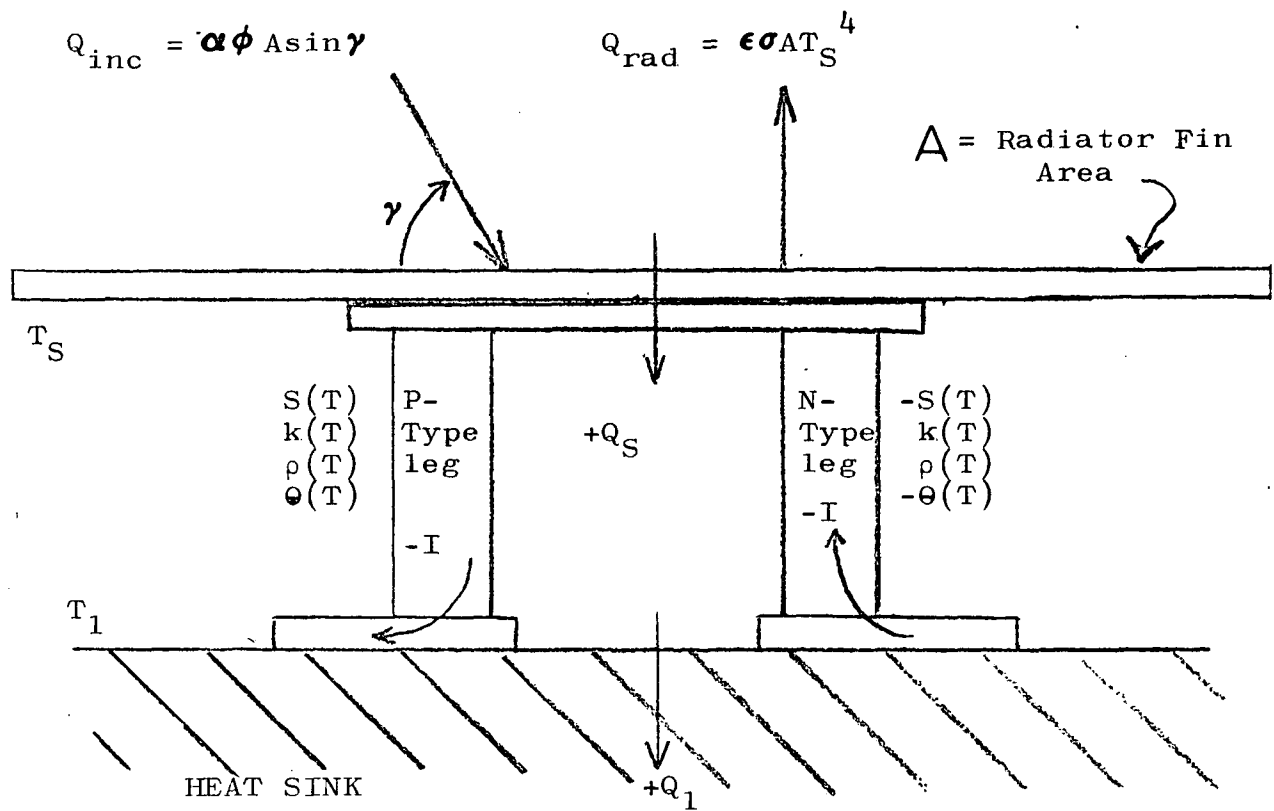
Introduction

Thermoelectric devices using standard Bi_2Te_3 alloys have been characterized as thermal control elements for spacecraft in earth orbit. The amount of heat that can be pumped into or out of a spacecraft to maintain it at a given control temperature has been found for a range of control temperatures from 270°K to 330°K . For each of these temperatures, TED behavior has been analysed for a number of radiator surface absorptivities and emissivities, and also for the radiator tilted with respect to the Sun, from full Sun intensity to a dark oriented surface.

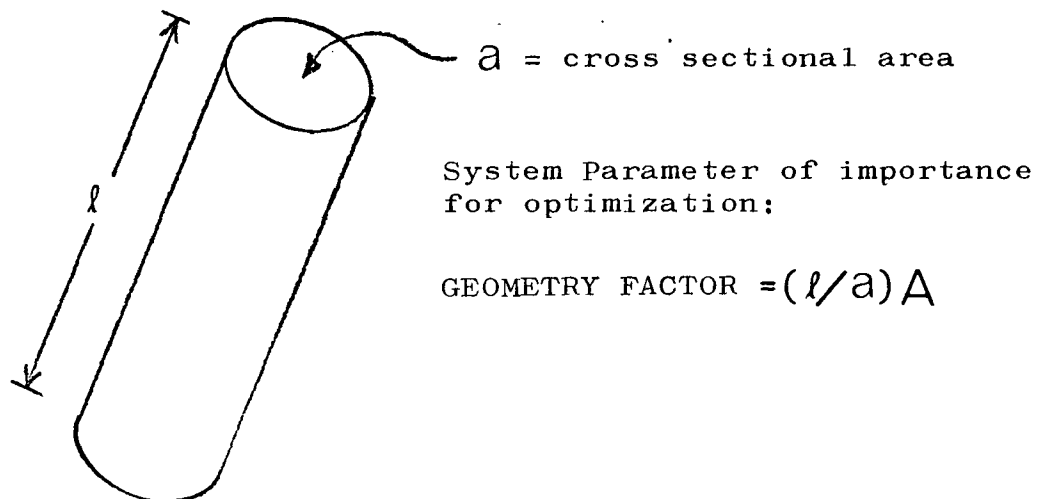
Basic Analysis

A heat sink at temperature T_1 was used to simulate the spacecraft, which was to be maintained at this fixed control temperature. This heat sink model is shown in Figure 3(a). The TED, consisting of one couple, is placed between the heat sink and a radiator fin with the surface parameters shown. The solar constant is $\phi=1.4 \text{ KW/m}^2$. The heat flow into or out of the heat sink, Q_1 , in Watts per m^2 of radiator area, is the quantity of interest. It is defined as positive when flowing into the heat sink. Positive electrical current, I causes an increase in Q_1 in the positive direction. The thermoelectric parameters listed beside each semiconductor leg are defined in Table II. The difference between Q_S and Q_1 is the electrical input power to the couple.

Figure 3(b) shows the dimensions of a semiconductor leg. The thermoelectric parameters of Bi_2Te_3 are close enough in magnitude that the cross sectional areas of the legs, a , can be kept the same. The thermoelectric parameters for n- and p-type materials are thus averaged together. It has been shown that the same results are obtained with TED's in a space environment having an (ℓ/a) value as long as the geometry fac-



(a) Spacecraft Model: Heat Sink with TED and radiator fin.



(b) Dimensions of TED Semiconductor leg, P- or N- Type.

Figure 3. Heat Sink Model With TED (a) and Semiconductor Leg Geometry (b).

TABLE II

DEFINITIONS: SEE FIGURE 3 AND TABLE III.

N - AND P - TYPE THERMOELECTRIC PARAMETERS ARE AVERAGED TOGETHER. MATERIAL IS Bi_2Te_3 .
THE TEMPERATURE VARYING THERMOELECTRIC PARAMETERS ARE FITTED WITH FOURTH ORDER
POLYNOMIALS.

THE PARAMETERS ARE AVERAGED OVER THE TEMPERATURE RANGE OF OPERATION USING THESE
POLYNOMIALS.

1. $S(T)$ = SEEBECK COEFFICIENT, $\mu\text{V}/^\circ\text{K}$
 S_1 IS EVALUATED AT T_1
 S_S IS EVALUATED AT T_S
2. $k(T)$ = THERMAL CONDUCTIVITY, $\text{WATTS}/\text{cm}/^\circ\text{K}$
3. $\rho(T)$ = ELECTRICAL RESISTIVITY, $\Omega\text{-cm}$
4. ΔT = $T_S - T_1$
5. ΔQ = $Q(I \neq 0) - Q(I = 0)$ = HEAT PUMPED, $\text{WATTS}/\text{COUPLE}$ OR $\text{WATTS}/(\text{m}^2 \text{ fin area})$
6. COP = COEFFICIENT OF PERFORMANCE = $\Delta Q/VI$, UNITLESS
7. I = CURRENT, AMPS
8. GEOMETRY FACTOR = $(l/a)A$, cm
9. COP x Q = COP WEIGHTED IN FAVOR OF NET TOTAL HEAT FLOW
10. COP x ΔQ = COP WEIGHTED IN FAVOR OF HEAT PUMPED
11. $\theta(T)$ = THOMSON COEFFICIENT, $T(ds/dT)$, $\mu\text{V}/^\circ\text{K}$

tor $(\ell/a)A$ remains the same, and that this factor is an important optimization parameter.

With the above model, radiation between the fin and spacecraft surfaces is assumed to be negligible. The effect of thermal barriers at the TED-fin and TED-spacecraft interfaces are taken into account by using a decreased TED Figure of Merit, Z , relative to the Z value of the bulk material, by picking a practical module Z of 2.55 (room temperature). The Seebeck coefficient of the bulk material is corrected to reflect the decrease in Z . The thermoelectric parameters are inserted into the computer program as 4th order polynomials in temperature, as demonstrated in the Second Quarterly Report.

The electrical analog circuit of the heat sink model is shown in Figure 4, and the major assumptions involved are listed, along with the sources of the heats to be summed at the two nodes. The fourth assumption implies that the differential equation for the temperature as a function of distance along the semiconductor leg has been linearized.¹ The temperature dependent parameters are written as integrals of polynomials, so that average thermoelectric parameters can be used for any temperature range. For example, the heat flow along a semiconductor bar, such as that shown in Figure 3(b), due to thermal conduction is

$$q = (a/\ell) \int_{\Delta x} k(T)(dT/dx)dx,$$

or, as an average,

$$q = (a/\ell)\bar{k}\Delta T$$

$$\text{where } \bar{k} = (1/\Delta T) \int_{\Delta T} k(T)dT.$$

The same operations are performed on the electrical resistivity and Thomson coefficient. Then one half of each of

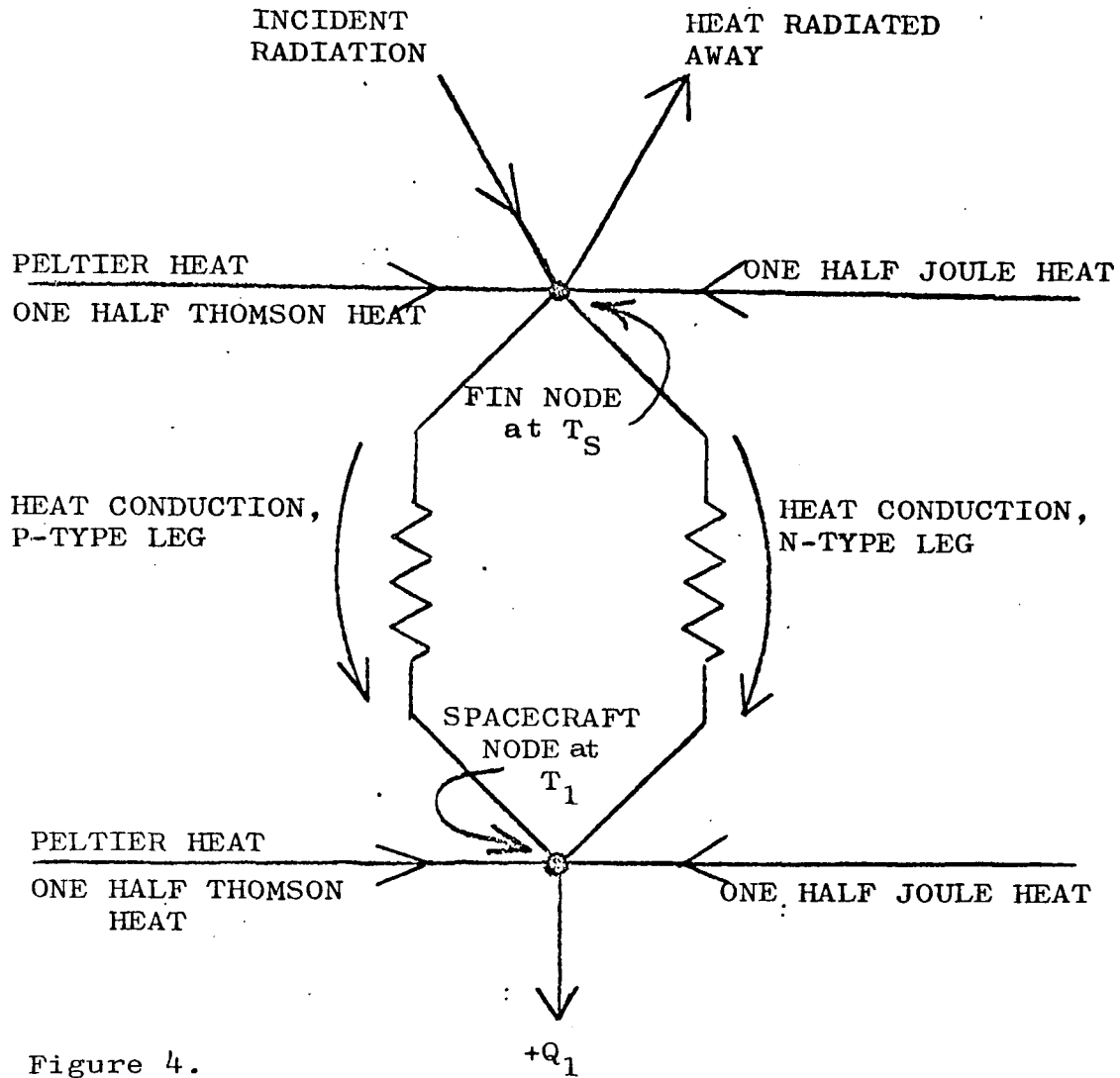


Figure 4.

ANALOG CIRCUIT FOR HEAT SINK MODEL

ASSUMPTIONS:

1. NO RADIATION LOSS FROM SURFACE OF FIN FACING HEAT SINK, OR FROM SIDES OF SEMICONDUCTOR LEGS.
2. THERMAL BARRIERS AT TED INTERFACES TAKEN INTO ACCOUNT WHEN TED THERMOELECTRIC PARAMETERS ARE MEASURED.
3. RADIATOR FIN IS ISOTHERM AT T_S .
4. ONE HALF THE HEAT DUE TO THE THOMSON AND JOULE EFFECTS APPEARS AT EACH NODE.

these sources of bulk heat flow is summed at each end of the TED. The complexities of an exact numerical solution to the above-mentioned differential equation are discussed by Sherman, et.al.,² and the errors involved in using average parameters are delineated. None of the examples given by them correspond to the material used in this study, but from past experience with Bi_2Te_3 , we estimate the errors in the results to be less than +15% in the heat pumping rate and fin temperature, and less than 5% in the power generation mode. This is because in the heat pumping mode the net heat flux is the difference between the Peltier heat and that due to the Joule effect plus thermal conduction, and the net heat flux is smaller than either of them at reasonably high current and temperature gradient. Thus small percentage changes in either of the latter two terms can make a large difference in the net heat pumping rate. On the other hand, in the power generation mode, the Peltier and thermally conducted heats are in the same direction and their sum is large compared to the Thomson and Joule heats for reasonable electric currents. Thus a small change in either term has less effect on the power generated. This can be seen in Figure 5, where the effect of adding the Thomson effect is shown to be considerably greater in the heat pumping regime at higher currents than in the power generation regime toward lower currents.

The equations for heat flow across the TED - heat sink interface are given in Table III. They were derived in the Second Quarterly Report from the analog circuit shown in Figure 2 of this report. Definitions of terms are given in Table II. Note that the COP defined here is with an initial ΔT across the module, in contrast to the usual case, where $Q(I=0) = 0$. Table IV lists the partial derivatives of the heat pumped, (ΔQ in Table II) with respect to (ℓ/a) and I . They are derived using Leibnitz' rule and the chain rule from equations 1 and 2 in Table III, and the heat flow at zero current:

$$Q(I=0) = 2(a/\ell)\bar{k}\Delta T.$$

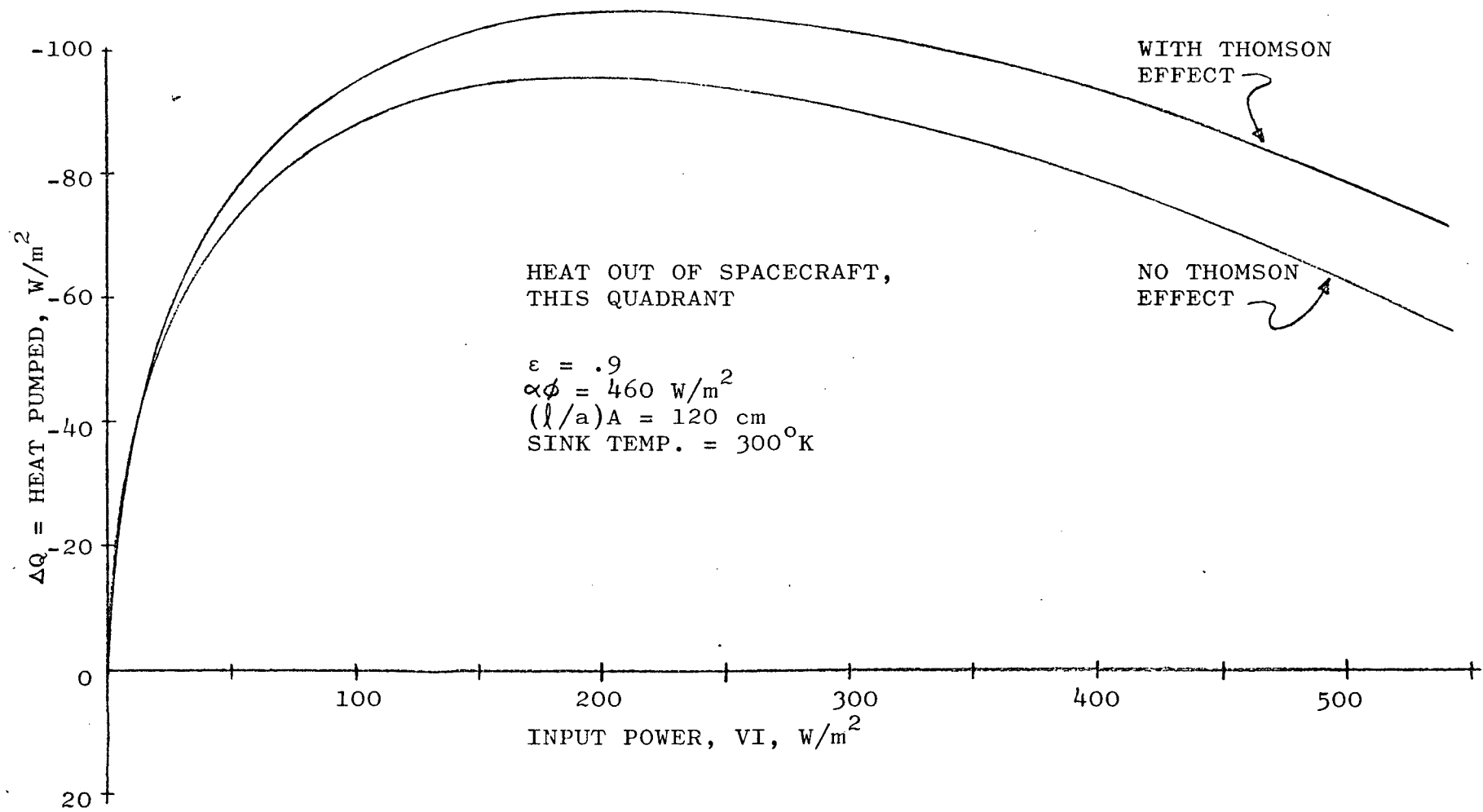


Fig. 5. Magnitude of Thomson Effect.

TABLE III

EQUATIONS ARE WRITTEN ON A PER COUPLE BASIS, WITH "A" cm^2 OF FIN AREA PER COUPLE.
HEAT IS PUMPED INTO OR OUT OF HEAT SINK DEPENDING ON CURRENT DIRECTION.

HEAT FLOW EQUATION AT SPACECRAFT NODE:

$$1. \quad Q_1 = 2(a/l)\bar{k}\Delta T + 2S_1T_1I + \bar{\rho}(l/a)I^2 + \bar{\Theta}I\Delta T \quad \text{Watts/Couple}$$

HEAT FLOW EQUATION AT SPACECRAFT NODE FROM ENERGY CONSERVATION AT THE RADIATOR NODE:

$$2. \quad Q_1 = \alpha\phi A \sin(\gamma) - \epsilon\sigma AT_S^4 + 2[S_1T_1 - S_S T_S]I + 2\bar{\rho}(l/a)I^2 + 2\bar{\Theta}I\Delta T \quad \text{Watts/Couple}$$

THIS IS THE SUM OF THE ELECTRICAL INPUT POWER AND THE RADIATION BALANCE AT THE FIN NODE.

ELECTRICAL INPUT POWER EQUATION:

$$3. \quad VI = 2\bar{\rho}(l/a)I^2 + 2[S_1T_1 - S_S T_S]I + 2\bar{\Theta}I\Delta T \quad \text{Watts/Couple}$$

TEMPERATURE AVERAGED THERMOELECTRIC PARAMETERS:

$$4. \quad \bar{k} = (1/\Delta T) \int_{T_1}^{T_S} k(T) dT \quad 5. \quad \bar{\rho} = (1/\Delta T) \int_{T_1}^{T_S} \rho(T) dT \quad 6. \quad \bar{\Theta} = (1/\Delta T) \int_{T_1}^{T_S} T(dS/dT) dT$$

EQUATIONS 1. AND 2. ARE SOLVED SIMULTANEOUSLY FOR THE FIN TEMPERATURE.

TABLE IV

THE PARTIAL DERIVATIVES OF $\Delta Q = Q(I \neq 0) - Q(I = 0)$ WITH RESPECT TO (l/a) AND I ARE USED IN A COMPUTER PROGRAMMED OPTIMIZING PROCESS TO FIND THE MAXIMUM ΔQ THAT CAN BE PUMPED OUT OF THE SPACECRAFT, AT OPTIMUM $(l/a)_A$ AND OPTIMUM CURRENT.

$$1. \quad \partial \Delta Q / \partial I = 0 = 2[S_1 T_1 - S_S T_S] + 2\theta_S I + 4(l/a)\bar{\rho}_S I \\ - \left\{ \left[2(l/a)\bar{\rho}_S I + \theta_S I + 2S_1 T_1 \right] \left[-2IS_S + 2(l/a)\rho_S I^2 / \Delta T \right. \right. \\ \left. \left. - 2(l/a)\bar{\rho}_S I^2 / \Delta T - 4\epsilon\sigma AT_S^3 \right] / \left[2k_S(a/l) - (l/a)\bar{\rho}_S I^2 / \Delta T \right. \right. \\ \left. \left. + (l/a)\rho_S I^2 / \Delta T + \theta_S I \right] \right\}.$$

$$2. \quad \partial \Delta Q / \partial (l/a) = 0 = 2\bar{\rho}_S I^2 + 8\epsilon\sigma AT_{SO}^3 \bar{k}_{SO} (T_{SO} - T_1) / \left[(l/a)^2 (4\epsilon\sigma AT_{SO}^3 + 2k_{SO}(a/l)) \right] \\ + \left\{ \left[-4\epsilon\sigma AT_S^3 - 2(l/a)\bar{\rho}_S I^2 / \Delta T - 2S_S I + 2I^2 (l/a)\rho_S / \Delta T \right] \right. \\ \times \left[2(\bar{k}_S \Delta T - \bar{k}_{SO} [T_{SO} - T_1]) (a/l)^2 + 4k_{SO} \bar{k}_{SO} (T_{SO} - T_1) / (l/a)^3 (4\epsilon\sigma AT_{SO}^3 + 2k_{SO}(a/l)) \right. \\ \left. \left. - \bar{\rho}_S I^2 \right] / \left[2k_S(a/l) + \theta_S I + (l/a)\rho_S I^2 / \Delta T \right. \right. \\ \left. \left. - (l/a)\bar{\rho}_S I^2 / \Delta T \right] \right\}$$

$T_{SO} = T_S (I=0)$; SUBSCRIPT "SO" DENOTES PARAMETER EVALUATED AT T_{SO} ; SUBSCRIPTS "S" AND "1" DENOTE PARAMETERS EVALUATED AT T_S AND T_1 , RESPECTIVELY.

For each optimization parameter (ℓ/a) and I , two equations are obtained, and $dT_S/d(\ell/a)$ and dT_S/dI are eliminated to obtain the final equations. Note that these equations are valid only at the extrema, but vary monotonically, so that they can easily be used in a computer program to find the optimum $(\ell/a)A$ and input power for maximum heat removal from the spacecraft. This will be discussed in more detail later.

TED Operation In General

The general features of the results of the TED analysis can be seen from Figures 6 and 7. These curves give the difference in heat flow, ΔQ , between the situation with the TED's powered and that with the TED's unpowered as a function of input electrical power. They are shown here over a much greater range of input powers than can be used, as will be explained shortly. The $(\ell/a)A$ value is an arbitrary value picked for purposes of illustration. To help visualize the geometry for $(\ell/a)A = 100\text{cm}$, take each leg to be a cube 1 cm on a side. Then the radiator would be a square 10 cm on a side. Figure 6 illustrates behavior as the absorbed incident radiation changes from Sun side, $\gamma = 90^\circ$, to dark side, $\gamma = 0^\circ$, at a constant sink temperature. Figure 7 shows how the curves shift as the heat sink temperature varies between 330°K and 270°K at a constant absorbed incident flux, Sun side in this case.

The observations that can be made concerning Figures 6 and 7 are these. There are three modes of operation. The first is shown in the first quadrant, and is heat pumped out of the spacecraft. Figure 6 shows that for $\gamma = 90^\circ$, or full sun incidence, there is a broad maximum in the curve at about $200 \text{ W/m}^2 = .4 \text{ W/couple}$ input power, above which Joule heating and thermal conductivity begin to dominate and decrease the heat rejection capability. The maximum moves toward lower input powers as the incident radiation decreases (going from 90° to 0°), and as the maximum ΔQ decreases. Note that the COP at the peak is

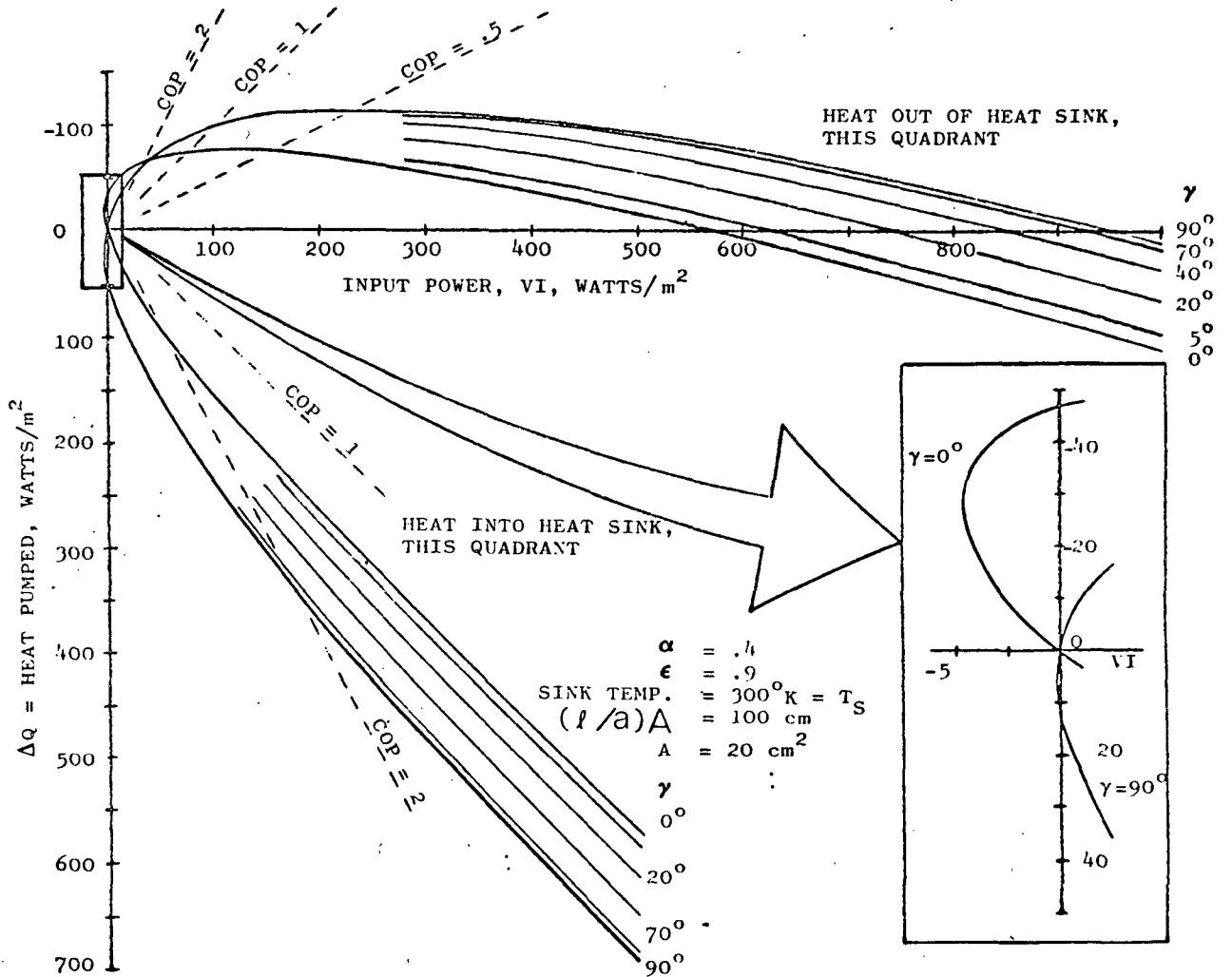


Figure 6. Illustration of the three modes of operation of the TED heat sink model for an arbitrary $(l/a)A$ and constant sink temperature. ΔQ is heat flow due only to the electrical input power to the TED. First quadrant is removal of heat sink, second and third quadrants are power generation (Inset) and fourth quadrant is heat piped into heat sink. The family of curves is for angle of tilt of surface with respect to Sun, from full Sun ($\gamma=90^\circ$) to dark side ($\gamma=0^\circ$). Multiply VI by $2 \times 10^{-3} \text{ m}^2/\text{couple}$ to get VI in Watts/couple.

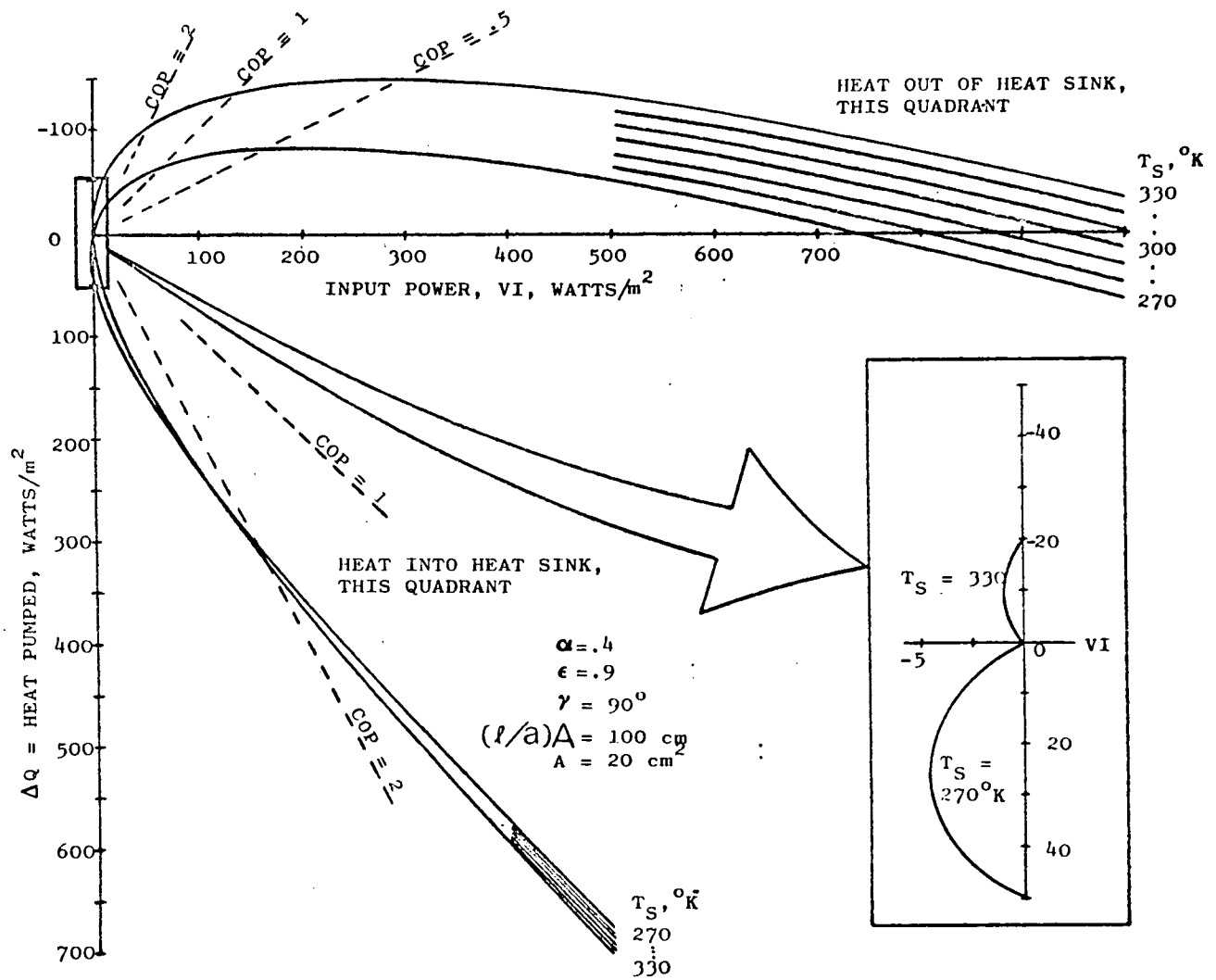


Figure 7. Illustration of three modes of operation of the TED heatsink model for an arbitrary constant $(l/a)A$ and full sun incidence ($\gamma=90^\circ$). ΔQ is the heat flow due only to the electrical input power to the TED. First quadrant is removal of heat from sink, second and third quadrants are power generation (Inset) and fourth quadrant is heat piped into heat sink. The family of curves is for different heat sink temperatures. Multiply VI by $2 \times 10^{-3} \text{ m}^2/\text{couple}$ to get VI in Watts/couple.

generally less than one, but (for $\gamma=90^\circ$) by reducing the ΔQ pumped by one half, the COP can be increased by a factor of 4. For $\gamma=0^\circ$, this is even more dramatic, since only 10% of the possible ΔQ need be sacrificed to increase the COP from .75 to 2. This implies that there is an important trade-off to be made between the maximum ΔQ that can be pumped out of the spacecraft and a reasonable cost in input power. For this reason, a better criterion for this model might be a weighted COP such as $COP \times \Delta Q$. It was also shown in the Second Quarterly Report that there is a maximum in these curves with respect to $(\lambda/a)A$. More will be said about this later.

The second mode of operation is the power generation mode, for negative input power, VI. It is expanded in the figure insets. The largest amount of power generated is for ΔQ out of the spacecraft on the dark side. The peak of each curve occurs where the load resistance is equal to the internal resistance of the module. A smaller amount of power is generated on the sun side for ΔQ into the spacecraft. There thus will be an angle of tilt, or a value of absorbed heat, for which there can be no power generated, and at $VI = 0$ there will be no ΔT across the module. From the inset, it can be seen that this will be a little less than $\gamma = 90^\circ$.

The third mode of operation, shown in the fourth quadrant, is for pumping heat into the spacecraft. In this case the Peltier term and the Joule term are of the same sign, and there is no optimum VI. At $VI = 200 \text{ W/m}^2$, almost four times as much heat can be pumped into the spacecraft as can be pumped out, for opposite current directions, of course. The COP is about four times as great also. This is true of the dark side as well, so that heat can be prevented from being radiated into space and therefore becomes part of the overall thermal control capability.

Figure 7 shows much the same phenomena for a constant $(l/a)A$ and γ over a variety of heat sink temperatures. Note that the heat sink temperature has less effect on the heat pumped in than on the heat pumped out. Comparing Figures 6 and 7, it is observed that the power generated for the $\gamma = 90^\circ$, $T_S = 270^\circ\text{K}$ case is about the same as for the $\gamma = 0^\circ$, $T_S = 300^\circ\text{K}$ case, but with the opposite direction of heat flow.

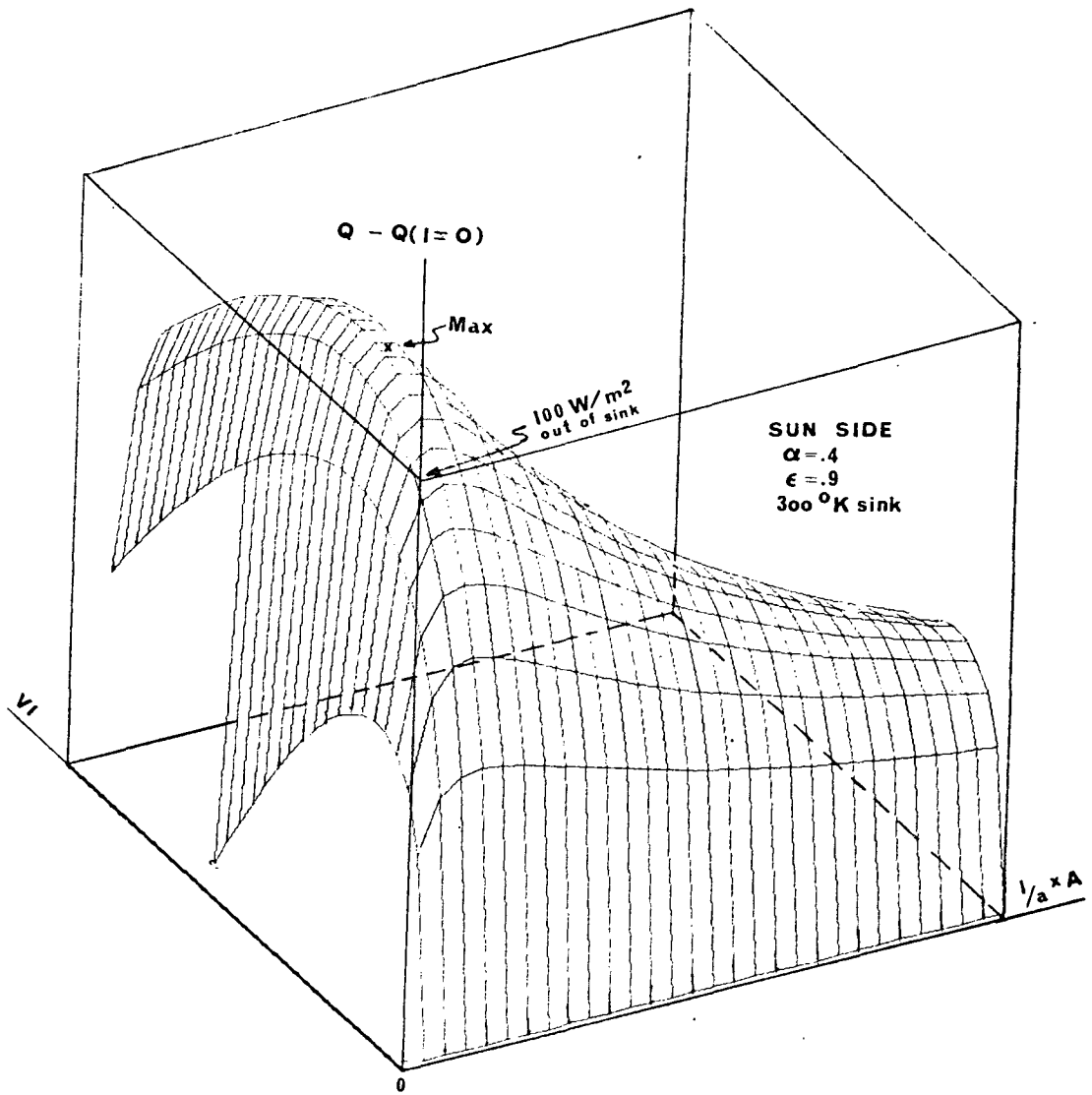
Three-dimensional graphs of various quantities of interest for two typical cases will now be presented:

1. Sun side illumination, sink temperature = 300°K .
2. Dark side illumination (ie., no illumination), sink temperature = 300°K .

ΔQ , T_S , COP, and COP x ΔQ are plotted against $(l/a)A$ and VI for each of these two cases. These surfaces are intended to give a qualitative picture of TED operation, and accurate numbers are obtained from a computer program that finds the peaks of the surfaces without calculating out all the points necessary for these plots.

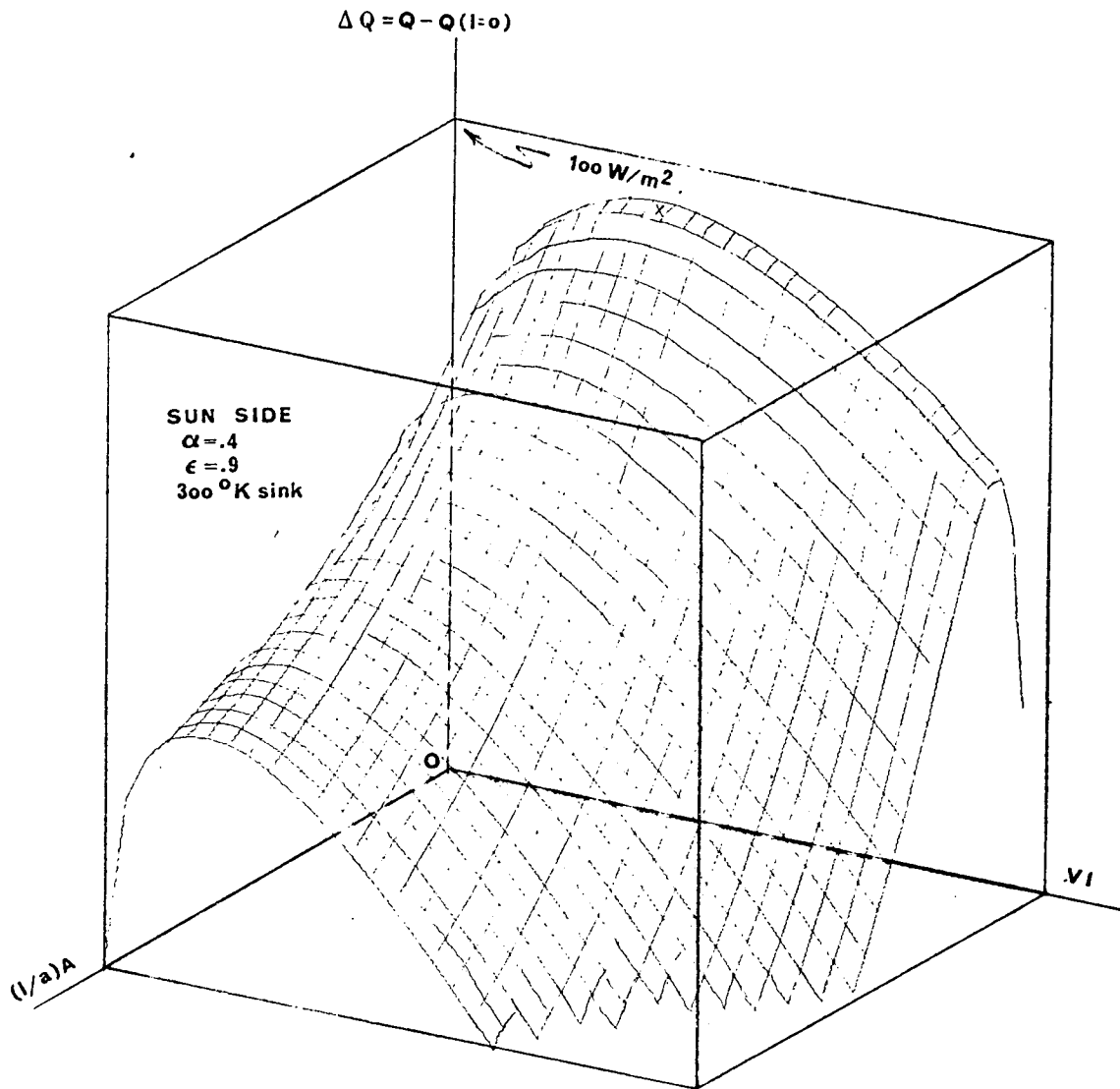
Figure 8(a) and 8(b) are two views of $\Delta Q = Q(I \neq 0) - Q(I = 0)$ for the Sun side. The curves running parallel to the VI axis are similar to those shown in Figures 6 and 7. The fifth curve from the VI axis is for $(l/a)A = 100\text{cm}$, and is identical to the first quadrant portion of the curve for $\gamma = 90^\circ$ and $T_S = 300^\circ\text{K}$ in Figures 6 and 7. There is obviously a maximum with respect to both VI and $(l/a)A$. Fortunately, the optimum $(l/a)A$ changes very little with VI for maximum ΔQ , as shown in Figure 9. This, then, will not be a design criterion when optimizing for maximum range of control, $\pm\Delta Q$.

The dark side ΔQ is presented in Figures 10(a) and (b). It has the same features as for the sun side, and in addition the general shape of the power generation region can be surmized from the shape of the line where the surface pierces the ΔQ ,



(a)

Figure 8 (a). Three-Dimensional View of $\Delta Q = Q(I \neq 0) - Q(I = 0)$ for the Sun Side. Demonstrates a maximum ΔQ with respect to both $(l/a)A$ and VI . VI increments are 20 W/m^2 and full scale is 580 W/m^2 . Multiply by $2 \times 10^{-3} \text{ m}^2/\text{couple}$ to get W/couple . $(l/a)A$ increments are 20 cm , and full scale is 580 cm . Heat is out of the spacecraft for the octant shown. ΔQ at maximum is 115 W/m^2 , optimum VI is 244 W/m^2 , and optimum $(l/a)A$ is 83 cm .



(b)

Figure 8 (b). Second view of Figure 8 (a). Same scale.

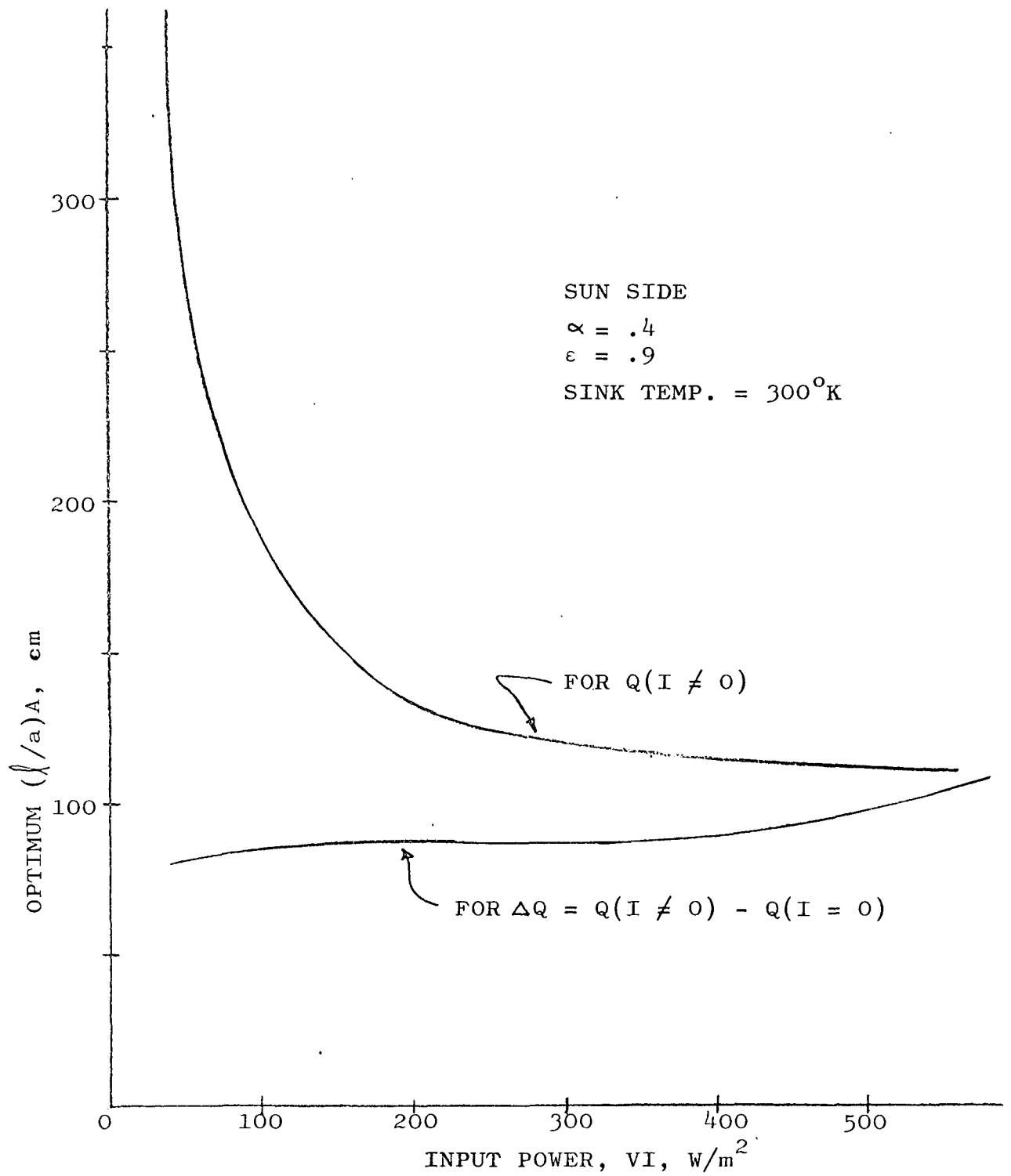
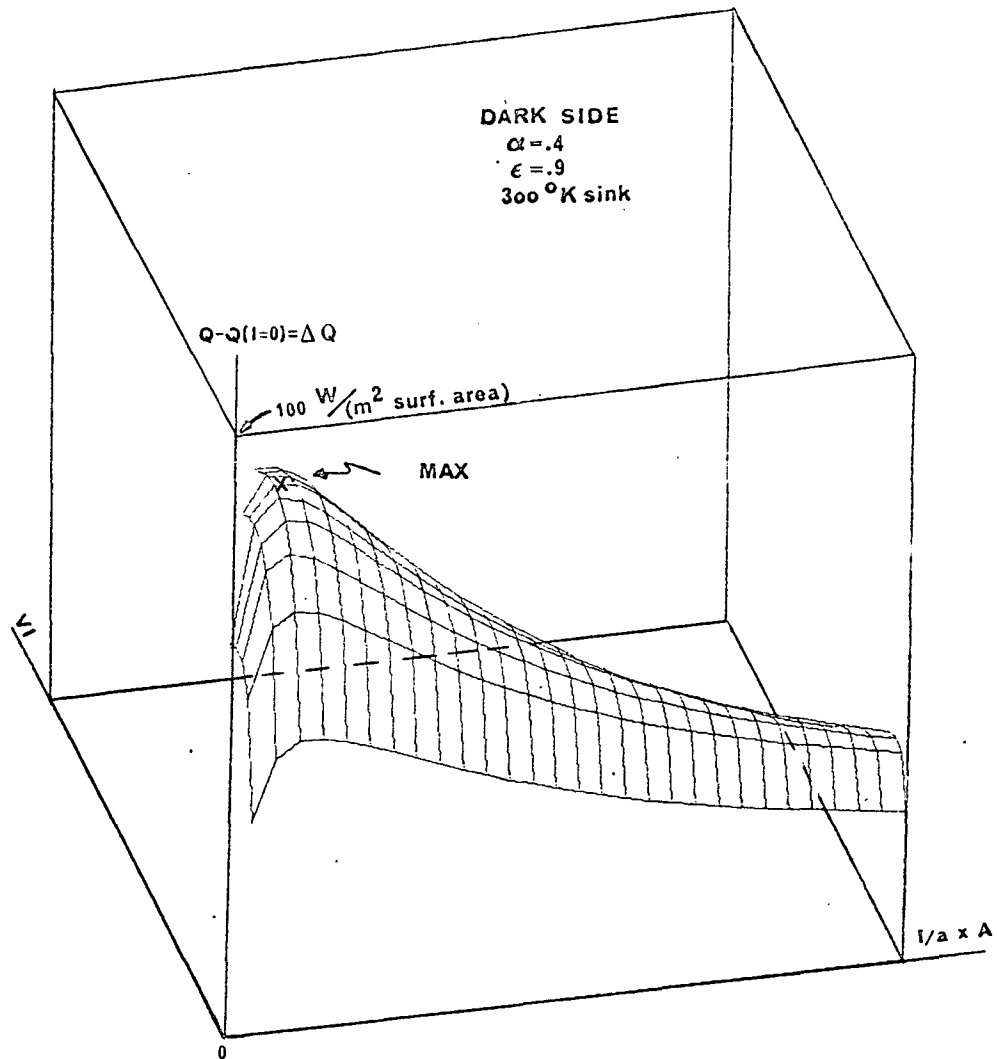
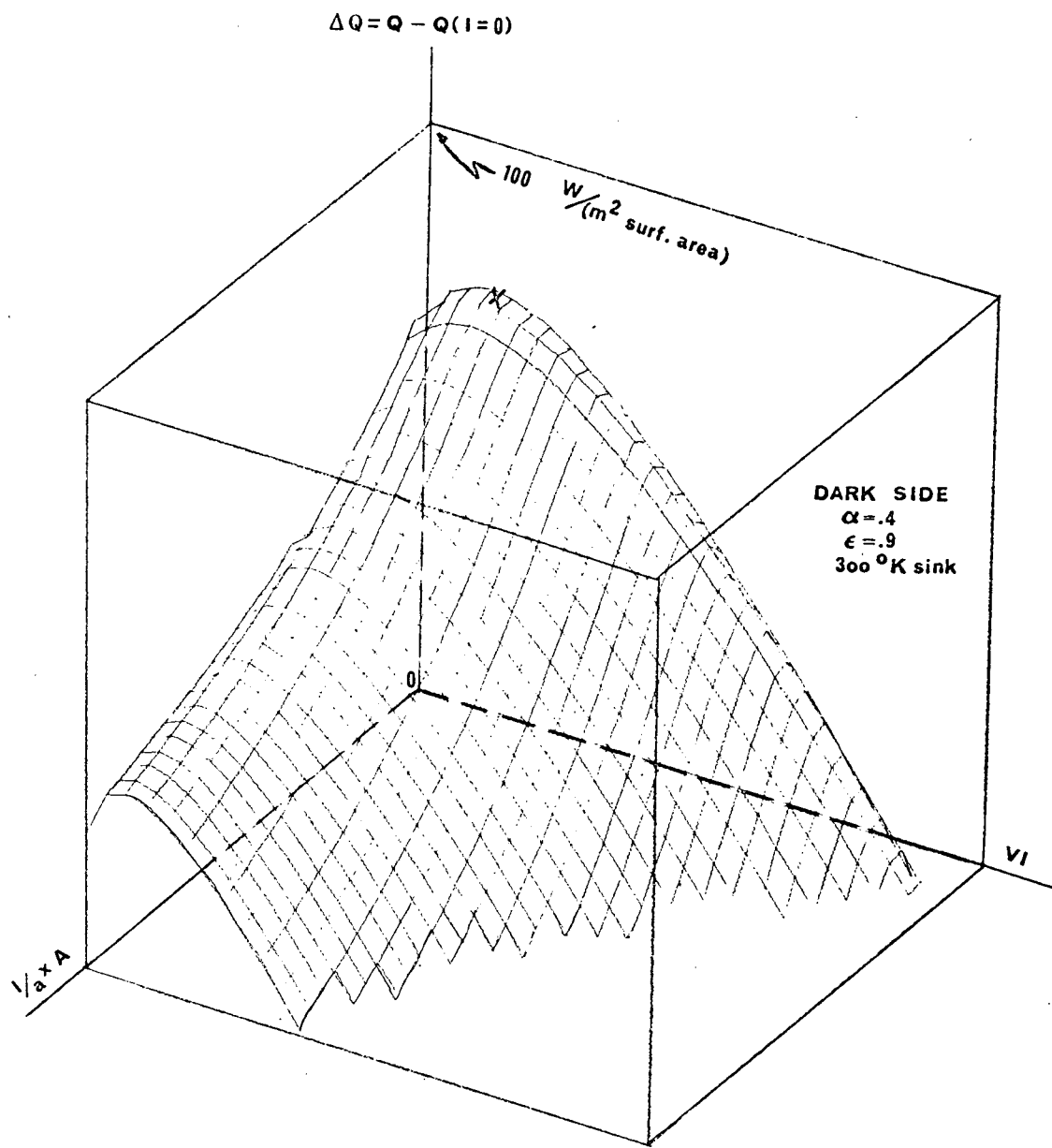


Fig. 9. Optimum $(l/a)A$ as a Function of Input Power for Q and ΔQ . Of importance if it is desired to operate at a lower V_I than optimum V_I (for maximum Q or ΔQ) to increase the COP.



(a)

Figure 10 (a). ΔQ for the Dark Side. Same scale as for Figure 8. Note that the line where the surface pierces the $(l/a)A - \Delta Q$ plane is where it enters the power generation region. Heat is out of the spacecraft for the octant shown. ΔQ at maximum is 80 W/m^2 . Optimum $(l/a)A$ is 65 cm. Optimum VI is 98 W/m^2 .



(b)

Figure 10 (b). Second view of 10 (a). Same scale.

$(\ell/a)A$ plane. There will also be optimum $(\ell/a)A$'s for the modes of heat pumped into the spacecraft and power generation, but the importance of operating at optimum $(\ell/a)A$ for heat pumped out of the spacecraft is evident.

The surfaces for COP are shown in Figures 11(a) and 11(b). They show the expected increase in COP with decreasing VI, and a maximum with respect to $(\ell/a)A$, occurring at about an $(\ell/a)A$ of 80 cm. The COP for the dark side rises faster than that for the sun side, as was seen from Figure 6 and 7.

The COP weighted with ΔQ , i.e., $COP \times \Delta Q$, is shown in Figures 12(a), 12(b) and 12(c). They have the same general characteristics as the COP. It is seen that COP increases faster than the heat pumping capability decreases, at least down to an input power of 0.04 W/couple, where the data ends. The numbers associated with two points on the surfaces are given in the captions for purposes of comparison.

The fin temperatures are displayed in Figures 13(a), 13(b), and 13(c) for the sun side, and Figure 13(d) for the dark side. Figures 13(b) and 13(c) are expanded scale views of 13(a). It can be seen that there is a rapid increase in radiator temperature as $(\ell/a)A$ increases from zero, and a more gradual rise as VI increases. The temperatures at the points at which maximum ΔQ is being pumped are marked with crosses.

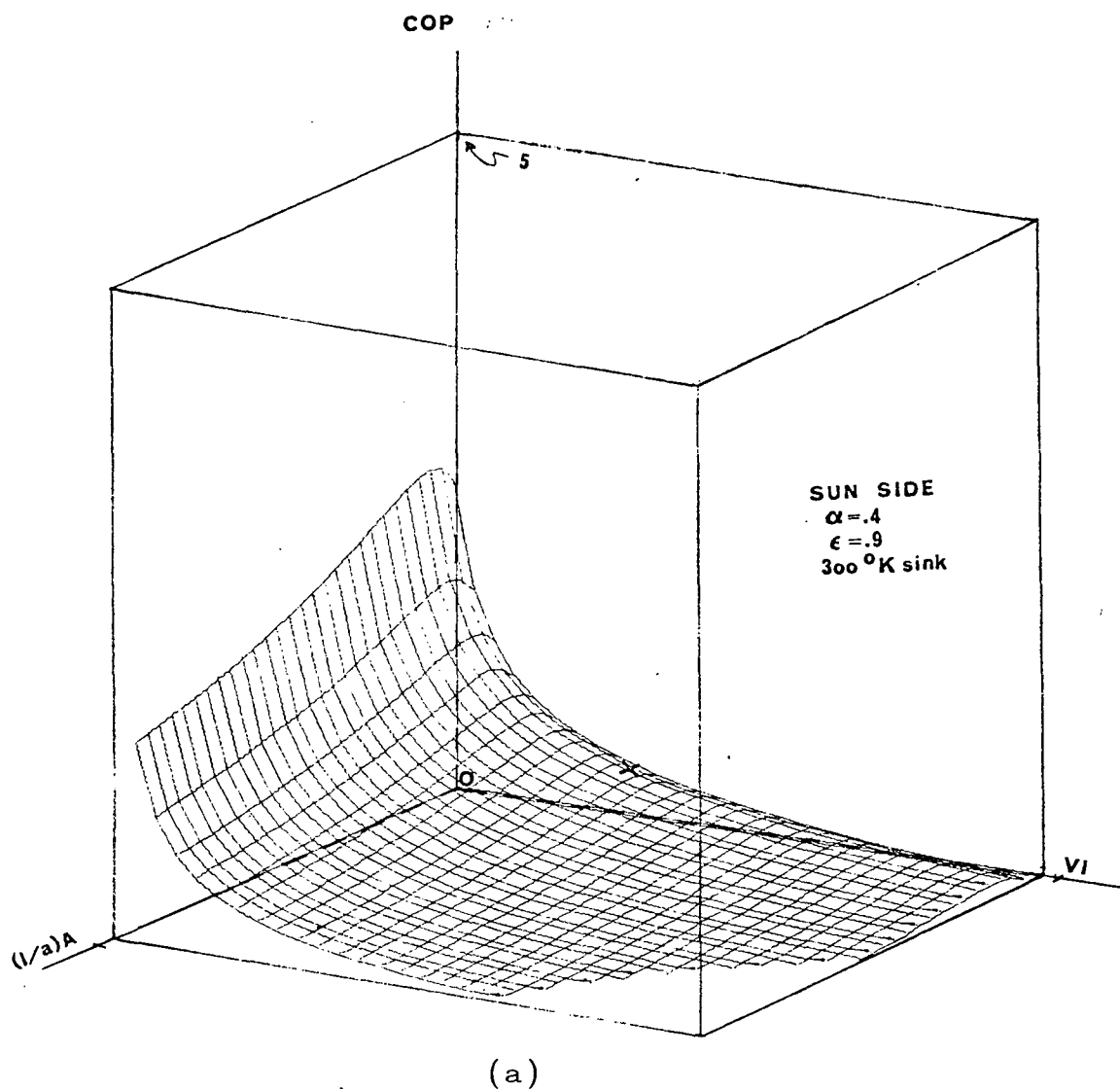
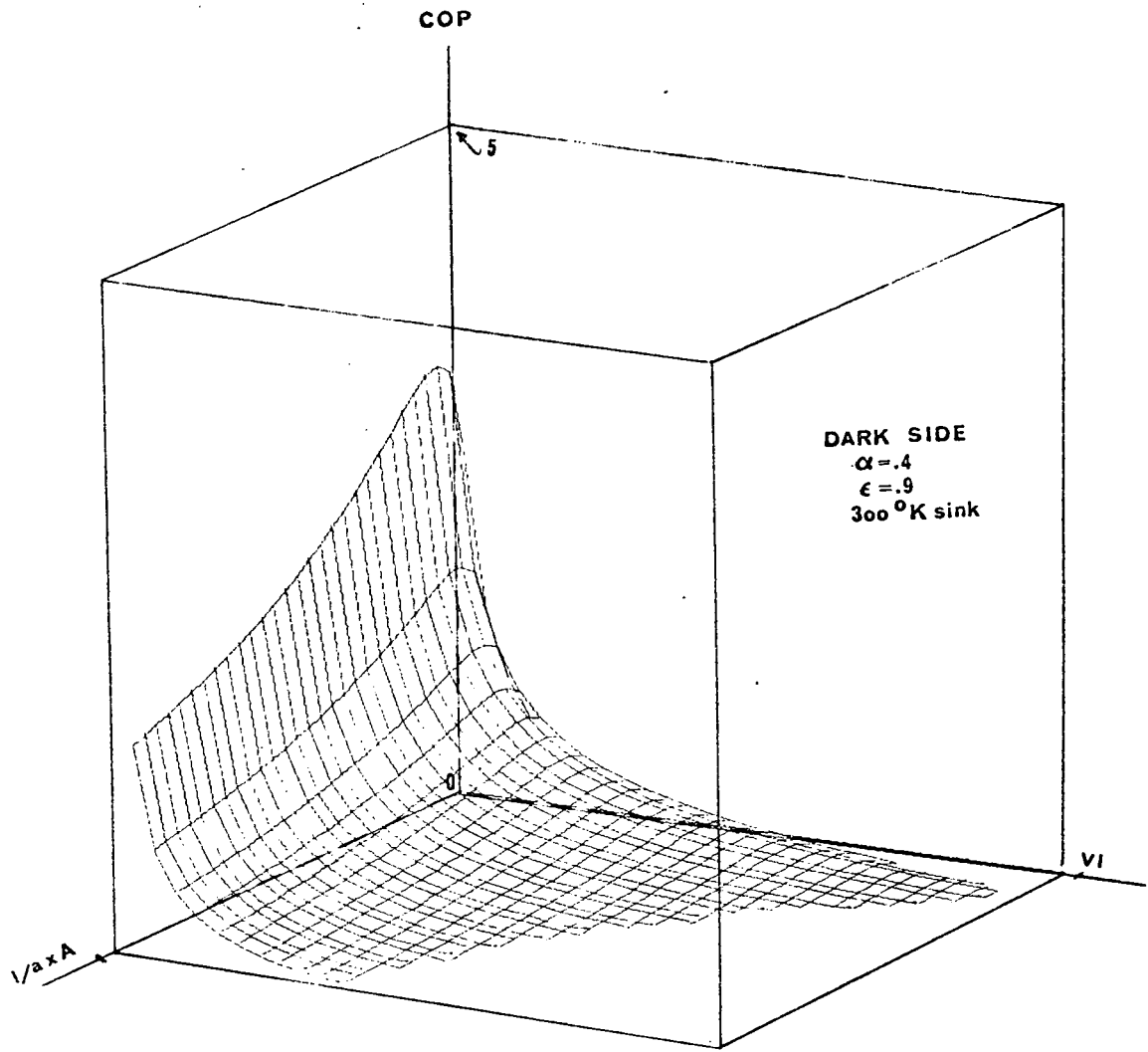


Figure 11 (a). Three-Dimensional View of Sun Side COP. Shows maximum with respect to $(l/a)A$ but not VI. $(l/a)A$ and VI scales are same as for Figure 8. COP at maximum ΔQ is marked with an x, and is about .5.



(b)

Figure 11 (b). Dark Side COP at Maximum ΔQ . Same scale as Figure 8. COP at maximum ΔQ is marked with an x, and is about .82.

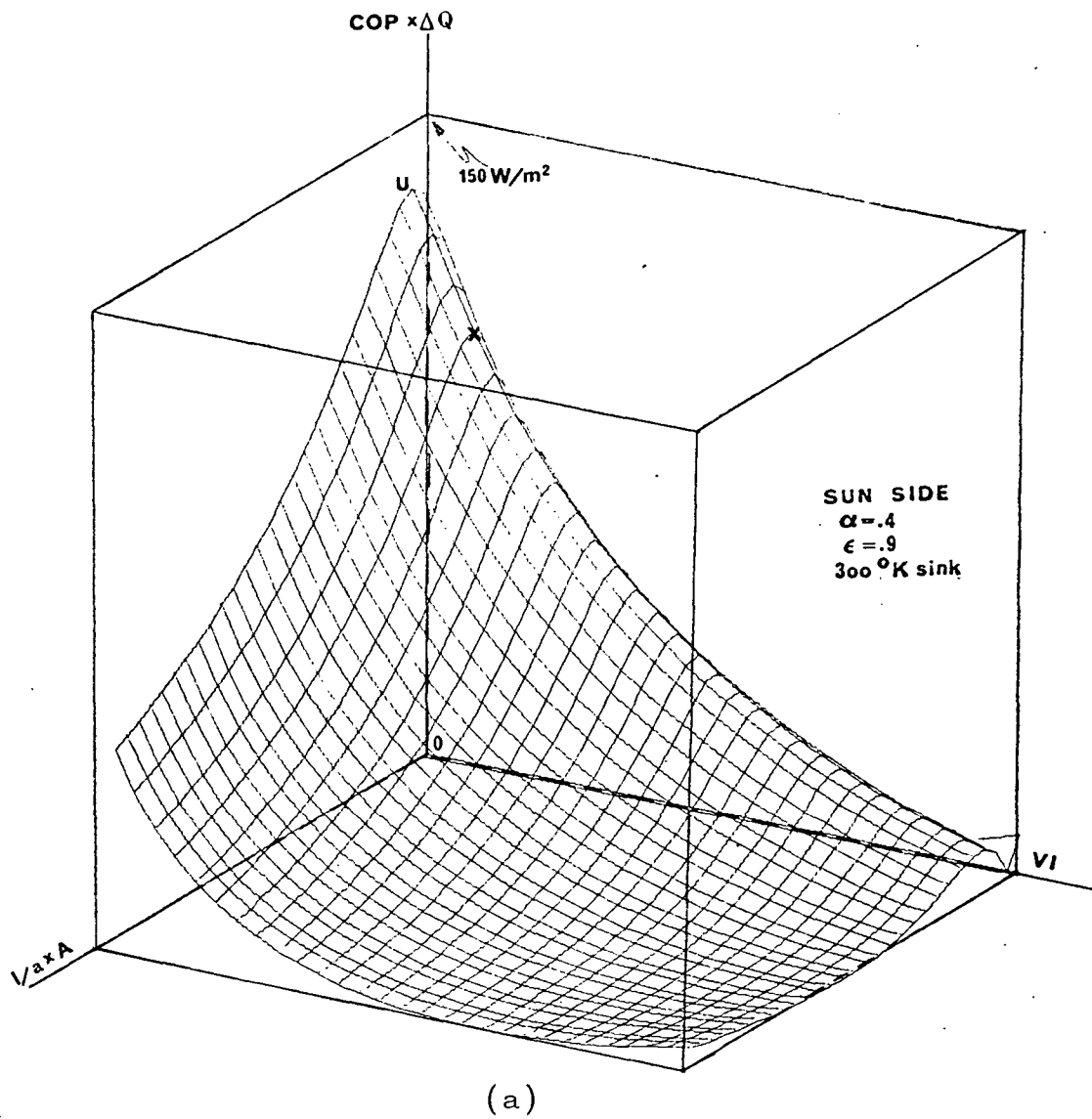


Figure 12 (a). Three-Dimensional View of COP Weighted With Respect to ΔQ , $COP \times \Delta Q$ for Sun Side. Displays maximum with respect to $(l/a)A$, but not with respect to VI. Same base plane scales as Figure 8. At point X, $\Delta Q=93 \text{ W/m}^2$ and $COP=1.16$. At point U, $\Delta Q=53 \text{ W/m}^2$ and $COP=2.6$.

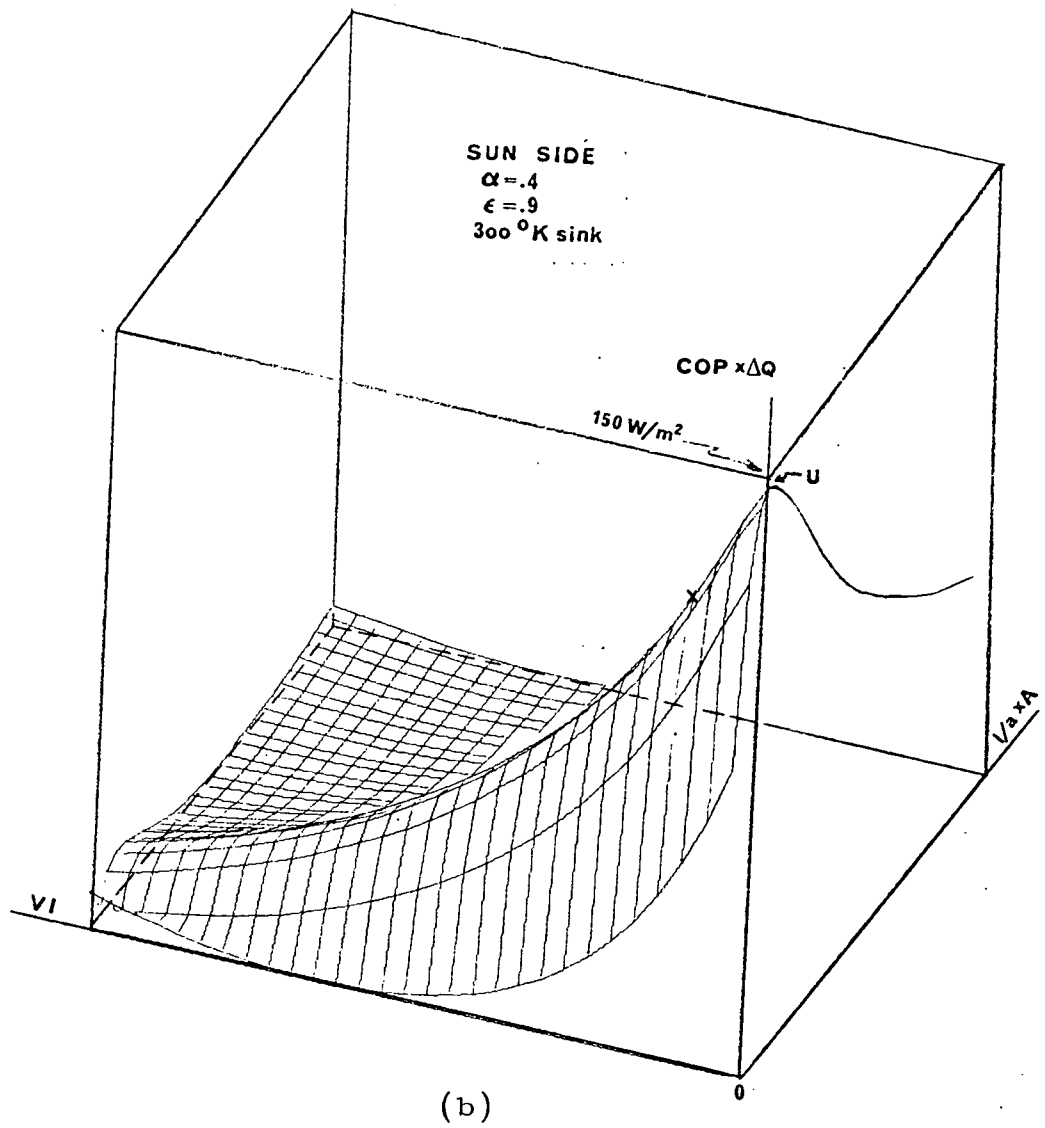
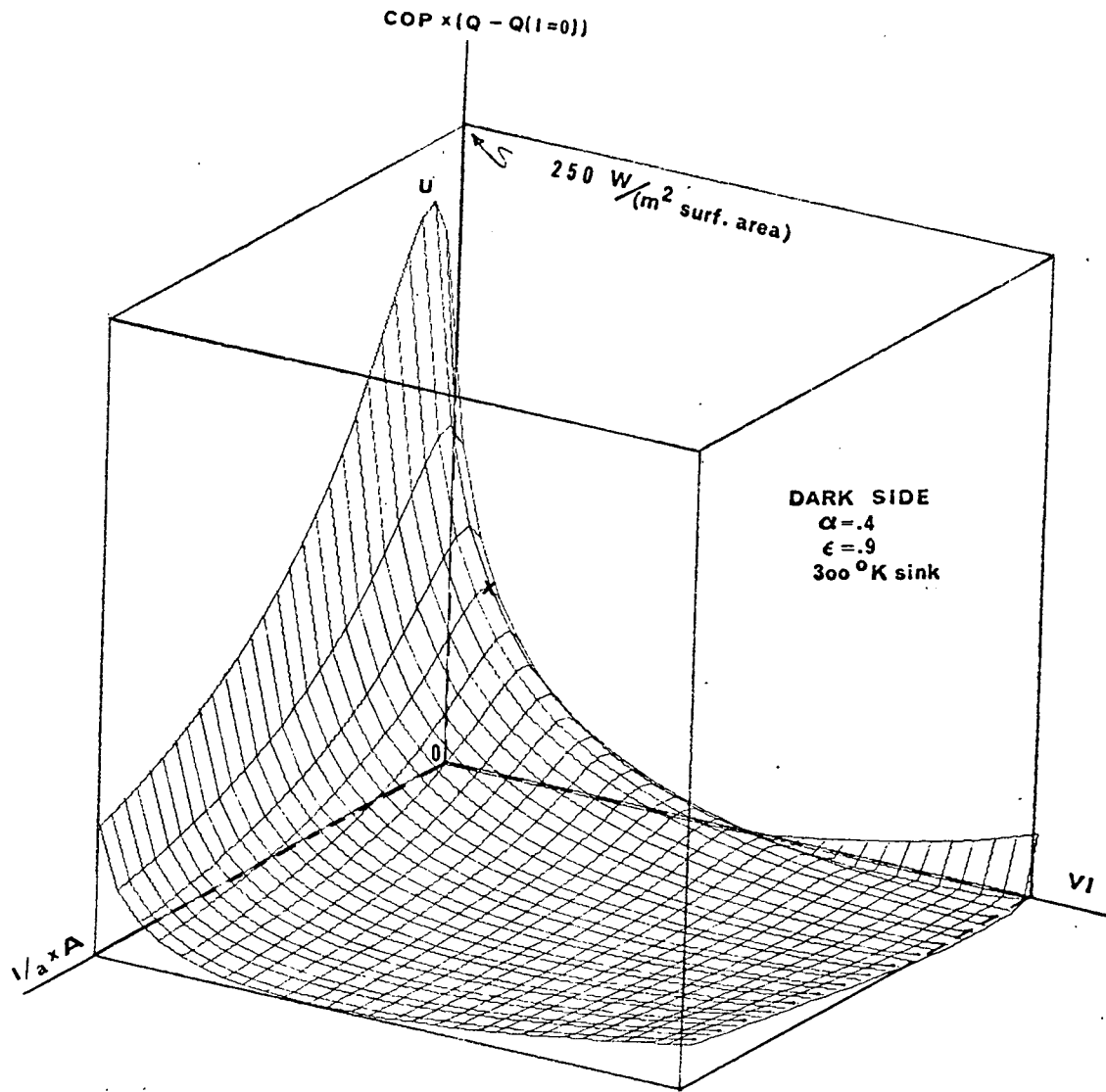
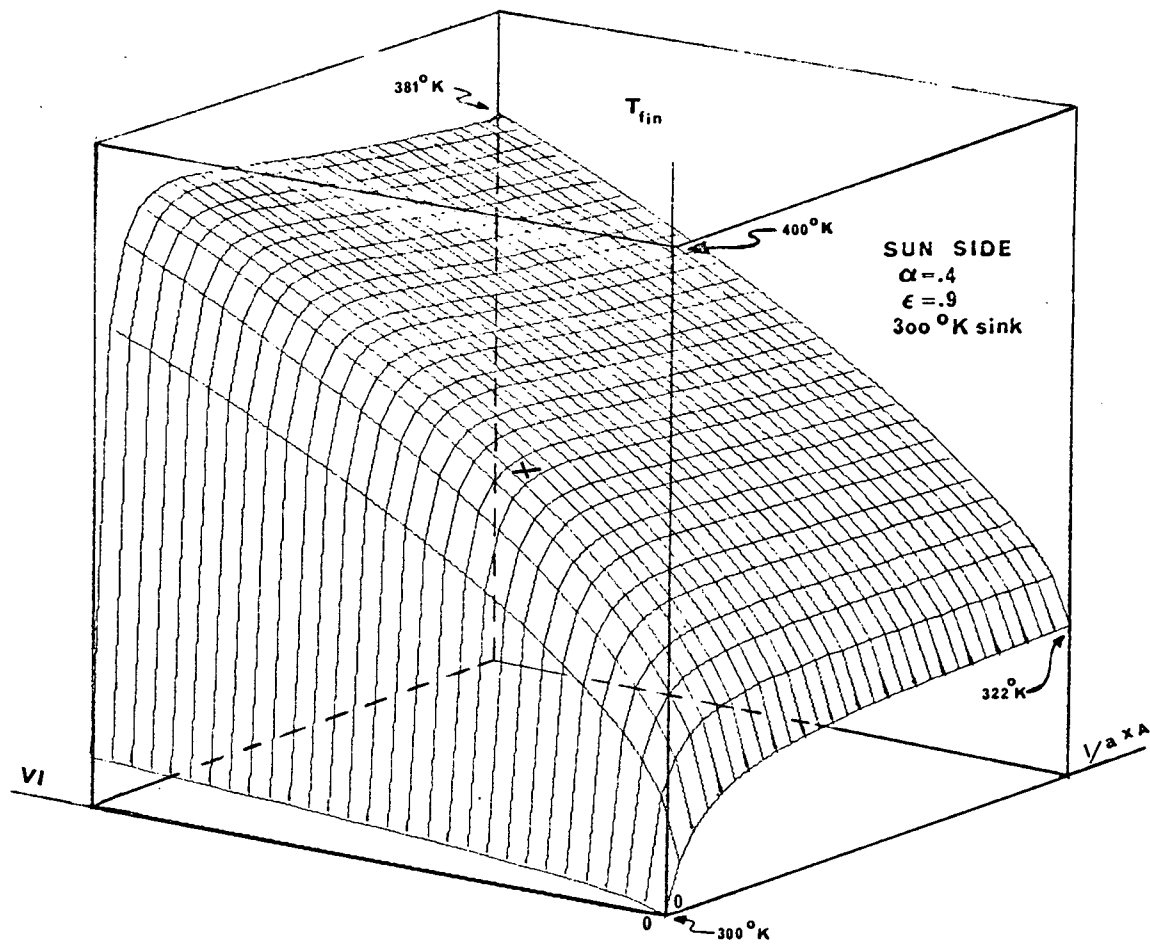


Figure 12 (b). Second View of Figure 12 (a). Same scale.



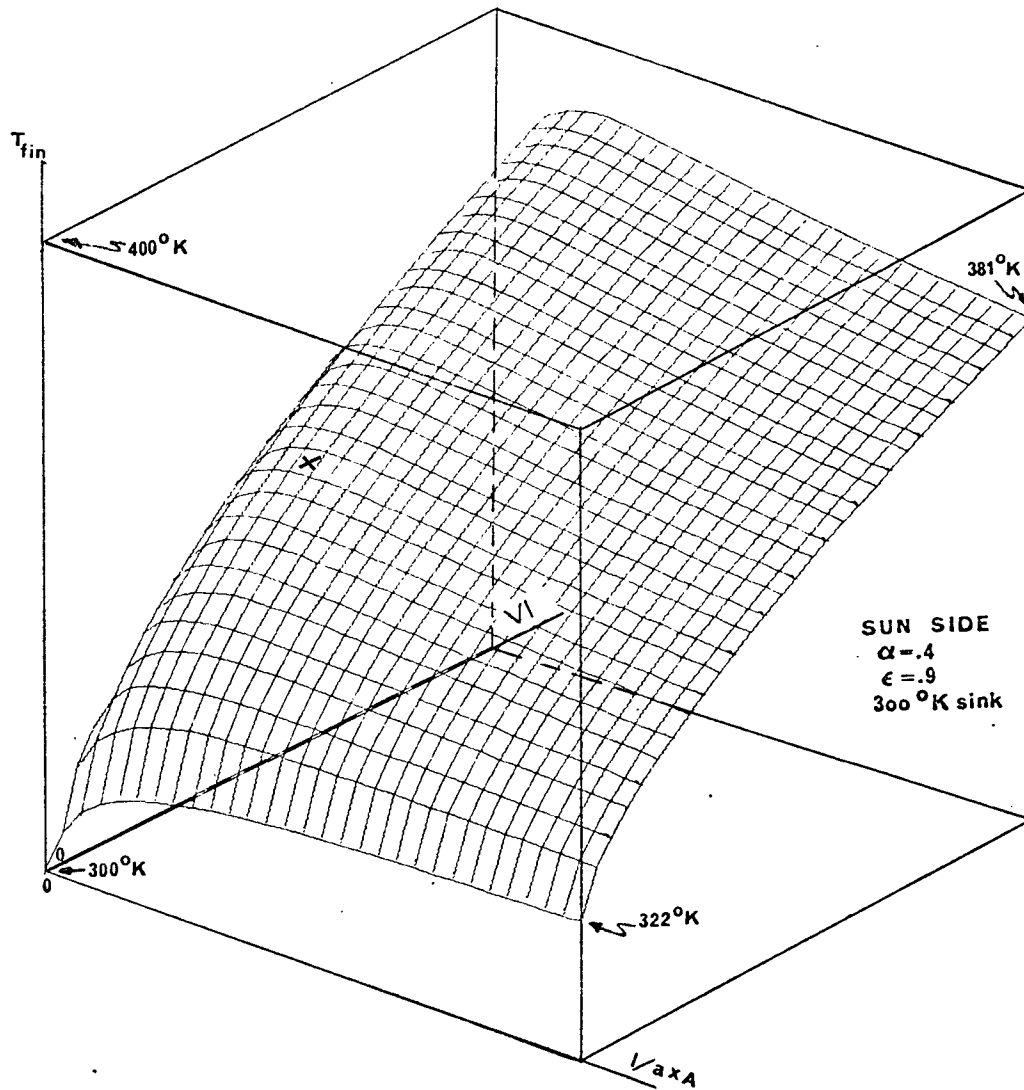
(c)

Figure 12 (c).. Dark Side COP x ΔQ . Same base plane scales as for Figure 12 (a). At point X, $\Delta Q = 80 \text{ W/m}^2$ and COP=1. At point U, $\Delta Q = 67 \text{ W/m}^2$ and COP=3.35.



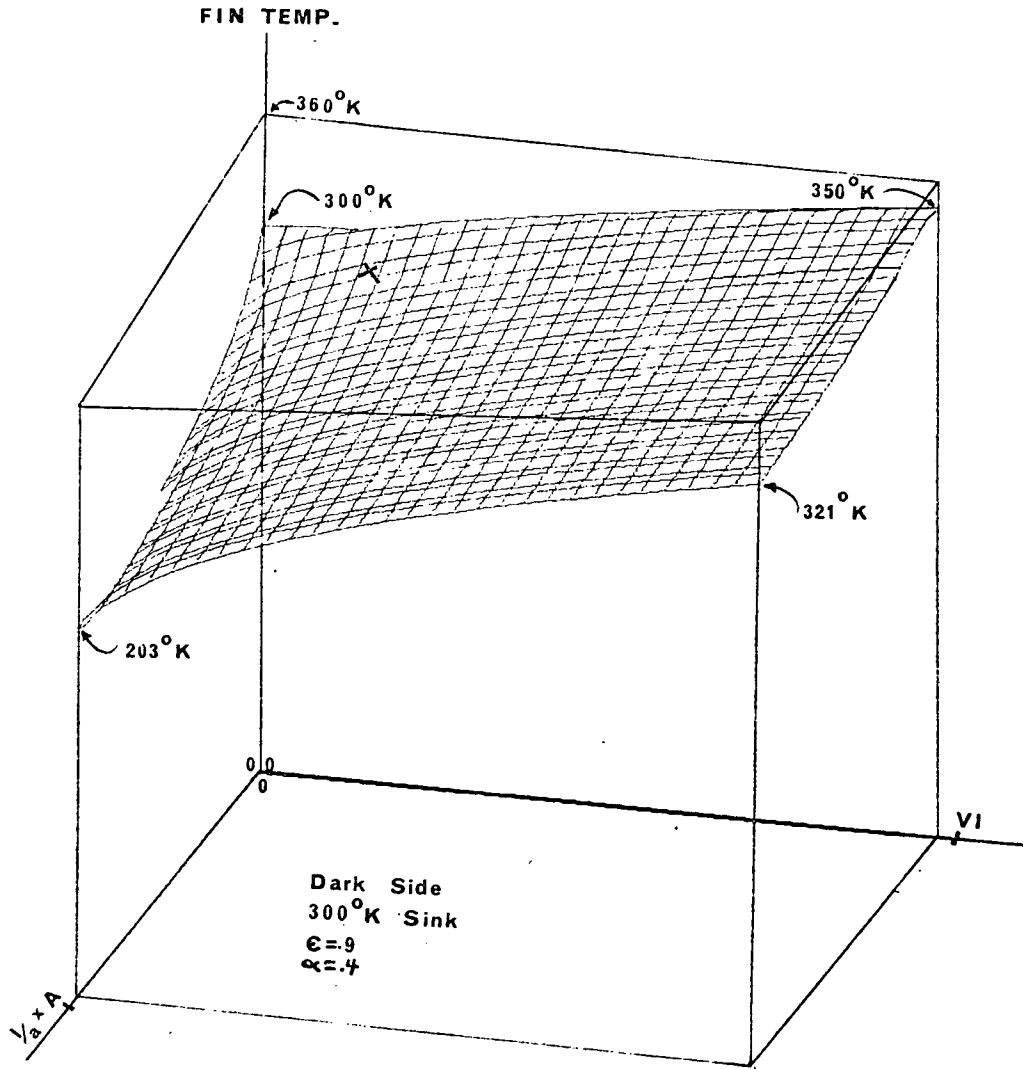
(b)

Figure 13 (b). Expanded Scale View of Figure 13 (a).



(c)

Figure 13 (c). Another View of Figure 13 (b).



(d)

Figure 13 (d). Dark Side Fin Temperature. Same scale as for Figure 13 (a). T_{fin} at maximum ΔQ is 296°K .

Optimization With Respect To ΔQ

Results of the optimization calculations are presented in Figures 14 through 18. They are the maximum heat that can be transferred out of the heat sink for a given heat sink temperature, α , ϵ , and γ . The abscissas of all the figures are the absorbed incident radiation = $\alpha \phi \sin(\gamma)$. The maximum value is for $\alpha = .5$ and $\gamma = 90^\circ$. Any combination of α and γ which produces an absorbed heat within this range is included. Four families of curves are given for values of $\epsilon = .9, .7, .6$ and $.5$. For each of these there are seven heat sink temperatures, from 330°K to 270°K . As Figure 14 shows, the heat that can be pumped out decreases with sink temperature because the material figure of merit decreases with temperature and because of the T^4 law. The decrease with absorbed radiation is for the same reasons and the decrease with decreasing ϵ is obvious.

The fin temperature, T_S , shown in Figure 15, decreases with the heat sink temperature because for fixed absorbed radiation the ΔT is very approximately a constant. Hence, the fin temperature tends to follow the sink temperature. It increases to partially compensate for decreasing ϵ . It decreases with decreasing absorbed incident radiation because there is less heat to radiate.

The equation at the fin node for the heat pumped is of the form.

$$\Delta Q = -\epsilon A \left[T_S^4 - {}^0T_S^4 \right] + VI,$$

where T_S is for $I \neq 0$ and 0T_S is at $I=0$. As the optimum T_S decreases with decreasing absorbed incident radiation or with decreasing sink temperature, the input power for maximum ΔQ would be expected to go down, as we see it does from Figure 16. Also from Figures 6 and 7, it can be seen that the power generation region moves into the quadrant for heat flow out of the spacecraft, which moves the optimum VI down in magnitude. However, the optimum VI decreases with

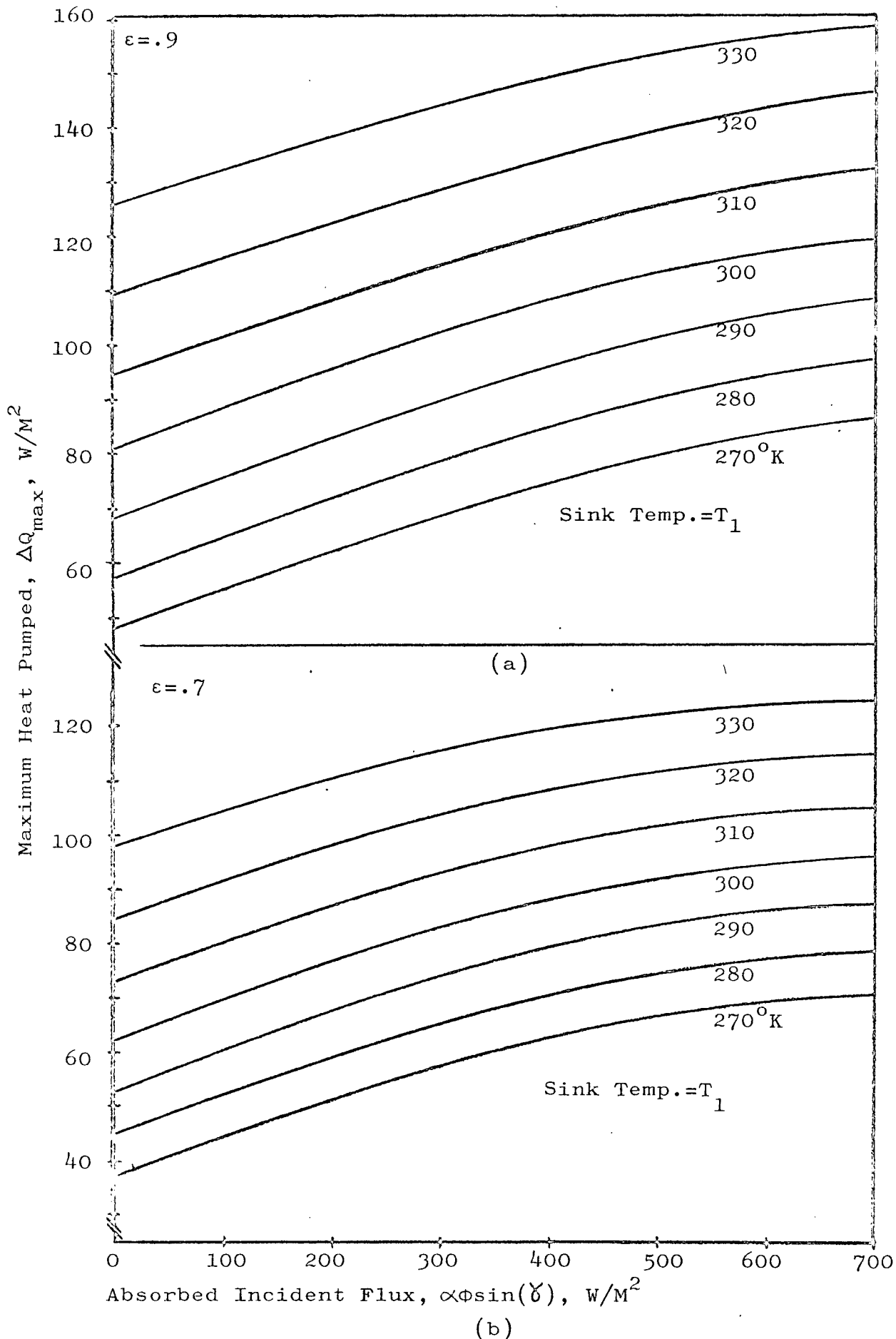


Figure 14. Maximum ΔQ that can be pumped out of spacecraft. $A=20cm^2$
 Every combination of α and γ is represented up to $\alpha=.5$, $\gamma=90^\circ$

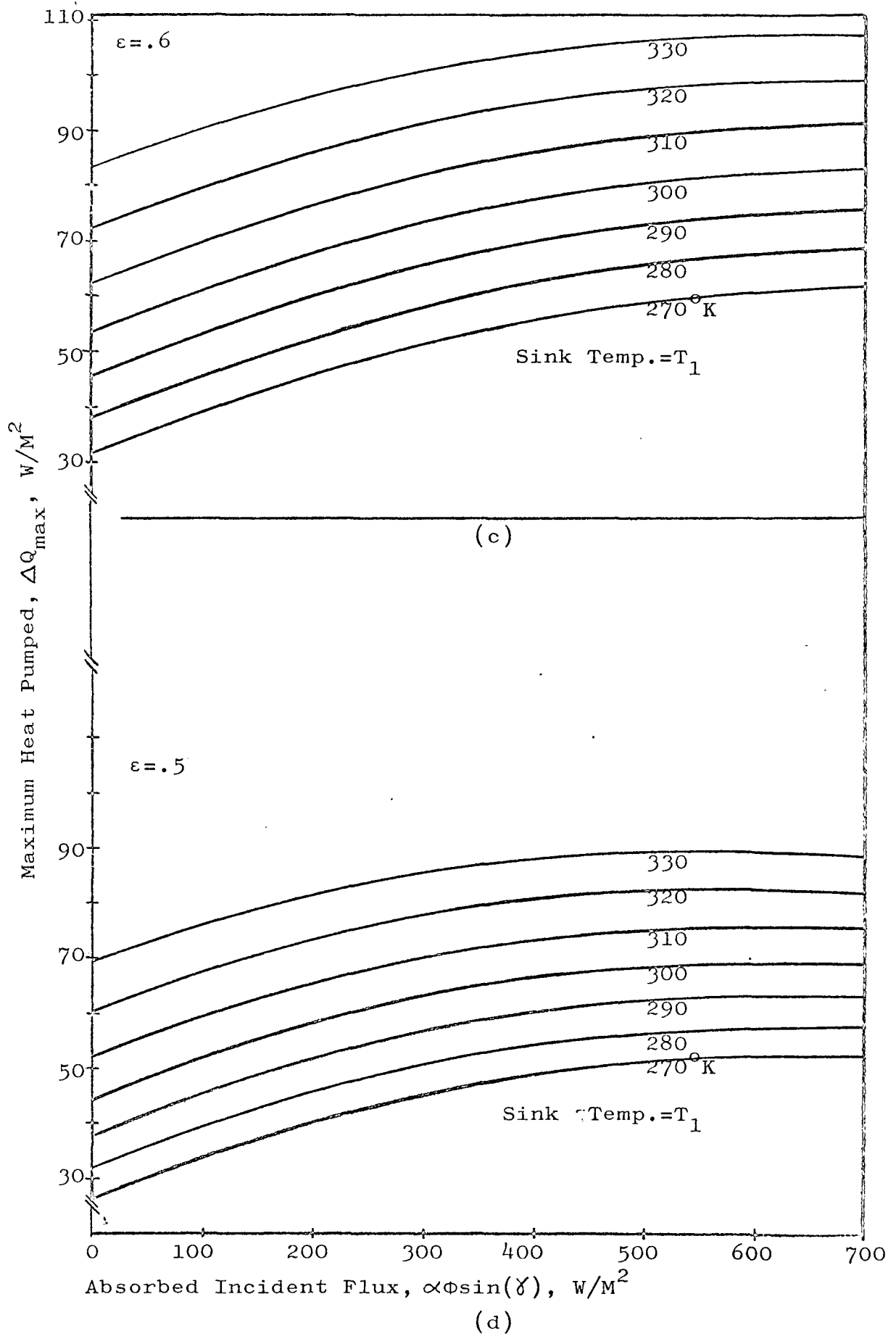


Figure 14. (c) $\epsilon = .6$, (d) $\epsilon = .5$

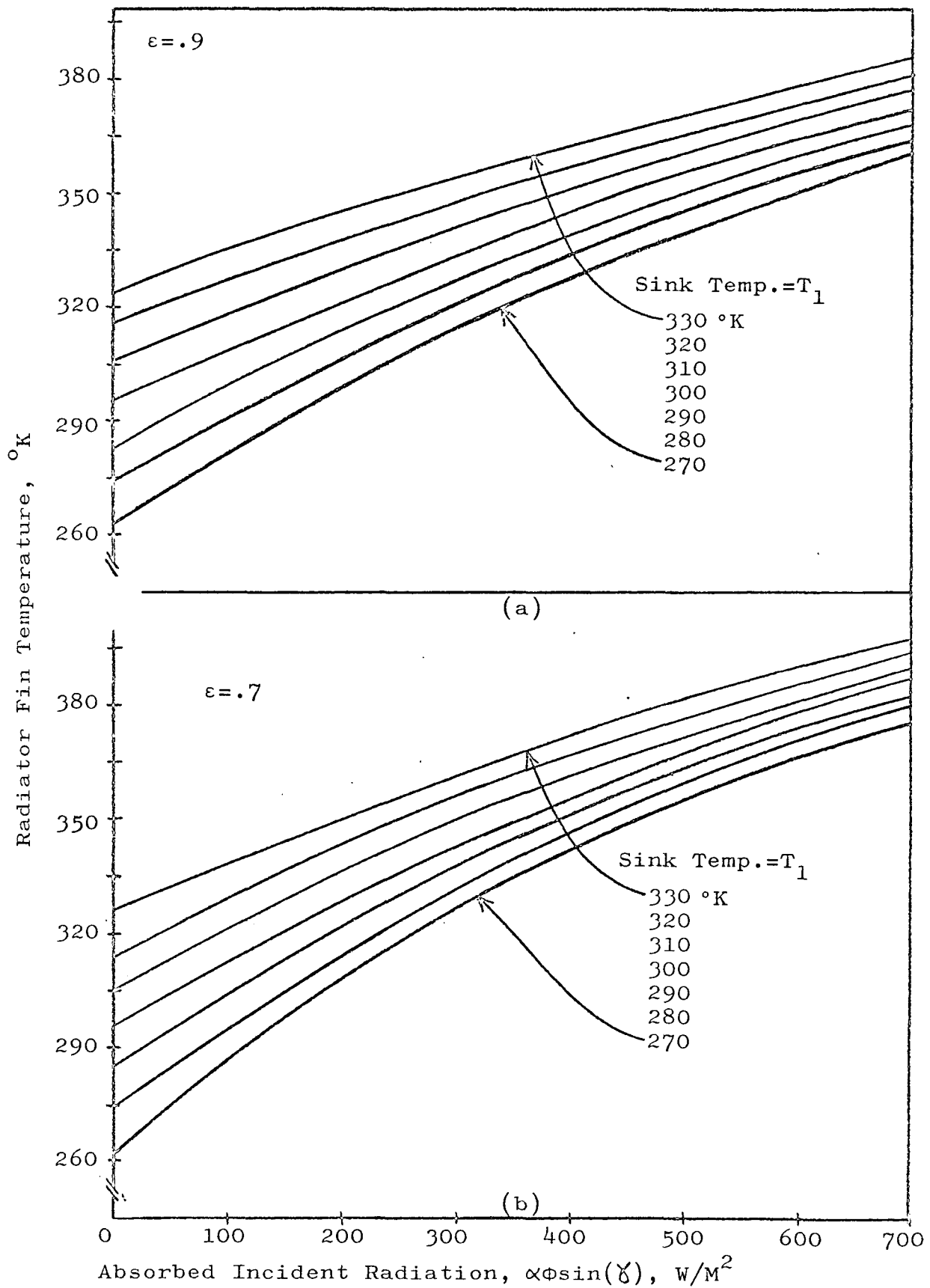


Figure 15. Radiator Fin Temperature at Maximum ΔQ . $A=20\text{cm}^2$. Every combination of α and γ is represented up to $\alpha=.5$, $\gamma=90^\circ$. $\Phi=1.4\text{KW/M}^2$
 (a) $\epsilon=.9$, (b) $\epsilon=.7$

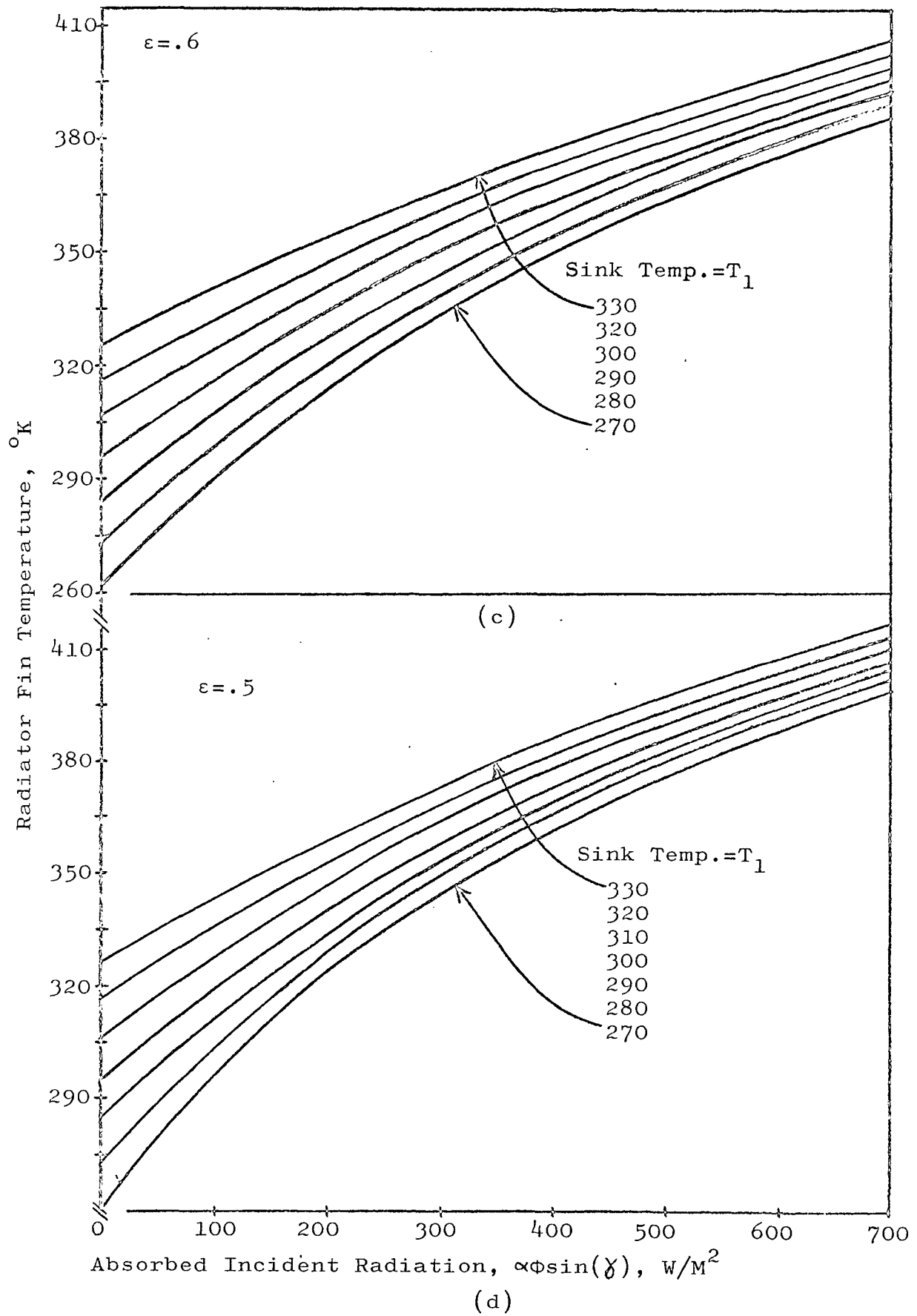


Figure 15. (c) $\epsilon = .6$, (d) $\epsilon = .5$

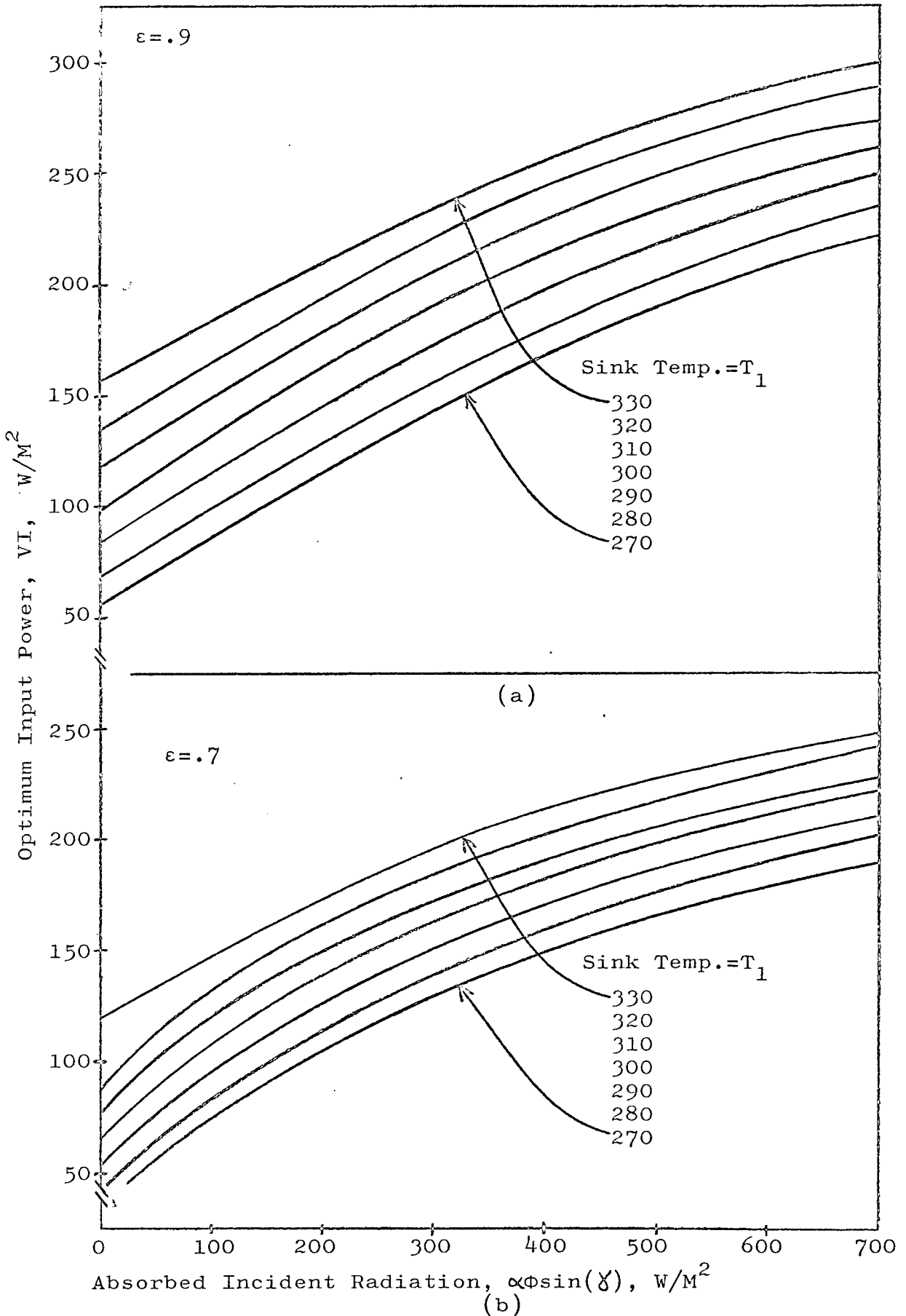


Figure 16. Optimum VI for Maximum ΔQ . Multiply VI scale by 2×10^{-3} $M^2/couple$ to get VI in Watts/couple. $A=20cm^2$. Every combination of α and γ is represented up to $\alpha=.5$, $\gamma=90^\circ$. $\phi=1.4KW/M^2$. (a) $\epsilon=.9$
 (b) $\epsilon=.7$

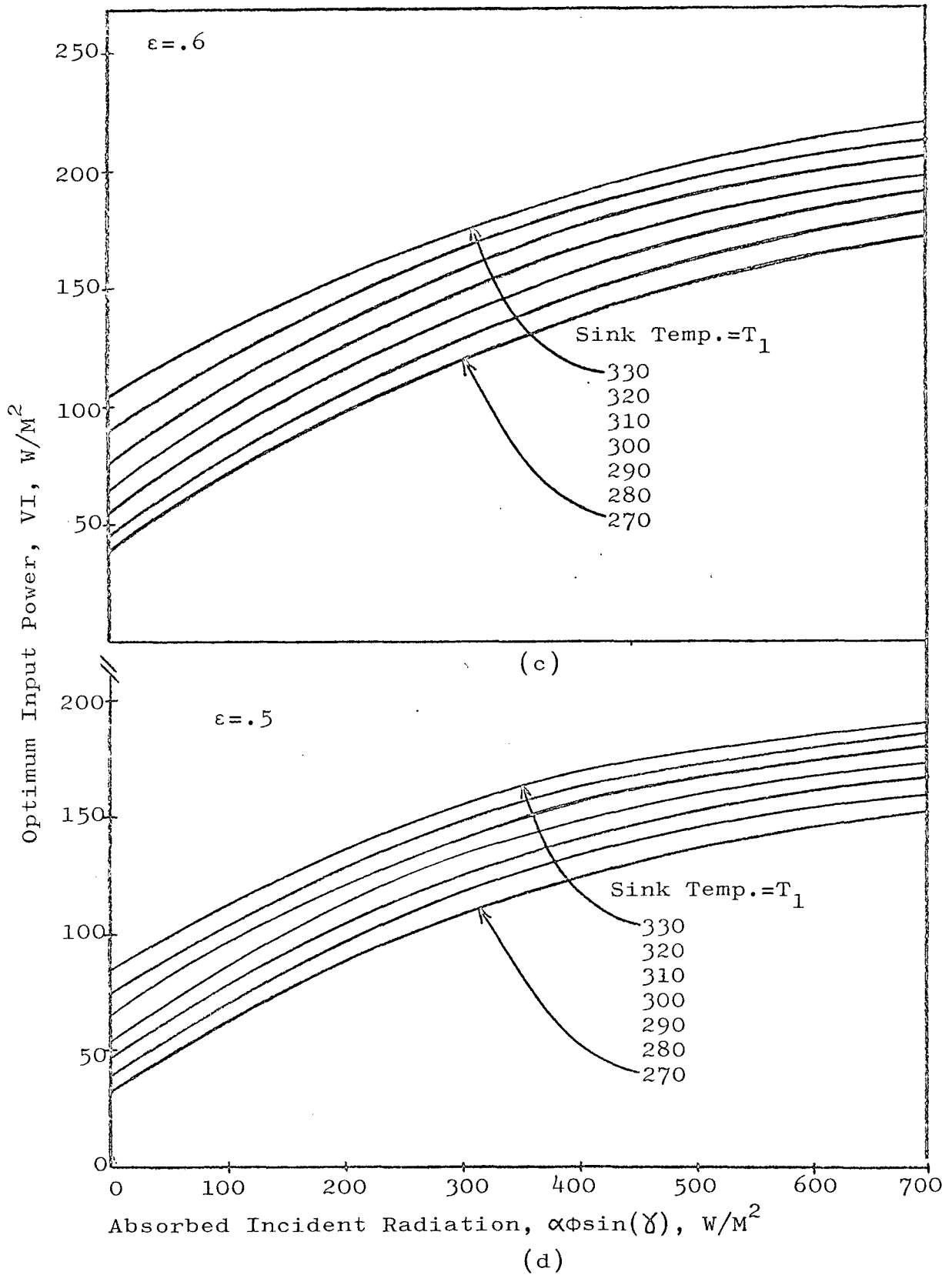


Figure 16. (c) $\epsilon = 0.6$, (d) $\epsilon = 0.5$

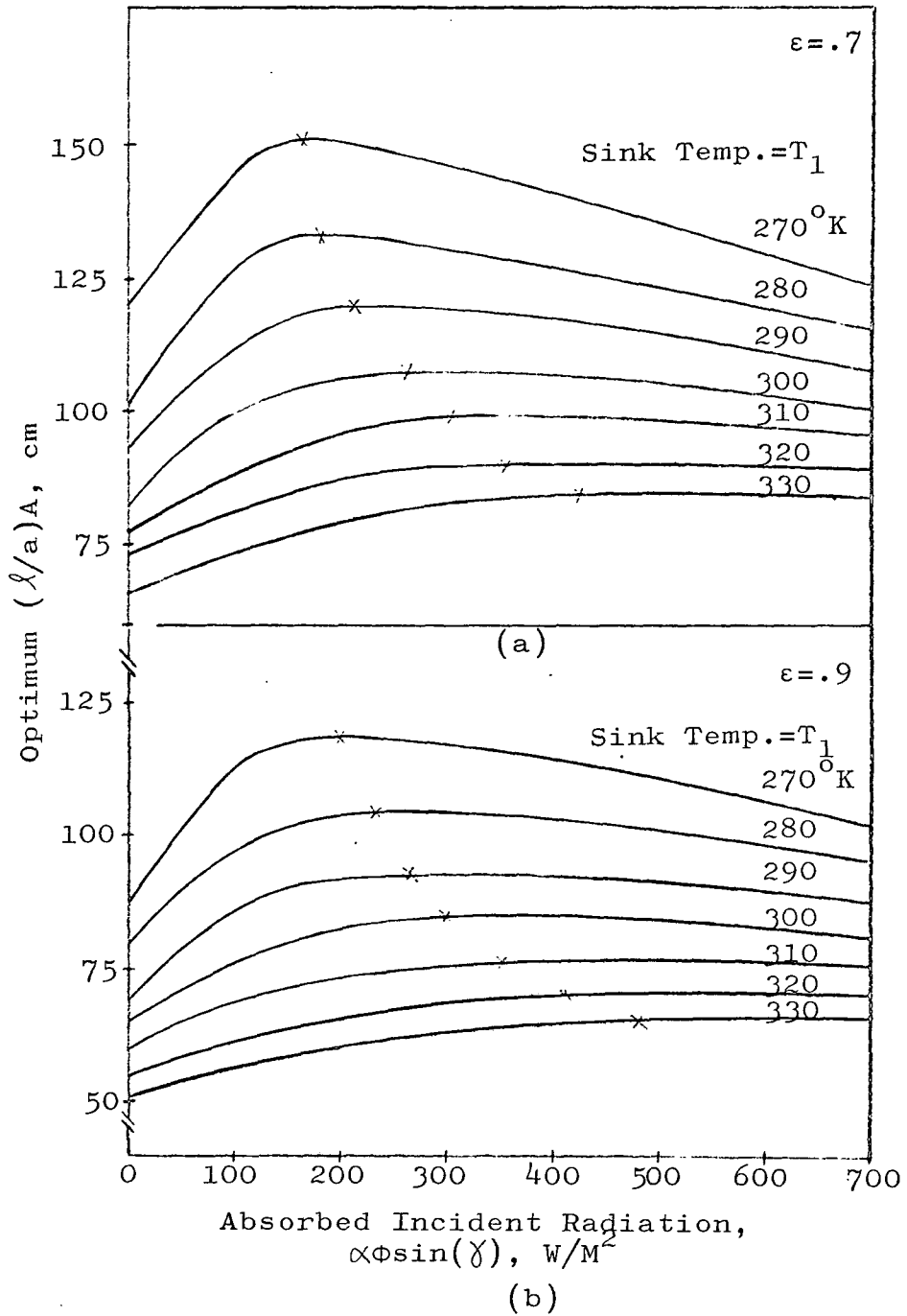


Figure 17. Optimum $(l/a)A$ at Maximum ΔQ . The parameter is sink temperature. $A=20cm^2$. Every combination of α and γ is represented up to $\alpha=.5$, $\gamma=90^\circ$. $\phi=1.4KW/M^2$. (a) $\epsilon=.7$, (b) $\epsilon=.9$

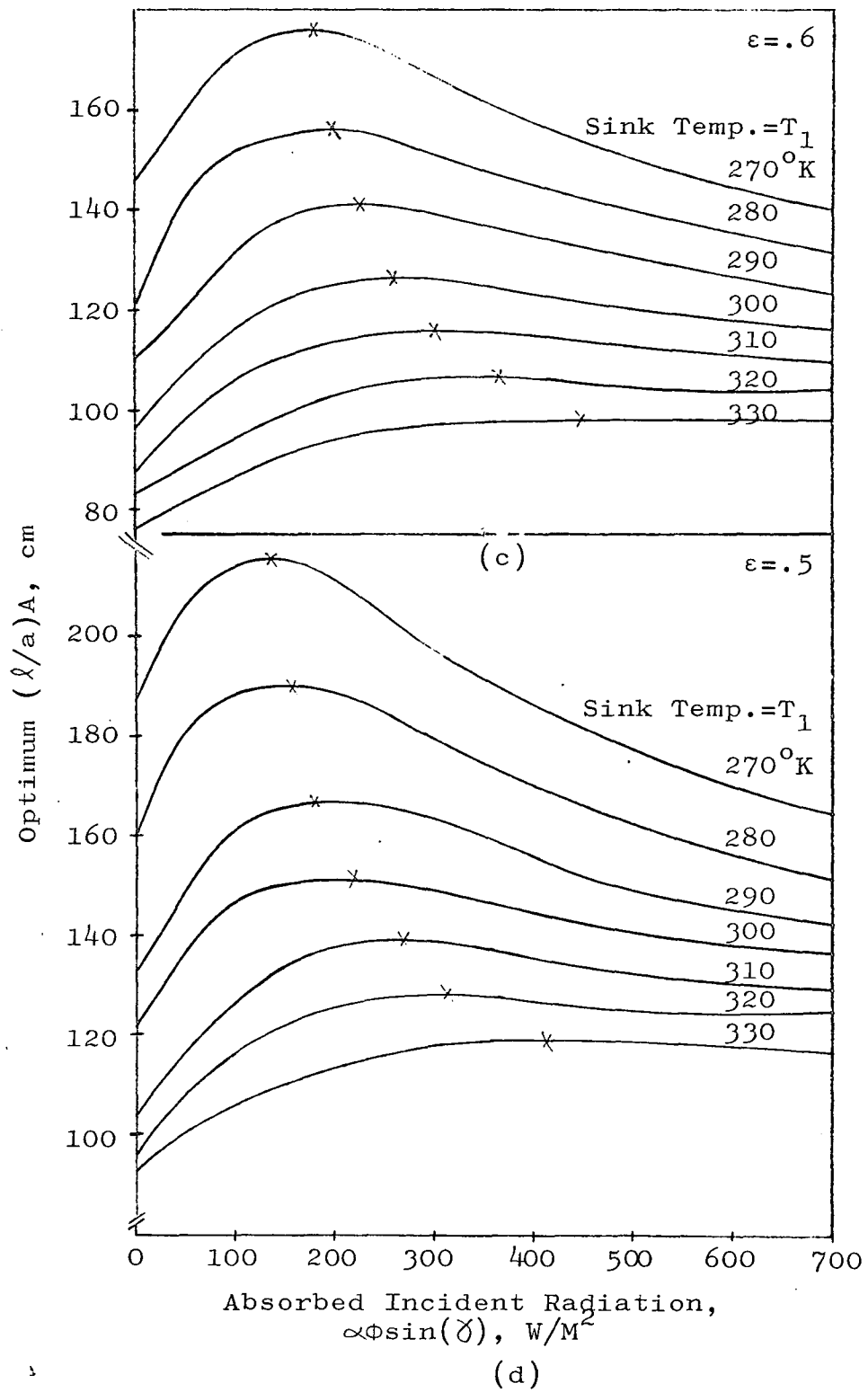


Figure 17. (c) $\epsilon = .6$, (d) $\epsilon = .5$

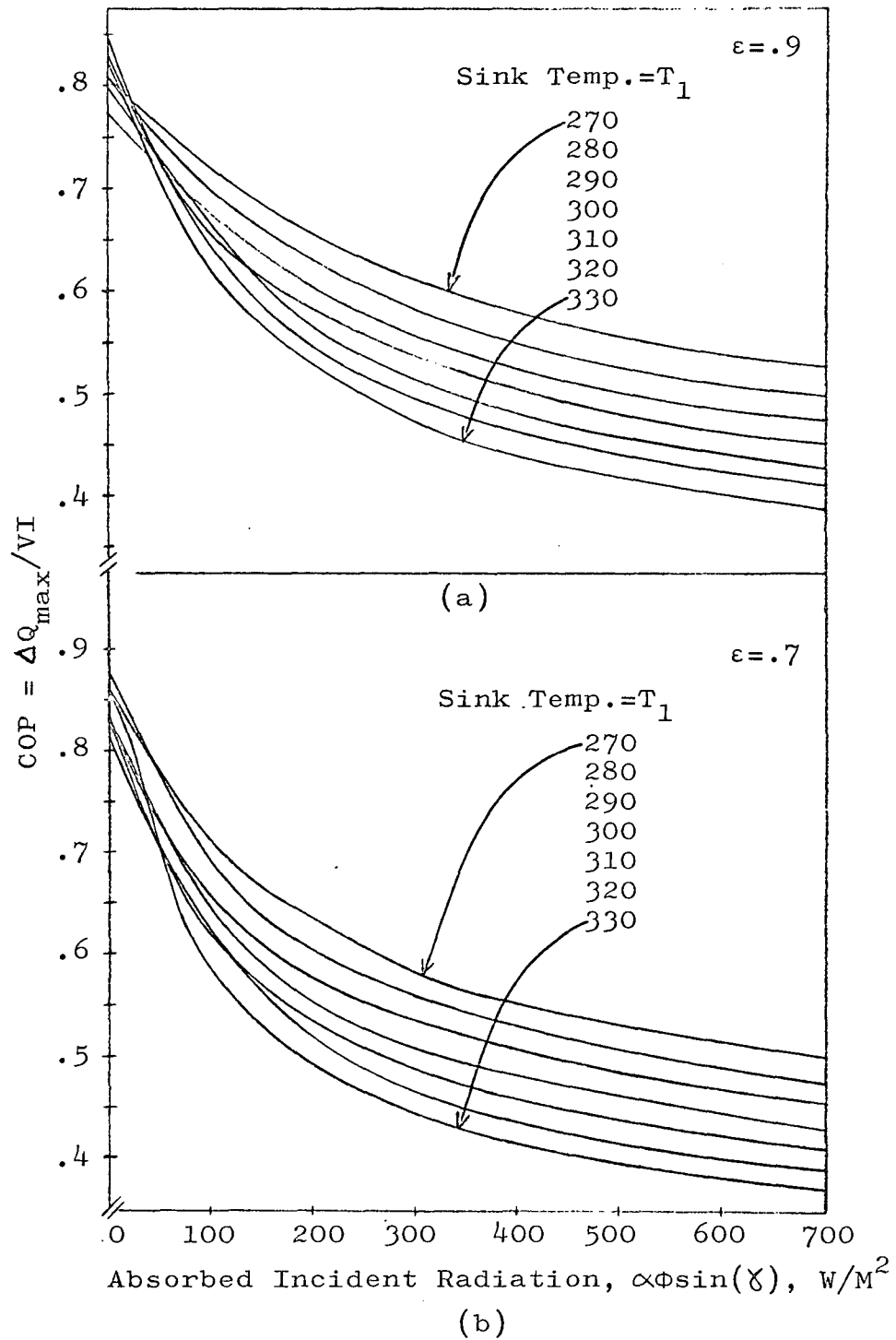


Figure 18. COP at Maximum ΔQ . The parameter is sink temperature. $A=20cm^2$. Every combination of α and γ is represented up to $\alpha=.5$, $\gamma=90^\circ$. $\Phi=1.4KW/M^2$. (a) $\epsilon=.9$, (b) $\epsilon=.7$

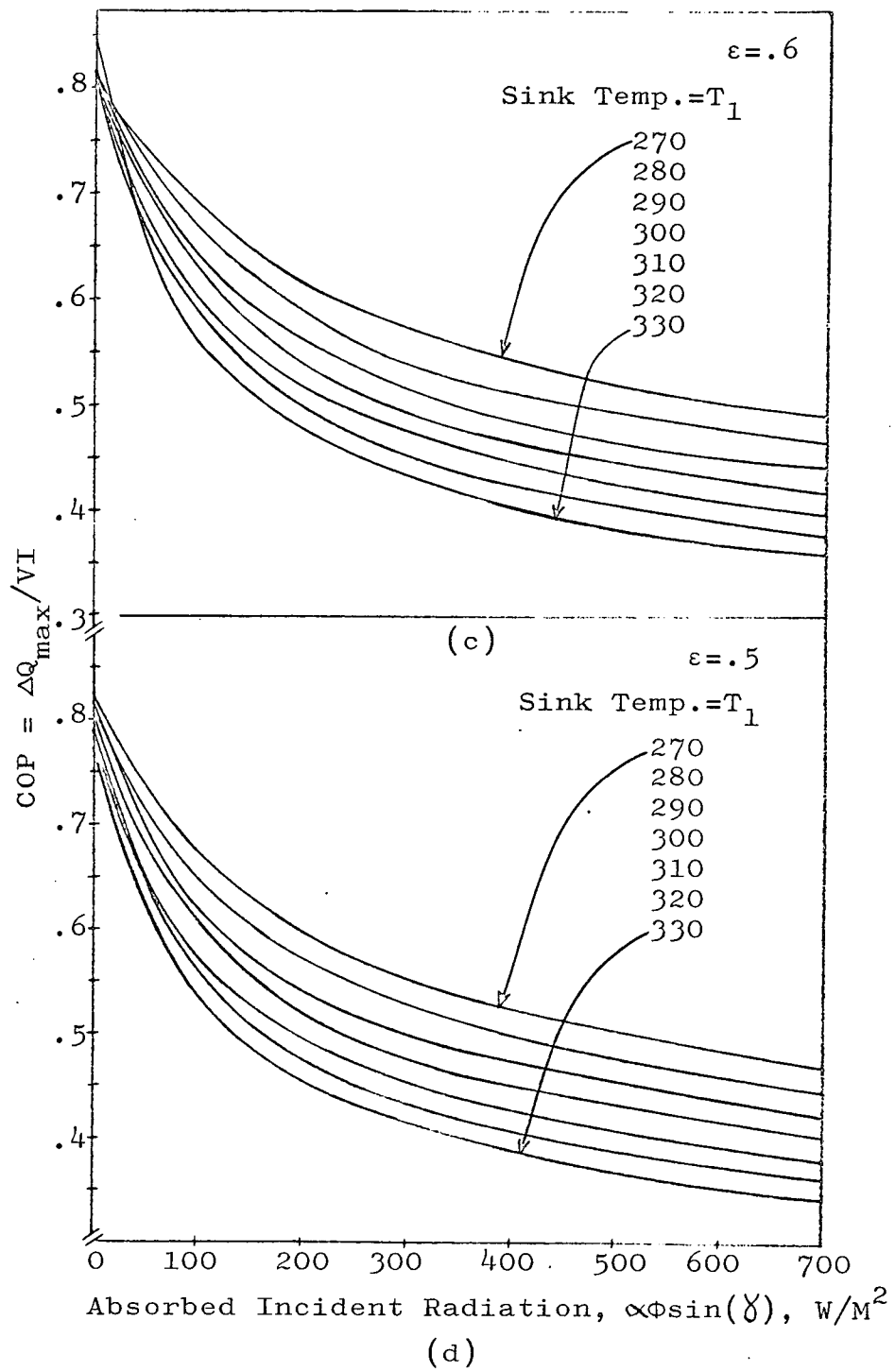


Figure 18. (c) $\epsilon = .6$, (d) $\epsilon = .5$

decreasing ϵ , while T_S increases. This is because the T^4 law does not quite make up for the decrease in ϵ , and the Joule heat and the thermal conductivity begin to dominate at lower VI's, moving the optimum VI to lower values.

The behavior of the optimum $(l/a)A$ is more complex than that of the other parameters because it depends more on interaction between them. As shown in Figure 17, it increases with decreasing sink temperature because as the resistivity decreases, the optimum VI decreases. Also, the Joule heat becomes less important while the thermal conductivity becomes more important. Further, the radiator temperature is increased which improves heat rejection. The optimum $(l/a)A$ increases with decreasing ϵ , again increasing the radiator temperature. The peaks of the optimum $(l/a)A$ curves vs. $\alpha\phi\sin(\gamma)$ occur when there is no temperature difference across the module at $I=0$, i.e., where the power generation mode changes from heat flowing into the spacecraft to heat flowing out. These points are marked by x's in Figure 7 and are calculated from $\alpha\phi\sin(\gamma) = \epsilon\sigma T_1^4 = \epsilon\sigma T_S^4$ (see discussion of Figures 6 and 7). When the absorbed heat is such that at $I=0$ there is a net flow into the spacecraft, the optimum $(l/a)A$ increases with decreasing absorbed flux (for a given sink temperature). This is because the optimum VI decreases, decreasing the importance of the Joule term, and the $(l/a)A$ can be increased to decrease the effect of thermal conduction. When the absorbed heat has decreased to the point where power is generated for heat flow out of the spacecraft, the peak in optimum $(l/a)A$ is crossed, and optimum $(l/a)A$ decreases with further decrease in absorbed heat. This is because heat conduction is favorable to the direction it is desired to pump heat, and there is benefit to increasing the effect of thermal conduction and decreasing the electrical resistance.

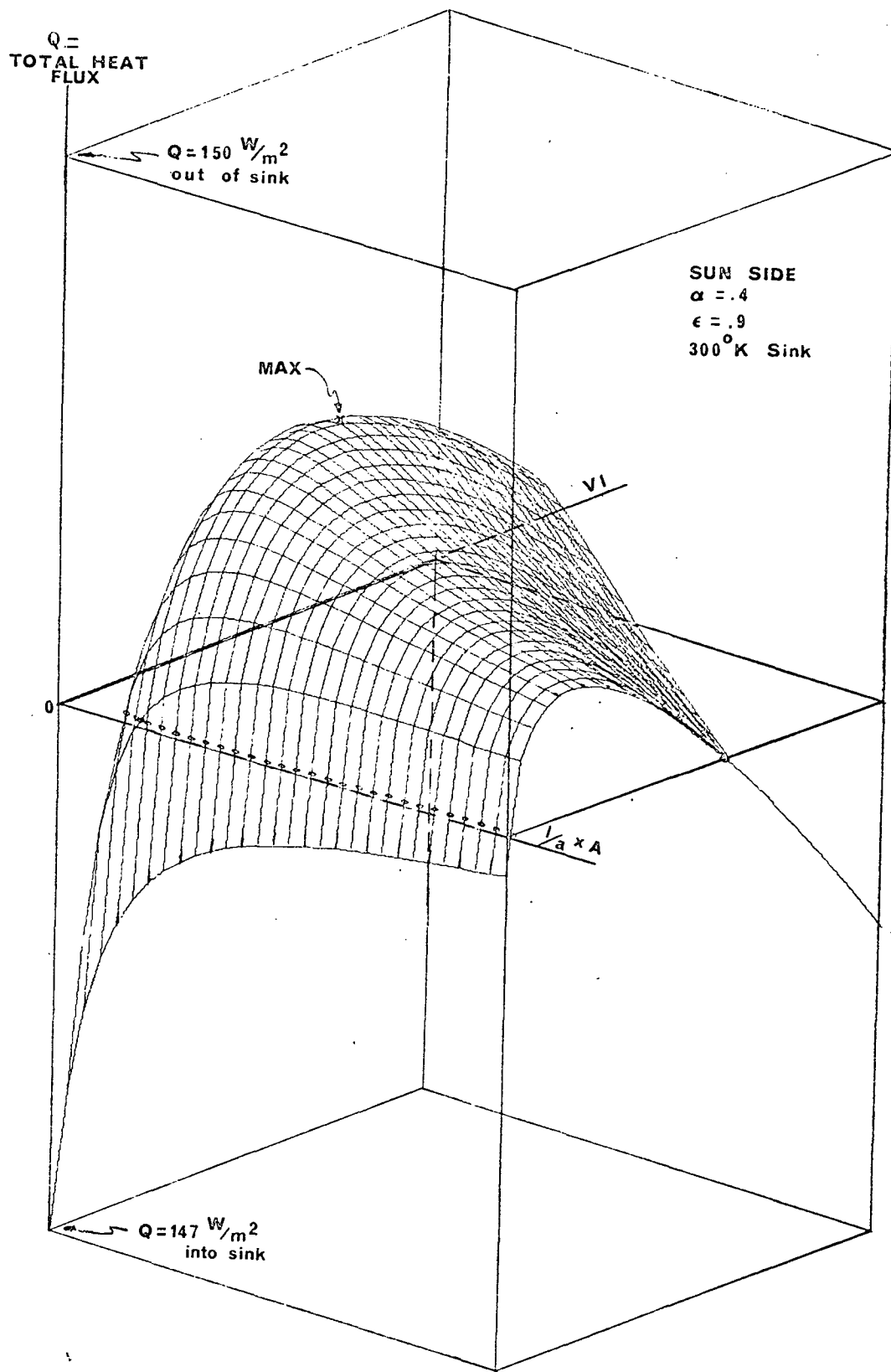
The COP at maximum ΔQ , shown in Figure 18, is just the value of ΔQ from Figure 4 divided by the corresponding VI values

from Figure 6. The COP increases toward the dark side, as discussed in relation to Figure 6 and 7. The curves cross at low incident fluxes because the optimum input power decreases faster than the maximum ΔQ at low heat sink temperatures.

Optimization With Respect To Q

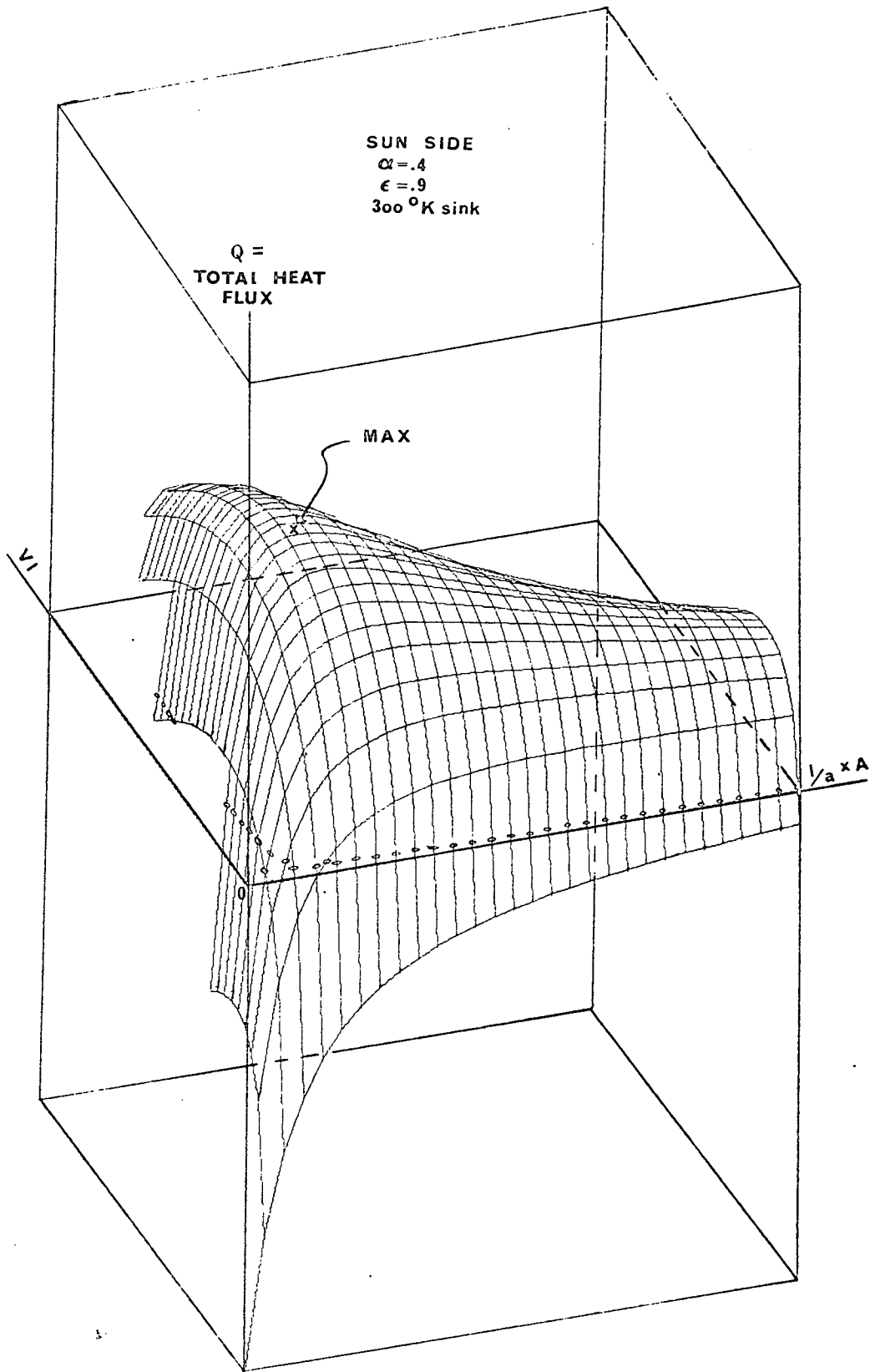
When designing a TED thermal control system or when investigating the application of TED's to a system which has already been designed with thermal control capability, such as the Phase B space station and its freon system, the total heat flow, Q , must be considered as well as the range of thermal control, $+\Delta Q$, discussed in the last section. To illustrate, consider that the unpowered TED placed in the Phase B system is simply an insulating layer. On the Sun side, it helps keep the spacecraft cooler, but on the dark side it hinders heat rejection. When powered at optimum VI, Sun side TED's can not only shut off all incoming heat, but pump a net amount out of the spacecraft. On the dark side, although the TED's can pump a finite ΔQ as has been shown, they cannot equal the heat rejection without TED's (for present materials and system arrangement). They provide a range of control, $+\Delta Q$, but for a given spacecraft geometry and its cooling system, a determination must be made as to whether or not the benefits of TED's on the Sun side can make up for the degradation on the dark side and what, if any, power is required. All modes of operation, such as powering Sun side TED's with generated power from dark side TED's, or short circuiting some TED's on the dark side to increase their thermal conductivity while powering others must be examined.

Figures 19 and 20 show total heat flow, Q , for the same conditions as shown in Figures 8 through 13. The maximum $Q(I \neq 0)$ indicated in Figure 19 occurs at a different optimum $(\ell/a)A$ and optimum VI than that for maximum $\Delta Q = Q(I \neq 0) - Q(I = 0)$ (See Fig. 8) because $Q(I = 0)$ depends on $(\ell/a)A$. This implies that a design choice must be made between maximum range of control, $+\Delta Q$, or



(a)

Figure 19. (a) Three-Dimensional View of Net Total Heat Flow, Q . Top octant is heat out of spacecraft, bottom octant is heat in. Same base plane scales as Fig. 8. Q at maximum is 68 W/m^2 , optimum VI is 230 W/m^2 , and optimum $(l/a)A$ is 130 cm .



(b)

Figure 19.(b) Second View of Fig.19 (a). Same scales.

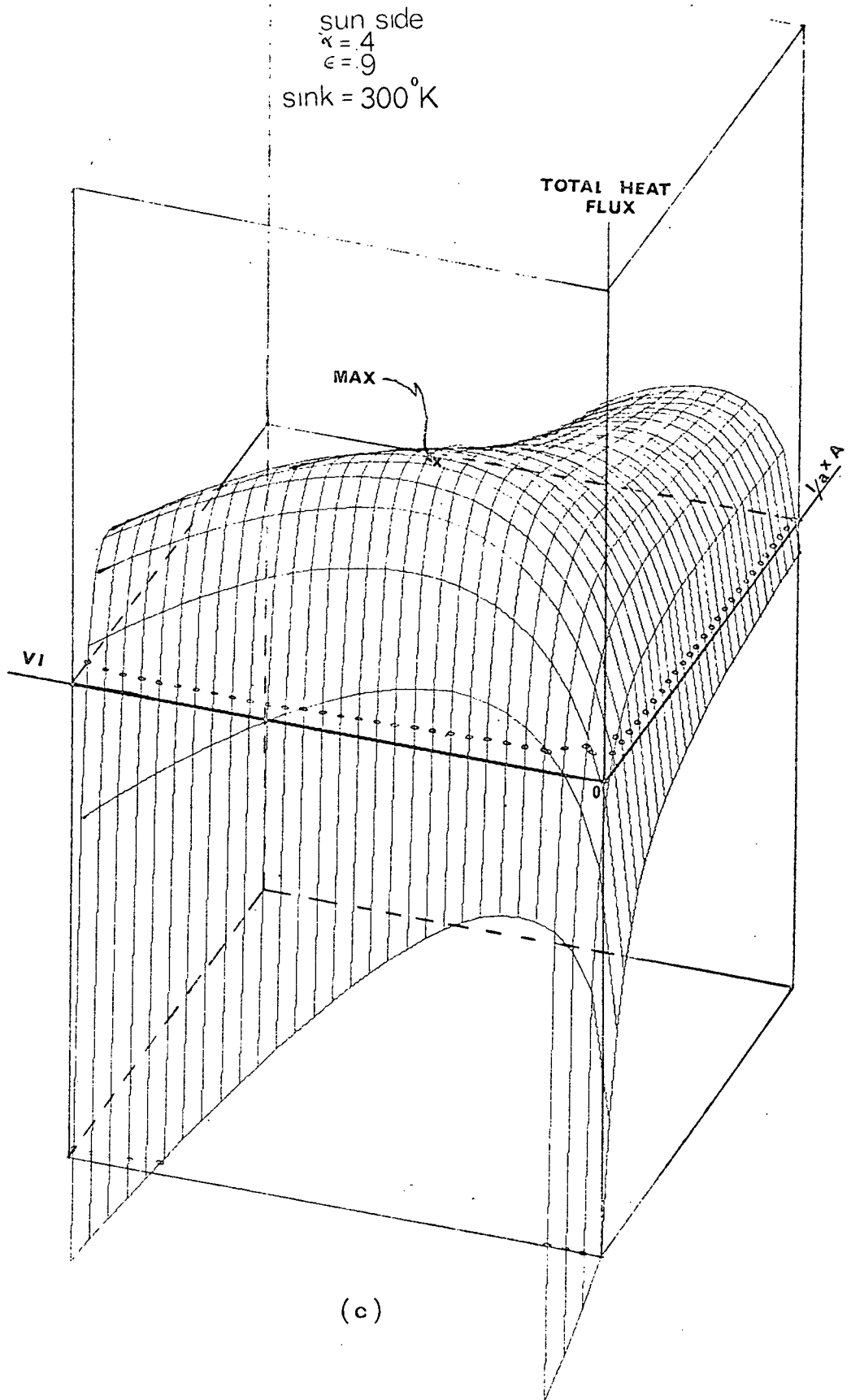
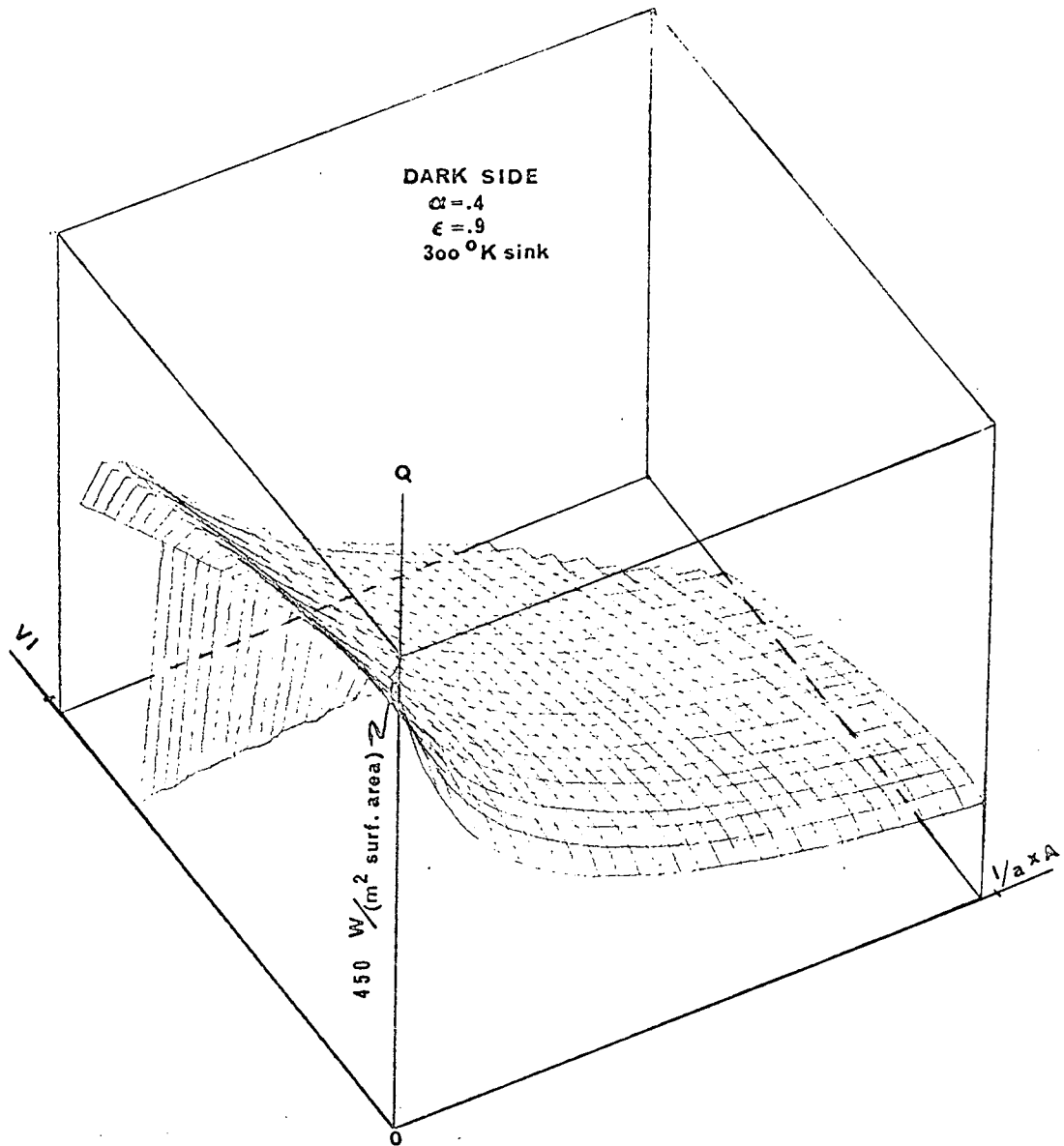
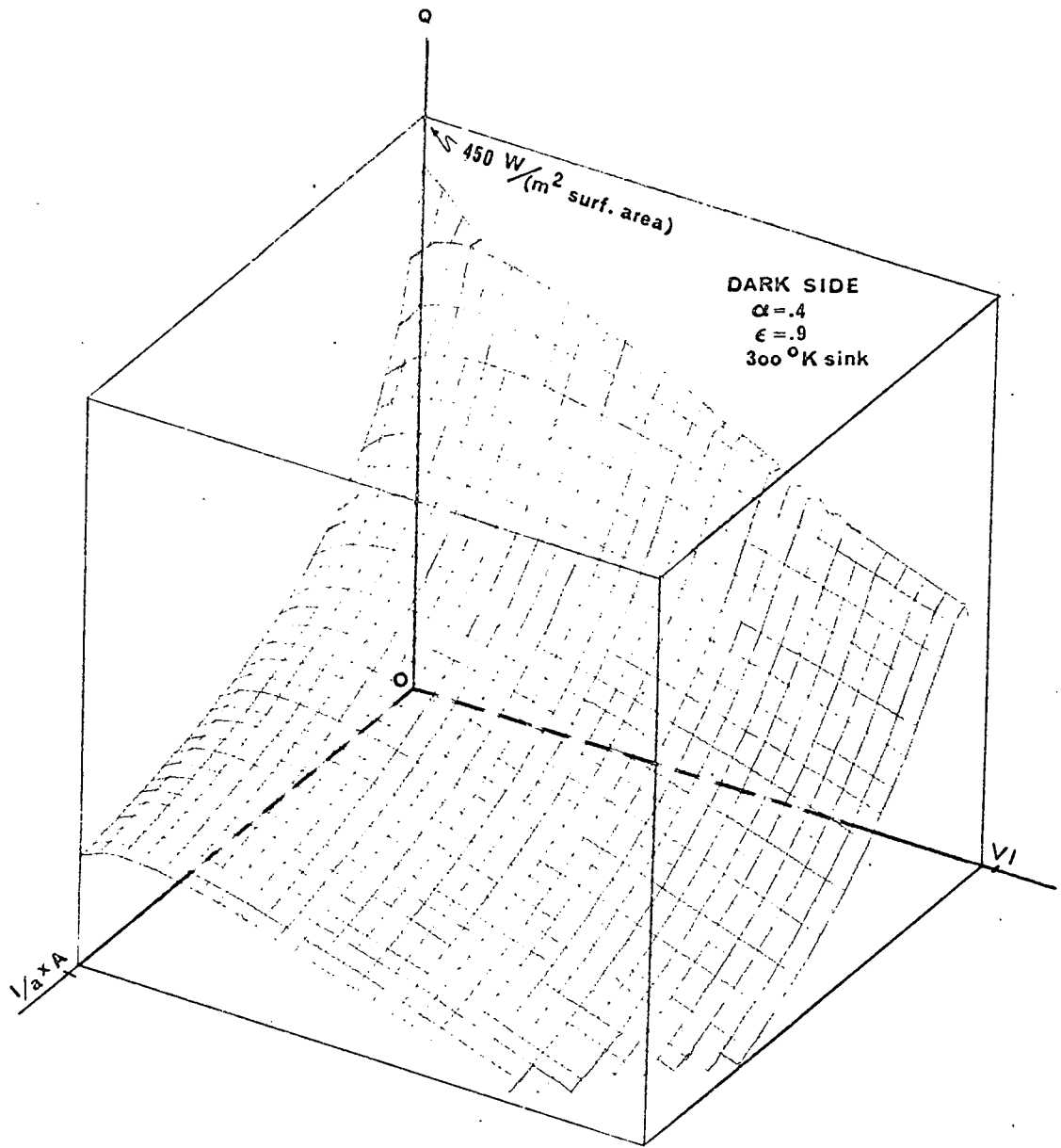


Figure 19.(c) Third View of Fig.19(a). Same scales.



(a)

Figure 20. (a) Dark Side Net Total Heat Flow, Q . Octant shown is for heat pumped out of spacecraft. Base plane scales are same as for Fig. 8. $(l/a)A$ along ridge is about 40 cm. Maximum Q out of spacecraft is 413 W/m^2 for sink without TED's.



(b)

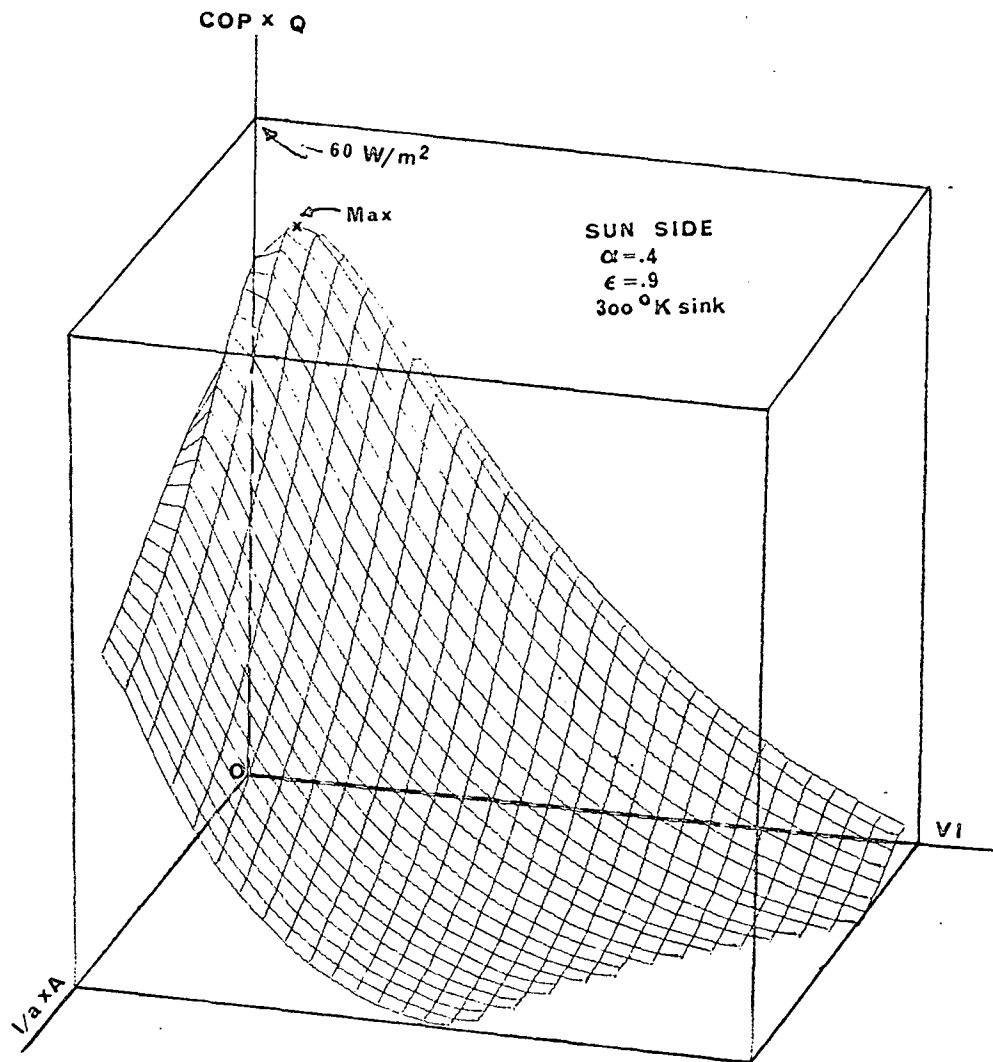
Figure 20.(b) Second View of Fig.20(a). Same scales.

maximum total heat rejection, or a compromise reached. Since the maxima involved are so broad, this is not likely to be too severe a limitation. In Figure 19, the lower base plane is the amount of heat flowing into the spacecraft (heat sink) with no TED's attached. Under conditions with TED's attached and powered, the Q curves pierce the zero-heat flow plane where indicated by the small circles, ie., heat flow into the spacecraft due to full solar radiation has been shut off. Eventually, at the proper $(\ell/a)A$ and VI, the maximum net total heat flow, Q, is reached. Note that the order of magnitude of the maximum Q's and ΔQ 's are on the order of the peak average heat rejection of the current freon system.

The dark side, shown in Figure 20, has the characteristics discussed previously. The heat flow out of the spacecraft is a maximum for no TED's, where the surface intersects the Q axis, and powered operation of the TED's cannot equal it. It is evident that operation along the ridge at about an $(\ell/a)A$ of 40 to 60 cm would be best. This is where the maximum shown in Figure 10 occurs for ΔQ on the dark side.

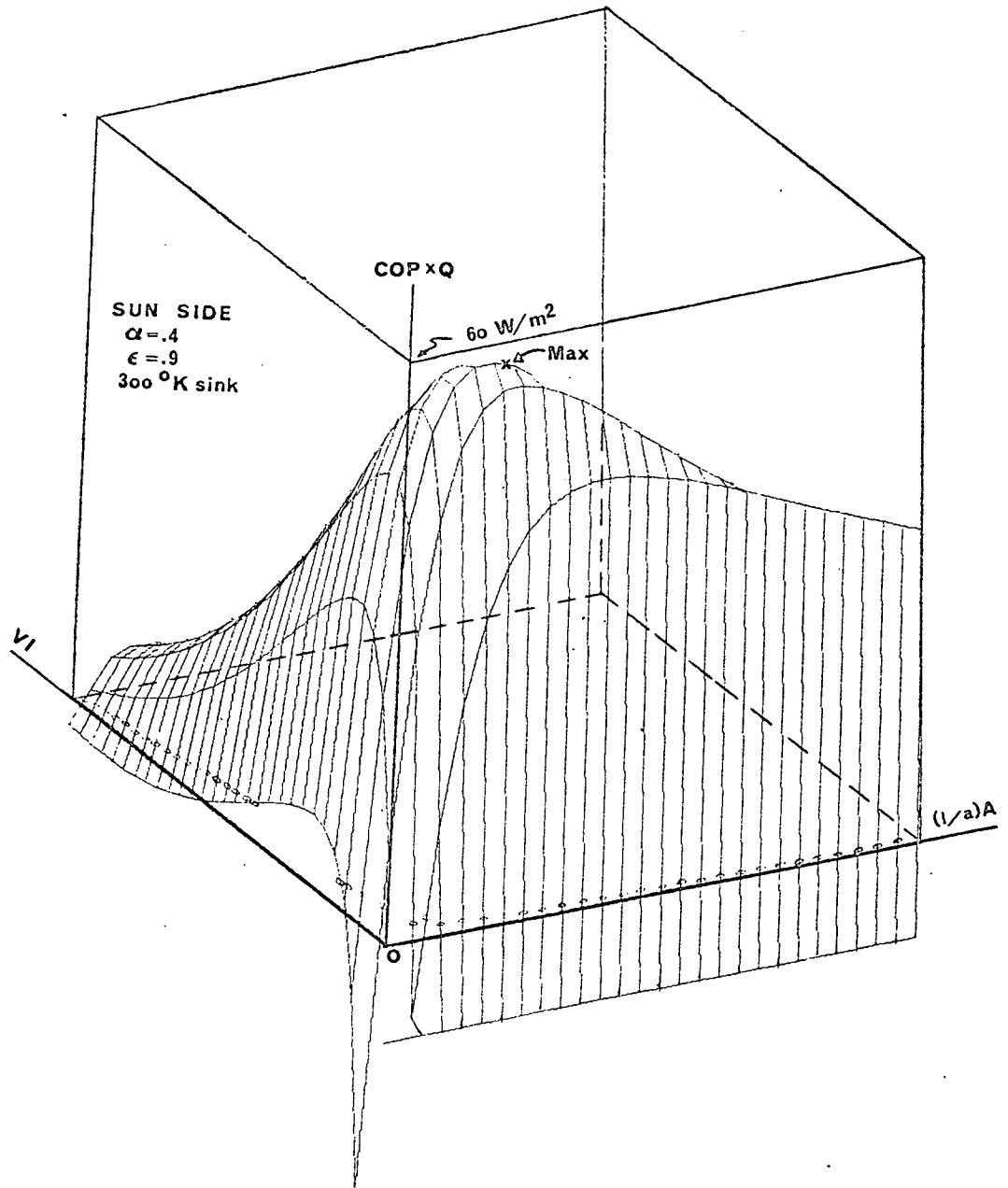
Figure 21 shows COP x Q, a COP weighted in favor of net total heat flow, Q. It has a maximum with respect to VI as well as $(\ell/a)A$, in contrast to COP. Remember that Q (out of the sink at this maximum) should be added to the heat that would be flowing into the spacecraft without TED's to obtain the benefits of heat rejection under these conditions. TED's on the dark side of the same $(\ell/a)A$ would hurt heat rejection but not by as much as the sun side was helped.

Data on the optimization of net total Q flow is presented in Figures 22 through 24. The purpose of presenting the data is similar to that for optimum ΔQ , as shown in Figures 8 through 11, although the results are quite different. In Figure 22, it can be seen that the optimum $(\ell/a)A$ increases with decreasing



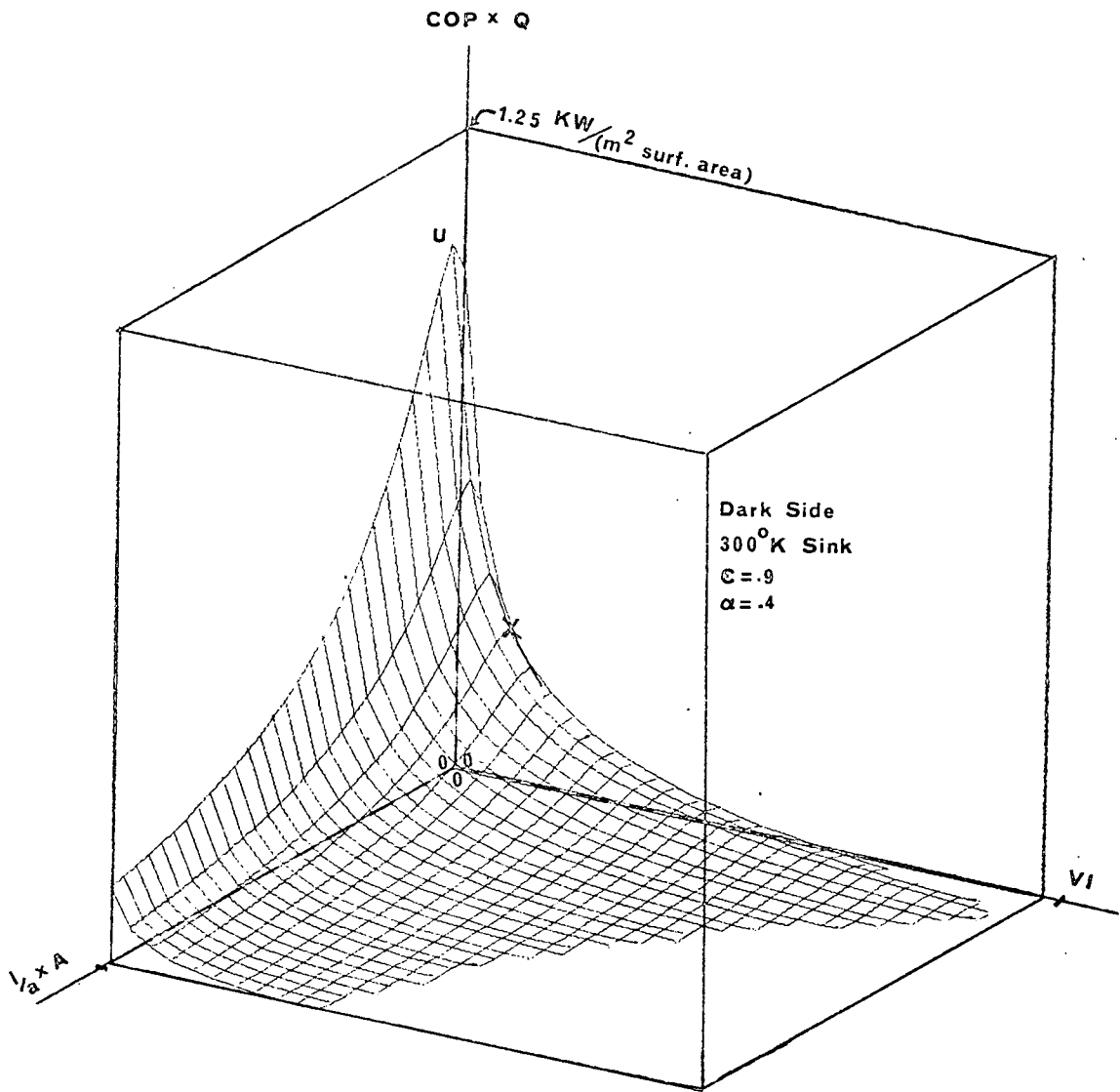
(a)

Figure 21. (a) Three-Dimensional View of COP Weighted with Q, or COP x Q, for Sun Side. Base plane scales are same as for Fig.8. Has maximum with respect to VI as well as $(l/a)A$. Q at maximum is 43 W/m^2 and COP is 1.65.



(b)

Fig.21.(b) Second View of Fig.21(a). Same scales.



(c)

Fig.21.(c). Dark Side COP x Q. Same scales for base plane as Fig.8. At point "x", $Q = 332 \text{ W/m}^2$ and $\text{COP} = .95$. At point "u", $Q = 321 \text{ W/m}^2$ and $\text{COP} = 3.2$.

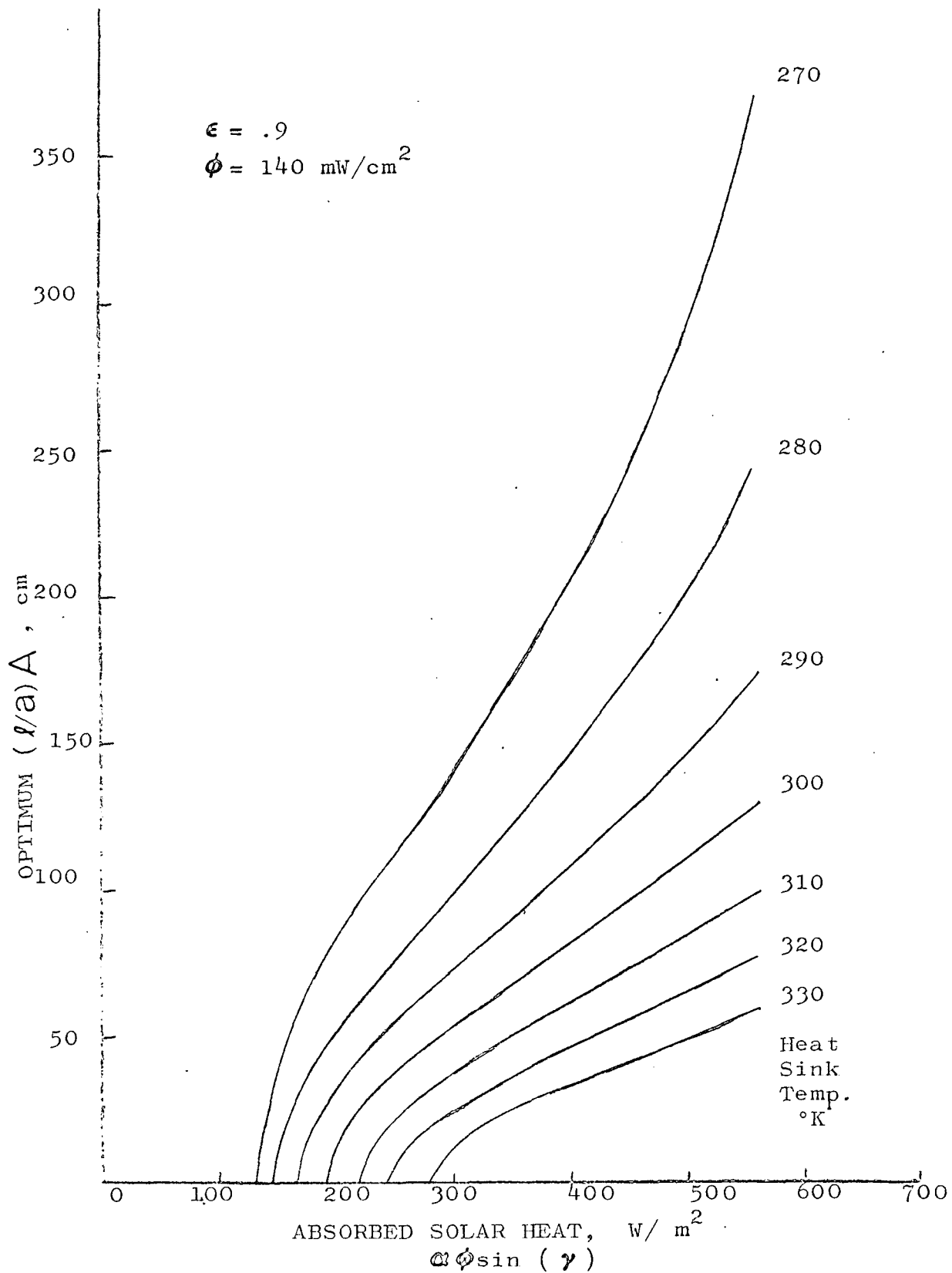


Figure 22. Optimum $(l/a)A$ for maximum net heat flow, Q , out of heat sink at optimum VI. Every combination of α and γ is represented up to $\alpha = .4$, $\gamma = 90^{\circ}$.

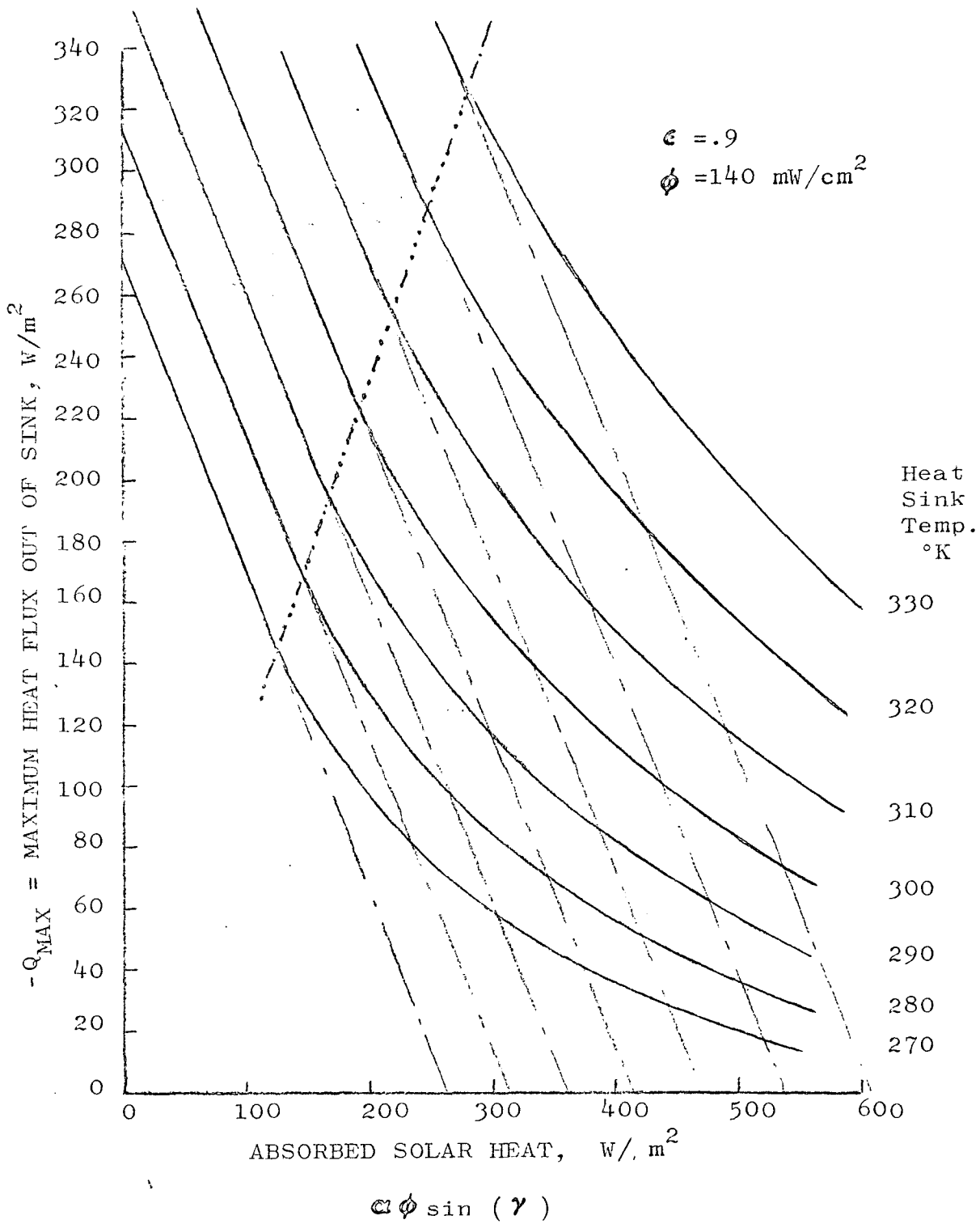


Figure 23. Maximum Net Amount of Heat Flow Out of Spacecraft at Optimum $(l/a)A$ and Optimum VI. ϵ is constant. Every combination of γ and ω is represented up to $\omega = .4$ and $\gamma = 90^\circ$. To the left of the dotted line the heat rejection is greatest without TED's on the sink, and the curves become $Q = \omega \phi \sin(\gamma) - \epsilon \sigma T_{\text{sink}}^4$.

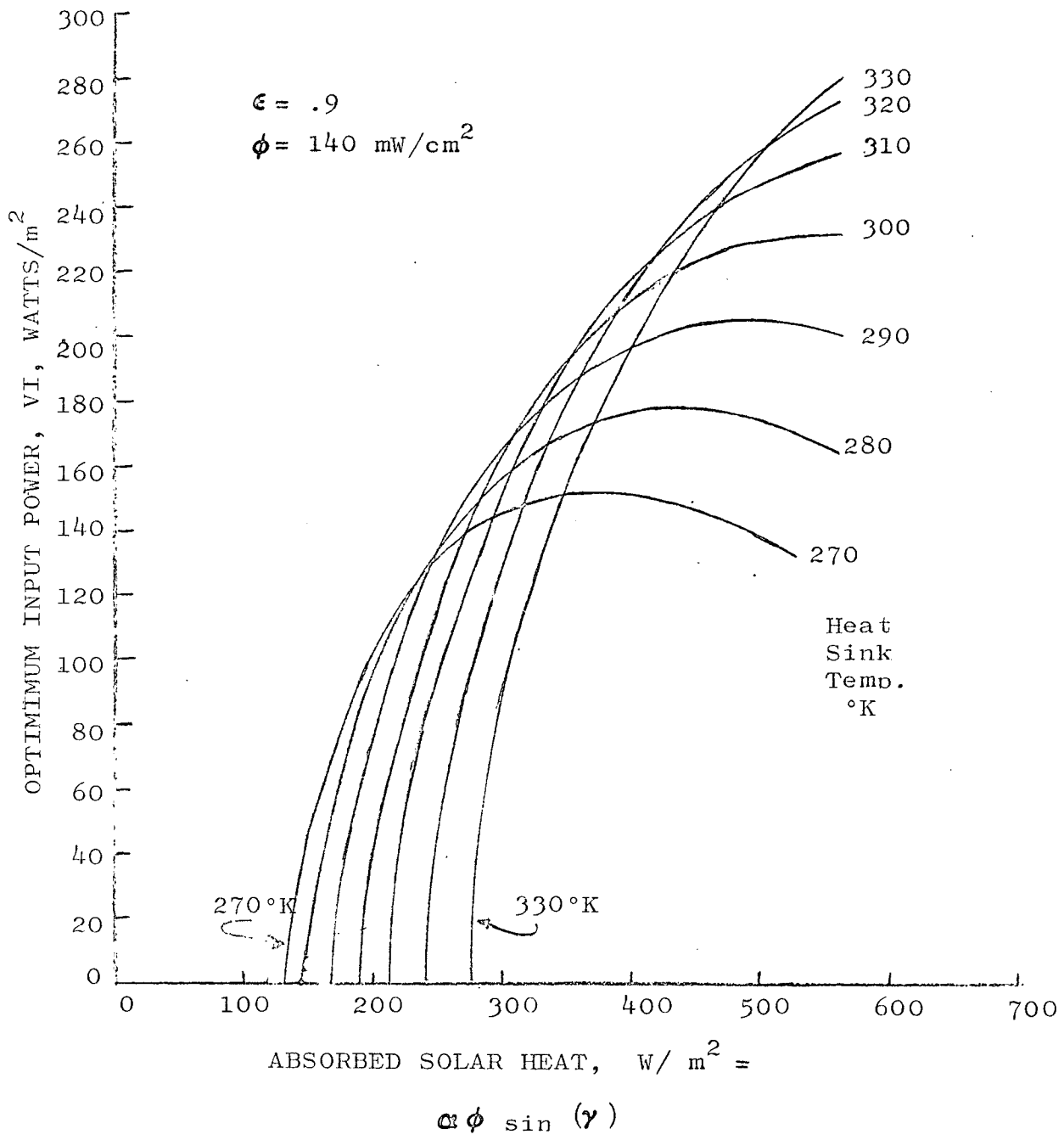


Figure 24. Optimum input power for maximum net heat flow, Q , out of spacecraft. Every combination of α and γ is represented up to $\alpha = .4$, $\gamma = 90^{\circ}$. Multiply VI by $2 \times 10^{-3} \text{ m}^2/\text{couple}$, to get VI in Watts/couple.

sink temperature. This happens because there is a need to increase the radiator area to offset the lower radiator temperature. The optimum $(\ell/a)A$ decreases with decreasing absorbed incident radiation also, until a point is reached for which the optimum $(\ell/a)A = 0$. This simply means, as mentioned above, that no net advantage can be gained by having TED's in the system for cooling purposes on the dark side, except for the $\pm\Delta Q$ control available. The points where the curves intersect the abscissa are where $-Q_{\max} = \alpha\phi\sin(\gamma) - \epsilon\sigma T_{\text{sink}}^4$.

Returning to Figure 9, it can be seen that the optimum $(\ell/a)A$ changes with operating input power, VI. This becomes a design criteria when designing for maximum Q if it is desired to operate at a VI lower than the optimum VI in order to increase the COP.

As the optimum $(\ell/a)A$ approaches zero, as in Figure 22, the maximum net total heat that can be rejected approaches the value for no TED's as shown in Figure 23. The maximum Q out of the sink increases as the absorbed radiation decreases and heat sink temperatures increase largely because the TED becomes less of an insulating layer, and can be powered more because of decreasing resistance and ΔT . At the points where the incident flux becomes too low for the TED's to give an advantage in cooling (dotted line in Fig. 23), the equation for the lines becomes $Q = \alpha\phi\sin(\gamma) - \epsilon\sigma T_{\text{sink}}^4$. To the high flux side of the dotted line, it can be seen that the curved portions of the lines fall above the lines for no TED's (dashed), showing the advantage of TED's.

The optimum input power shown in Figure 24 increases with absorbed incident radiation at first, and then decreases because the advantage of an insulating effect becomes dominant. The same thing happens for decreasing sink temperatures, so the curves cross as shown. The points of intersection on the

abscissa correspond to those in Figure 22.

Correlation With Phase B Results

Closed form equations were derived in the Second Quarterly Report for Q which employed a Taylor expansion linearization of the T^4 law and constant TED parameters. The optimum $(\ell/a)A$ found from it predicted that below a certain value of Q_N , the optimum $(\ell/a)A$ would be zero, and above a certain value of Q_N it would be infinite (perfect insulator), where

$$Q_N = \alpha \phi \sin(\gamma) - \epsilon \sigma T_{\text{sink}}^4$$

This is the heat that would be flowing when no TED's were on the spacecraft. Figure 25 shows that the two models agree qualitatively and fairly well quantitatively also.

Summary

The operation of TED's radiating into space has been characterized by the maximum amount of heat, ΔQ , that can be pumped away from a heat sink at a temperature T_1 , with a given amount of incident radiation. Since it has been shown that, with a reversal of input current but the same input power, several times more heat can be pumped into the spacecraft as out, the range of thermal control is limited by this maximum ΔQ . It has also been shown that for ΔQ out of the spacecraft there is an optimum $(\ell/a)A$ and an optimum VI. Visualization of these characteristics is provided by Figures 6 and 7 and by the three dimensional surfaces. Quantitative characterization is provided by Figures 14 through 18.

It should be emphasized again that in a design procedure for thermal control of a body in Earth orbit operating in a barbeque mode, it is necessary to find a compromise $(\ell/a)A$ and VI since all surfaces will be exposed to the full radiation flux range. Considerations include the fact that individual TED's would receive different amounts of incident radiation

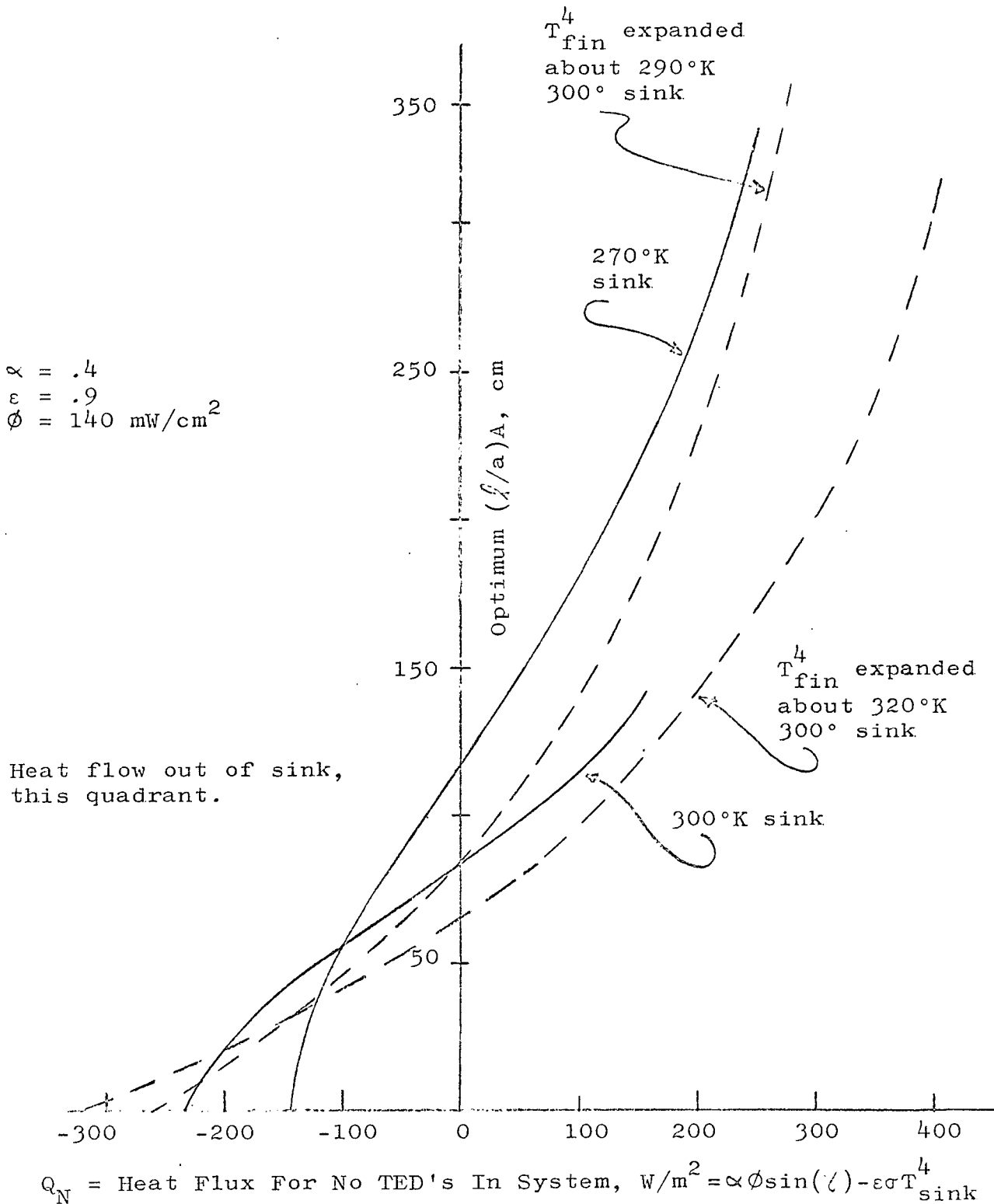


Figure 25. Correlation of closed form optimization equation as used in Phase B₄ comparison with optimum $(\lambda/a)A$ found with heat sink model using T^4 law and temperature varying parameters. Dashed curves are closed form solution with linearized T^4 law and constant TED parameters. Solid curves are from the heat sink model. Optimum $(\lambda/a)A$ is for maximum net total heat flow, Q , out of spacecraft.

at different times, and that the COP may have to be kept above some minimum for reasons of electrical power cost under worst possible incident radiation conditions. It should be kept in mind that, in designing a system to be cooled by TED's, the optimum geometry $((\ell/a)A)$ and operating input power will be different if examined with respect to the maximum range of thermal control $(+\Delta Q)$ than with respect to maximum net heat flow out of the spacecraft (Q) . It will be necessary to decide which is more important when comparing with other cooling systems. Considerations such as precise control and lack of moving parts and fluids will be important also.

If this model were to be applied to a spacecraft of the Phase B type, each TED-fin section would have to be weighted with respect to heat sink temperature and incident flux according to its position on the surface. From these results, an optimum $(\ell/a)A$ could be determined for each position, then trade-offs would have to be considered between COP, optimum $(\ell/a)A$ (for maximum heat pumped), available electrical power, and operating mode (open circuit, short circuit, power generation, or powered). These considerations would provide the basis for predicting total heat rejection and control. If heat rejection is greater than that without TED's in the system, the spacecraft will be cooled beyond what the fluid system will do. If the radiator surface area can be adjusted for specific thermal load requirements so that the correct average amount of heat can be rejected with the TED's passive, the range of control will be maximized.

The data in this section represents the completion of the Intermediate TED Analysis Study. The derived information will be employed during the next and final quarter of the existing contract to present useful predictions and engineering descriptions of various TED applications and characteristics.

CONCEPTS STUDY

Introduction

Several concepts for application TED Thermal Control other than for the specific Phase B comparison based on bulk module studies have been examined during the past quarter.

These include:

1. Cooling of EVA equipment.
2. Moon station.
3. Solar array cooling for both moon and space stations.
4. Critical isolated communications, electronic or instrument packages.
5. Space station control geometries other than that of the Phase B system.
6. Thin film geometries.

Items 1-3 are related to applications of a TED thermal control systems having a dependence on an associated radiator of finite area and some sort of sink through which heat flow is controlled. Unique to items 4 and 5 are special problems of isolation. Critical temperature control in a changing thermal environment or special means of applying TED's. Item 6 involves investigating thin film or thin layer geometries suitable for thermal control which differs from the bulk module approach taken in this study.

The first 3 items are strictly applicational oriented and a discussion of control capability would be superfluous at this time since it would depend on a practical TED system, the load level, load variability and geometry. The fourth item relates to spot thermal control of critical components with heat sinks either connected to the surrounding structure or radiators. Further it includes thermal control between two radiators located within the space craft one of which is TED controlled and connected to an isolated system. This concept has been considered as a means for cooling the camera structures in the LST.

Included in 5 are the possibilities of utilizing TED's between two fluids in a heat exchanger and also between a heat exchanger and radiator webbed with heat pipes. The latter would employ a high packing density TED. Item 6 is self explanatory.

Consideration has been given to the concepts in general. Although none of them can be given the attention applied to the Phase B investigation two were selected for further examination. The selections, to be separately discussed, were based on there being sufficient difference between them and the Phase B study.

TED's With Heat Pipe Radiator

Figure 26, shows a sketch of an applicational concept where the TED's are connected between a radiator and a heat exchanger. If we assume no interface temperature drop on either side of the TED then $T_{Fin} = T_1$ and $T_x = T_{sink}$.

The TED pack would consist of a high density of thermo-electric couples which would control the heat flow from the heat exchanger to the isothermal radiator through the connecting heat pipe. Thermal control would be different than that found in the Intermediate TED or the Phase B analysis.

Computations based on this concept were made regarding TED packing density and radiator area. Assuming an isothermal cylindrical radiator with its length 5 times its diameter, calculations were made and results obtained on a per square meter basis and are given in Table V. The $(l/a)A$ value was selected from the Phase B analysis to be 60 cm. The l/a value was 3.24. Hence there are 538 couples required per square meter. If each couple occupies $.03 \text{ cm}^2$, a module area of about 16 cm^2 or 4 cm on a side is obtained. Sun was incident on one side and no radiation from earth was considered.

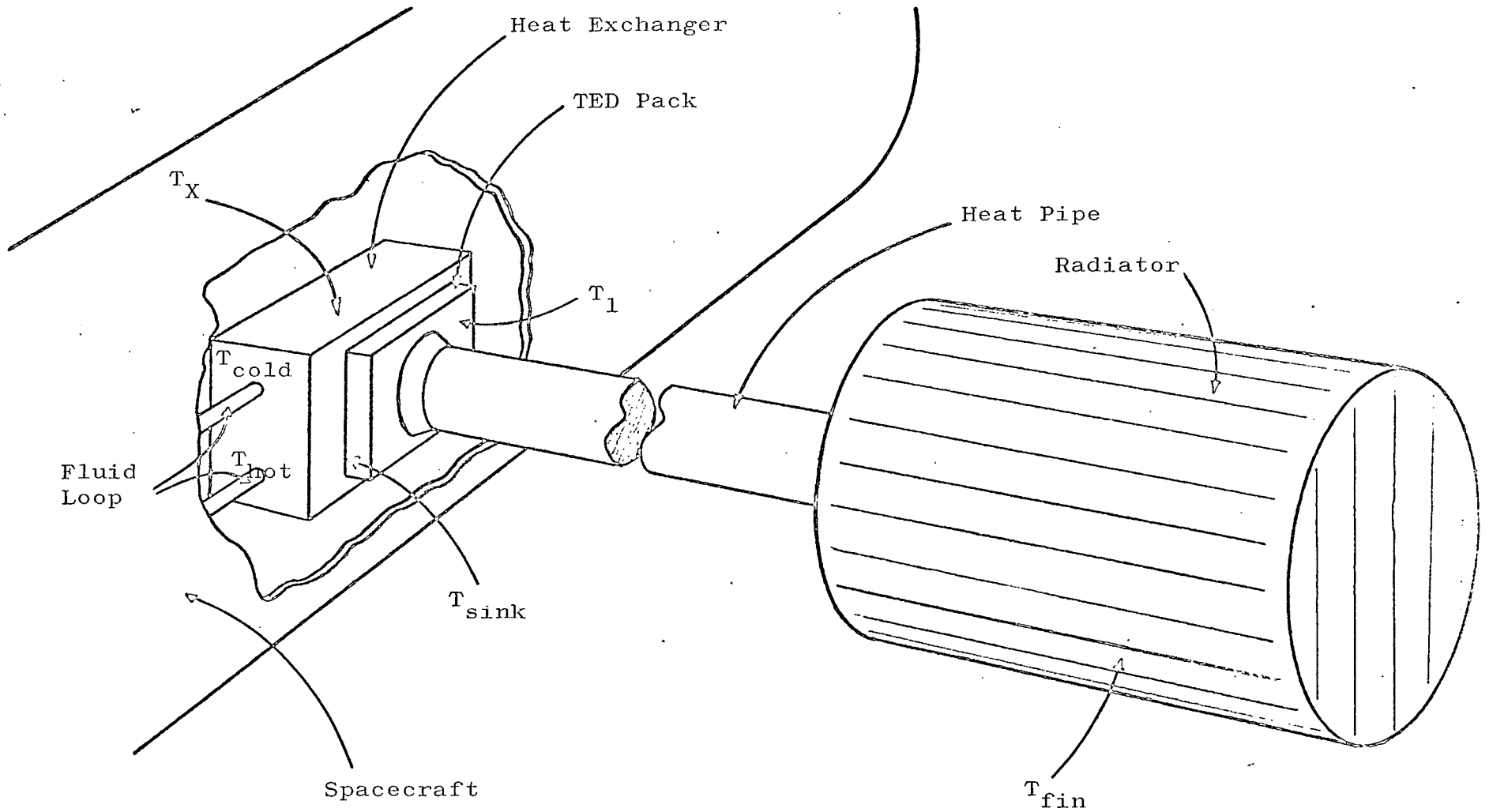


Figure 26. TED'S With Heat Pipe Radiator.

TABLE V.

Control Capability Of A TED-Heat Pipe Radiator

Current (amps)	Electrical Power (Watts)	T_x (°K)	T_{Fin} (°K)	Rejected Heat
0	0	270	257	55
1.85	15.5	270	270	100

Note that with 1.85 amps the heat rejection is very nearly doubled giving an additional 45 watts/m^2 heat rejection at a cost of 15.5 watts. Since 1.85 amps is below the value for maximum heat rejection a greater control range is expected. Control, closer to the 55 W/m^2 point would be even more efficient than indicated in Table V. The power generation mode was not considered in this analysis.

Thin Film TED Radiators

The concept of employing thin film TED's has been a long range goal in our studies. During the past quarter period consideration was given to means of constructing such a system and its geometric layout.

Figure 27, is a schematic of a thin film TED radiator section. Preliminary calculations based on results of the Phase B study indicates that about 50% of the total radiator surface would be utilized for the TED thermal control radiator portion.

Behavior of the thin film system is such that the insulating effects are reduced over that found in the Phase B comparison utilizing a bulk approach. Therefore, differences in heat rejection between the unpowered TED thin film system and the Phase B system will be much smaller than found in our present study.

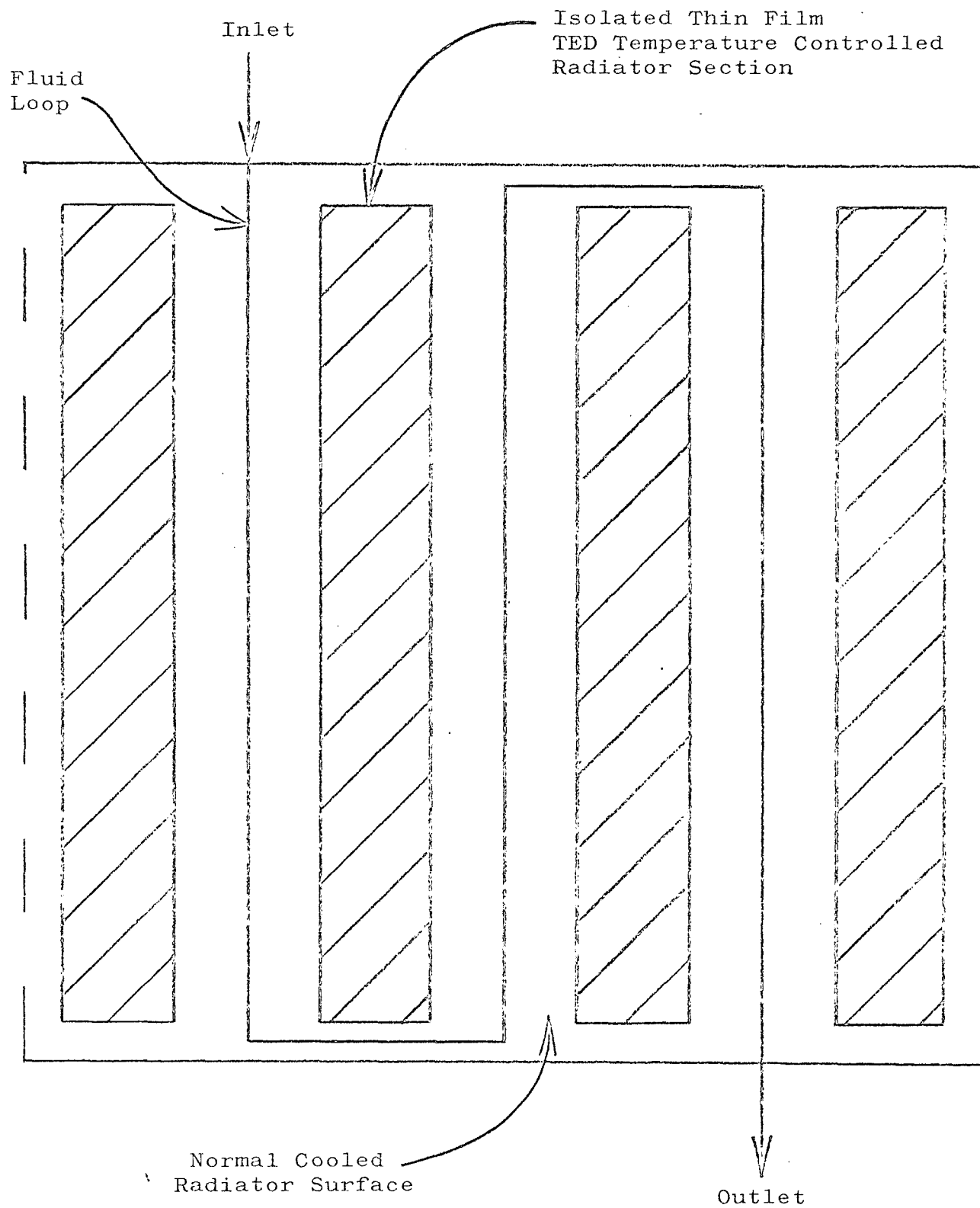


Figure 27. Schematic of Thin Film Radiator

Along with the above, other characteristics of the thin film system indicate a superiority over the bulk approach. Mechanical integrity is improved. Most of our present method of analysis will apply to the thin film system. A detailed program outline is being prepared to implement a thin film study as a separate task.

PLANS FOR FUTURE WORK

During the next and final quarter period of the present contract the following work is planned.

1. Finalize a specific TED Analysis based on the completed Intermediate TED study. This will be a system characterization without a comparison compromise.
2. Finalize the Phase B comparison study.
3. Finalize a TED concept evaluation and make recommendations.
4. Identify other spacecraft applications of TED.
5. List the conclusion reached during this year's work and make recommendations where continued effort would be beneficial to the overall objectives of the program.

REFERENCES

1. Domenicali, C.A., Stationary Temperature Distribution in An Electrically Heated Conductor, J.A.P., 25, 10, October 1954.
2. Sherman, B., Heikes, R.R., and Ure Jr., R.W., Calculation of Efficiency of Thermoelectric Devices, J.A.P., 31, 1, January, 1960.